MAO-B INHIBITORS PROTECT AGAINST LIPOPOLYSACCHARIDE-MEDIATED EPITHELIAL BARRIER LOSS AND CYTOKINE RELEASE

by

Vincent Wally James Senini

B.Sc., The University of British Columbia, 2009

A THESIS SUBMITTED IN PARTIAL FULFILLMENT OF
THE REQUIREMENTS FOR THE DEGREE OF

MASTER OF SCIENCE

in

The Faculty of Graduate Studies

(Craniofacial Science)

THE UNIVERSITY OF BRITISH COLUMBIA
(Vancouver)

August 2011

Abstract

Epithelial tissues play a critical role in maintaining systemic health by establishing a functional barrier that separates the external environment from the host to provide an innate defense against environmental insult. Epithelial barrier disruption is suspected to play a central role in the onset of chronic inflammatory disease, although, fundamental knowledge of the underlying pathogenesis remains poorly understood. Thus, identifying factors that mediate epithelial barrier loss is clinically relevant as it will open the possibility that novel interventional strategies may be developed to mitigate early disease-associated signaling events.

Lipopolysaccharide (LPS) is a Gram-negative bacterial virulence factor implicated in periodontal disease onset. Amphiregulin (AR) is a ligand for the epidermal growth factor receptor (EGFR) and downstream mediator of tumor necrosis factor-alpha (TNF-α) (Chokki et al., 2006) that is normally sequestered at cell-cell contacts in stable epithelial barriers. AR and corresponding signaling components modulating the EGFR pathway are altered in a rat model of periodontal disease that exhibited concomitant altered barrier architecture (Fujita et al., 2011; Firth et al., 2011). Treatment of this model with monoamine oxidase (MAO) inhibitors ameliorated disease indices (Ekuni et al., 2009).

This study employs an *in vitro* histiotypic model of epithelium to provide evidence that LPS-reduced epithelial barrier function associated with chronic inflammatory disease may be mediated by altered AR and TNF-α secretion. MAO-B inhibition by ($-$)-deprenyl enhanced barrier model transepithelial electrical resistance (TER), prevented LPS-, AR- and H_2O_2-induced reduction in TER and attenuated LPS-induced AR and TNF-α secretion and H_2O_2-induced AR secretion. Furthermore, immunostaining of barrier model cultures showed

that markers of cell-cell junctions were altered by LPS challenge and treatment of the model with (−)-deprenyl protects against this disruption. This study addresses the underlying mechanism by which (−)-deprenyl protects against bacterial virulence factor-induced epithelial barrier disruption and points to a significant role for AR as a central mediator of barrier integrity. Ultimately, this project aims to provide *in vitro* evidence for the efficacy of (−)-deprenyl treatment of LPS-induced epithelial barrier disruption, which may promote development of enhanced MAO-B inhibitors and lead to an effective clinical treatment for disease-associated epithelial barrier loss.

Table of Contents

List of Tables

List of Figures

List of Abbreviations

ADAM	a disintegrin and metalloproteinase
AJ	adherens junction
AJC	apical junctional complex
AR	amphiregulin
EGF	epidermal growth factor
EGFR	epidermal growth factor receptor
ERK1/2	extracellular signal-regulated kinase 1/2
H_2O_2	hydrogen peroxide
IBD	inflammatory bowel disease
IEC-6	intestinal epithelial cell line-6
IFNγ	interferon-gamma
IRF-5	interferon regulatory factor-5
IL	interleukin
JE	junctional epithelium
LPS	lipopolysaccharide
MAO	monoamine oxidase
MDCK-I	Madin-Darby canine kidney epithelial cell line-I
MDCK-II	Madin-Darby canine kidney epithelial cell line-I
MLCK	myosin light chain kinase
NF-κB	nuclear factor kappa-light-chain-enhancer of activated B cells
PLE	periodontal ligament epithelial cell line
ROS	reactive oxygen species
TACE	tumor necrosis factor-alpha converting enzyme
TGF-α	transforming growth factor alpha
TJ	tight junction
TLR	toll-like receptor
TNF-α	tumor necrosis factor-alpha
ZO-1	zonula occludin-1

Acknowledgments

1 Introduction

Epithelial tissues play a critical role in maintaining systemic health by establishing a functional barrier that physically separates the external environment from the host. Epithelial barriers cover or line all organs and have a tissue-specific level of permeability, which facilitates the controlled transepithelial transport of molecules and fluids conducive to the optimal function of the particular tissue it protects. This barrier provides an innate non-specific defense that serves to protect underlying tissues from environmental stresses, chemical damage and bacterial infection. Furthermore, maintaining the normal balance between competence to respond to pathogens and not generating an inflammatory response to commensals appears to depend on the integrity of the epithelial barriers (Rakoff-Nahouman et al., 2004; Fukata et al., 2005; Brown et al., 2007). Loss of barrier function that accompanies alterations of cell-cell junctional proteins is associated with chronic epithelial inflammatory processes typified by periodontal disease, psoriasis, chronic airway inflammatory diseases, conjunctivitis, various forms of kidney proximal tubule disease as well as gut related barrier disruption seen in inflammatory bowel disease (IBD) (Fujita et al., 2010; Chung et al., 2005a; He et al., 2009; Kucharzik et al., 2001; Xavier and Podolsky, 2007; Sartor, 2006; Runswick et al., 2007; Balkovetz, 2009; Wine et al., 2009). In this regard, disruption of epithelial barrier is suspected to play a central and general role in the onset of chronic inflammatory disease. While serious itself, there is also evidence that loss of barrier may lead to disease at distant sites. For example, chronic loss of both gut and periodontal barrier has been associated with chronic heart disease and various systemic diseases, possibly due to prolonged systemic access by pathogens (Ebersole et al., 2010;

Nakajima et al., 2010; Haapamäkia et al., 2010; Actis et al., 2011). Fundamental knowledge of the underlying pathogenesis remains poorly understood. Therefore, identifying factors that mediate epithelial barrier loss is clinically relevant, as it will open the possibility that novel interventional strategies may be developed to mitigate disease-associated signaling.

1.1 Epithelium in Health and Chronic Inflammation

Development and survival of multicellular organisms, from sea sponges to mammals, is dependent on the ability to maintain unique structural integrity and chemical composition of specialized internal compartments. This is achieved by establishing cell barriers that separate body compartments from the external environment. Multicellular organisms rely on tissue compartmentalization to interface with the external environment while supporting specialized internal functions. The cells that define this interface between the organism and the external environment are a characteristic of all multicellular eukaryotes and play a critical role in barrier maintenance. To establish boundaries, cells that cover the external surface and line internal compartments must form barriers to inhibit unrestricted exchange of materials. Accordingly, barrier function is defined as the ability of epithelial and endothelial-lined surfaces to restrict free passage of water, ions, and large solutes. Simple epithelial linings in the gastrointestinal, respiratory, renal and reproductive systems are composed of monolayers of polarized cells with extended lateral surfaces that ensure maximum contact between opposing cells. The plasma membranes of these cells effectively restrict most hydrophilic solutes from crossing the boundary. In addition, the paracellular pathway between cells must also be sealed. This later function is the responsibility of the apical junctional complex (AJC), which is composed of the tight junction (TJ) and the subjacent adherens junction (AJ). In simple epithelia, TJ and AJ are closely positioned in the apical

2

part of the lateral plasma membrane (Figure 2). It is generally believed that the AJC plays a

key role in formation and maintenance of epithelial barriers (Tsukita et al., 2001; Blaschuk

and Rowlands, 2002). Desmosomes are localized along the lateral membranes beneath the

AJ (Figure 2). While the TJs seal the paracellular pathway, the AJs and desmosomes provide

strong adhesive bonds necessary to maintain cellular proximity and enable assembly of TJs.

AJs are also critical for epithelial polarization and differentiation, mucosal morphogenesis

and tumor suppression, which are processes that rely on a multitude of interactions between

AJs and other proteins, including actin and β-catenin.

A proposed model for inflammatory disease incorporates roles for microbiota,

epithelium and the innate and adaptive arms of the immune system (Clayburgh et al., 2004).

This model proposes a self-potentiating cycle by which small defects in any of these

components become amplified and result in disease. For instance, an episode of

inflammatory challenge may damage the epithelial barrier and enable microbiota to enter the

basal lamina and underlying connective tissue. The anti-inflammatory response elicited may

be limited by alterations in IL-10 expression, such as that found in IL-10 knockout mice or

in patients with polymorphisms adjacent to the IL-10 gene (Jarry et al., 2008; Powrie et al.,

1994; Fisher et al., 2008). This may result in epithelial immune activation proceeding

unchecked and lead to excessive release of cytokines, such as TNF-α, that increase loss of

barrier function, which in turn would cause further leakage of luminal bacteria and

perpetuate the pro-inflammatory cycle. Alternatively, the defect may be a deficiency of the

epithelial barrier function. In this case, aberrant immune regulation or altered composition of

the microbiota could enable initiation of the pro-inflammatory cycle. Lastly, alterations in

innate immunity, such as those associated with abnormalities in Toll-like receptors (Uematsu

et al., 2008; Fukata et al., 2008; Vijay-Kumar et al., 2007; Sutmuller et al., 2006), or defects in adaptive immunity, demonstrated by the presence of antibodies to bacterial components (Sanders et al., 2006; Lodes et al., 2004), may trigger this self-amplifying inflammatory cycle. This model of disease progression may explain the therapeutic effects of immunosupressants (D'Haens et al., 1999), immunomodulators and probiotocs (Bibiloni et al., 2005) as well as the benefits of attenuating inflammatory disease by employing novel methods that preserve barrier function (Arrieta et al., 2008). As a result, efforts to improve the understanding of the role of epithelial barrier in mediating interactions between adherent microbiota and host epithelial and immune cells, may lead to novel therapies that mitigate loss of epithelial barrier function associated with inflammatory disease pathogenesis.

1.1.2 Lipopolysaccharides and chronic inflammation

Lipopolysaccharides are essential structural components of the outer membrane of Gram-negative bacteria and potent endotoxins. LPS typically consists of three domains: the lipid anchor domain of LPS (lipid A), a short core oligosaccharide and an O side chain that may be a long polysaccharide (Raetz and Whitfield, 2002; Miller et al., 2005). Lipid A is the main pathogen-associated molecular pattern of LPS. The innate immune system recognizes bacterial pathogens such as LPS via a family of pathogen recognition receptors called Toll-like receptors (TLRs). Among them TLR4 is predominantly involved in recognition of LPS in epithelium and the receptor elicits an immune response that serves to control infection processes (Akira et al., 2006; Poltorak et al., 1998). Engagement of TLR4 with LPS induces dimerization, which brings together two signaling domains that subsequently serve as a platform for the recruitment of various intracellular adaptor molecules (Kenny and O'Neill, 2008). MyD88 is an adaptor used by TLR4 and functions to activate a transcription factor

called nuclear factor kappa-light-chain-enhancer of activated B cells (NF-κB) as well as the

mitogen-activated protein kinases (MAPKs). MyD88 also activates the transcription factors

AP-1 and interferon regulatory factor 5 (IRF-5) further downstream. These transcription

factors induce expression of specific proinflammatory cytokine genes (Lu et al., 2008). In

addition, these events drive cellular signaling which culminates in dynamic changes in the

expression of genes that encode chemokines and cell adhesion molecules as well as markers

of dendritic cell maturation (West et al., 2006; Van Vliet et al., 2007). Responses elicited by

TLR activation represent a double-edged sword. In the context of local acute infection, TLR-

induced events are critical in immune defense and the survival of the host by functioning to

provoke the innate immune response and enhance adaptive immunity against infection

(Akira et al., 2006). Even so, when a long-term association exists between TLRs and their

respective foreign agonists, receptor activation often is debilitating, and sometimes fatal, in

the context of systemic inflammation leading to sepsis, or in the setting of chronic

inflammatory disease resulting in tissue damage (Zuany-Amorim et al., 2002).

     In vivo, periodontal disease offers a model of such chronic inflammatory conditions

caused by prolonged exposure to pathogenic bacteria and/or their secreted virulence factors,

which may result in pathological tissue changes (Robson et al., 1999). The periodontal

sulcus is located in a strategic location between the tooth and surrounding gingival tissue and

is composed of junctional epithelium, which interfaces with periodontal soft and mineralized

tissue. The recess of the sulcus favors population by an adherent bacterial biofilm and may

experience chronic challenge by bacterial virulence factors. Conversion of this biofilm to a

Gram-negative, LPS-rich microbial population is associated with the conversion of the

junctional epithelium to pocket epithelium, which is regarded as a marker of disease

initiation (Bosshardt and Lang, 2005). Periodontitis is associated with oxidative stress (Akalin et al., 2007), decreased total antioxidant status (Chapple et al., 2007) and/or increased lipid peroxidation in gingival crevicular fluid and saliva (Tomofuji et al., 2006).

In a number of tissues, LPS can act directly on epithelial cells to increase paracellular permeability (Hanson et al., 2011). LPS is capable of disrupting mucosal architecture and increasing mucosal permeability in the stomach and intestine (Wallace et al., 1987). Also, the breakdown of the basement membrane in chronic periodontal inflammation suggests that LPS could be penetrating into the stroma (Takarada et al., 1974a) and thereby affecting the behavior of underlying fibroblasts. It has previously been reported that LPS signals through gingival fibroblast TLR2 and 4 to induce expression of keratinocyte growth factor expression, a paracrine mediator of epithelial proliferation (Putnins et al., 2002). This suggests that LPS penetration to the underlying stromal may be inducing changes in fibroblast protein expression, which subsequently alters epithelial behavior. In support of this, the responses of gingival fibroblasts to either bacterial components or inflammatory mediators have been reported to largely determine the overall cytokine environment in the gingiva (Takashiba et al., 2003; Dunford, 2006; Kuboniwa et al., 2007). Nevertheless, which tissue initiates the signaling interaction between the two cell types and to what degree this cell-type ligand-receptor crosstalk participates in the onset and or maintenance of chronic inflammation is poorly understood.

Ekuni et al previously used an LPS-induced rat model of periodontitis to study chronic bacterial virulence factor-induced inflammation (Ekuni et al., 2009). In this model, LPS was added daily to the periodontal sulcus. Chronic inflammation in this model manifested over 8 weeks with the development of elongated rete ridges, hyperplasia and

apical migration of junction epithelium and elevated infiltration of polymorphonuclear

leukocytes. Localized inflammation was further associated with more distant effects on

elevated systemic oxidative stress and alveolar bone loss (Ekuni et al., 2009). LPS-induced

inflammation was found to be associated with hyperplasia and elevated MAO-B-mediated

increases in H_2O_2 and TNF-α activity in junctional epithelial (Firth et al., 2011). Loss of

normal junctional epithelial barrier structure resulting in the penetration of bacterial

virulence factor into the underlying stroma (Firth et al., 2011) was mediated by ROS and

TNF-α. Further analysis showed that MAO inhibitors phenylzine and ($-$)-deprenyl

significantly reduced the TNF-α induction and ameliorated disease-associated epithelial

tissue changes and alveolar bone loss (Ekuni et al., 2009). Recently, a study that performed a

global analysis of genes that change with disease has shown that these changes are

associated with upregulation of AR expression and depression of EGFR pathway signaling

(Firth et al., 2011). Since this work suggested inflammation-induced changes to epithelial

architecture could be reduced by MAO inhibitor phenylzine, an objective of my project was

to study the effect of MAO inhibitors on an *in vitro* model of epithelial barrier chronically

challenged by LPS.

1.1.3 Chronic barrier disease in the junctional epithelium

The junctional epithelium (JE) is the epithelial component of the dento-gingival

complex that is in contact with the tooth surface. The innermost cells of the JE form and

maintain a tight seal against the mineralized tooth surface, the so-called epithelial attachment

(Schroeder and Listgarten, 1997). The JE is regarded as the most interesting structure of the

gingiva. The JEs interposition between the underlying soft and mineralized connective

tissues of the periodontium (*i.e.*, gingival connective tissue, periodontal ligament, alveolar

bone, and root cementum) points to its important roles in tissue homeostasis and defense against microorganisms and their products (Schroeder and Listgarten, 1997).

In contrast to other appendages, such as scales of reptiles, hair, feathers, fingernails, claws, antlers and hoofs, teeth are transmucosal organs. As such, they are permanently exposed to a contaminated environment, since the permanently wet, warm, and nutrient-rich oral cavity forms a habitat in which microorganisms thrive. These microorganisms form complex ecological systems that adhere to a glycoprotein layer on solid and nonshedding surfaces and are called biofilms. Since a biofilm quickly forms on the exposed tooth surface, the tissues in the vicinity of this biofilm are constantly challenged. Defense mechanisms do not preclude the development of extensive inflammatory lesions in the gingiva, and, occasionally, the inflammatory lesion may progress to the loss of bone and the connective tissue attachment to the tooth. Figure 1 presents a set of histological images showing healthy and diseased epithelial tissues of rat maxillary molars taken from a study that employed an *in vivo* LPS-induced periodontal disease model (Ekuni et al., 2009). In this disease model, the direct application of a daily treatment of *Escherichia coli* LPS, to the area of potential space between the tooth enamel and the surrounding gingival tissue (the gingival sulcus) was performed and effectively modeled normal disease pathobiology. Progression of chronic inflammation over 8 weeks could be confirmed by histological changes to the JE that is consistent with the disease state. In these histological studies of JE, the cemento-enamel junction (Figure 2, black arrowhead) is a commonly used reference point to measure morphological indicators of disease onset. The JE is of interest to the study of epithelial barrier since it located at a strategically important interface between the gingival sulcus, populated with bacteria, and the periodontal soft and mineralized connective tissues that

require protection from becoming exposed to bacteria and their products. In the LPS-induced periodontal disease model, the LPS treatment groups exhibited detachment of tissue and apical migration of JE characteristic of the disease (Figure 1D). LPS-induced tissue alterations lead to increased pocket depth below the cemento-enamel junction, which is normally associated with disease and this pocket depth can be probed by clinicians to test for the presence of periodontitis. The conversion of the JE to pocket epithelium is regarded as a hallmark in the progression of gingivitis to periodontitis. Furthermore, the lack of a tight physical seal by the JE may also allow bacteria and their products to penetrate the JE, thereby directly challenging the epithelial cells and attenuating their defense mechanisms. Bacteria such as *Porphyromonas gingivalis* have developed sophisticated strategies aimed at perturbing the structural and functional integrity of the JE, a mechanism that may significantly contribute to the initiation of pocket formation and attachment loss. Currently, data documenting triggering pathogenic factors and the subsequent cascade of cell and extracellular events leading to pocket formation are limited.
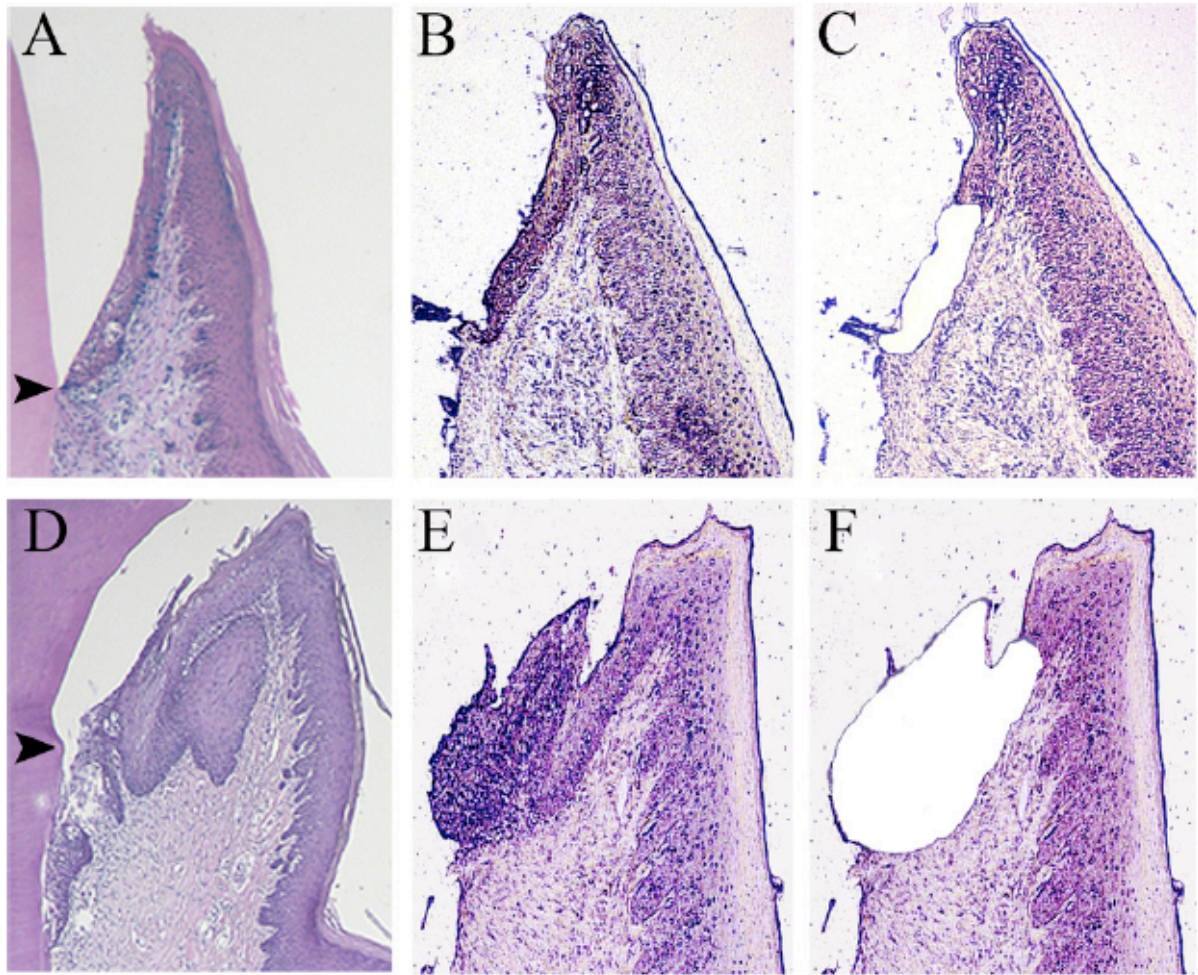
Figure 1. *In vivo* **rat periodontal disease model**

These histological images show the enamel space of mineralized tissue with the surrounding soft periodontal tissue. In these representative tissue samples, the black arrowhead indicates the epithelial cell apical boundary called the cemento-enamel junction that is normally associated with health **(A)** or disease **(D)**. The cemento-enamel junction is a commonly used reference point to measure morphological indicators of disease onset. In disease, detachment of tissue **(D, below arrowhead)** and proliferation of cells in a downward direction below the cemento enamel junction is observed **(D)**. Cryopreserved histiological tissue sections were prepared for precise laser-capture microdissection, which permitted tissue extraction for microarray analysis specific to healthy **(B, C)** and diseased **(E, F)** junctional epithelium. Reproduced with permission from Ekuni et al., 2009.

1.2 Epithelial Barrier Organization and Function

Normal barrier function requires an intact epithelial cell layer and sealing of the paracellular pathway (Turner, 2009), which is the route of transepithelial transport that involves passive movement through the space between adjacent cells. Consequently, epithelial cell damage induced by irritants or cytotoxic agents result in loss of barrier function. The primary responsibility for epithelial barrier function resides with the epithelial cell plasma membrane, which is impermeable to most hydrophilic solutes in the absence of specific transporters. In the presence of an intact epithelial cell layer, the paracellular pathway between cells must be sealed to create a barrier against the free diffusion of water and solutes. This function is mediated by the AJC (Figure 2). The most apical AJC component, the TJ, visualized by freeze-fracture electron microscopy, appears as a continuous network of intramembranous strands or fibrils obliterating the intramembranous space (Staehelin, 1973). The AJs are also components of the AJC and are located subjacent to TJs in polarized epithelial cells. AJs are distinguished ultrastructuraly as a prominent electron-dense plaque along the plasma membrane (Miyaguchi, 2000). Both TJs and AJs comprise clusters of transmembrane and cytosolic proteins (Tsukita et al., 2001; Blaschuk and Rowlands, 2002; González-Mariscale et al., 2003). Lastly, both TJs and AJs are supported by a perijunctional ring of actin and myosin that can mediate barrier function (Perez-Moreno et al., 2003) (Figure 2).

AJs require the activity of lineage-specific Ca^{2+}-dependent adhesion proteins, termed cadherins. Cadherins are a family of transmembrane proteins that establish homotypic interactions with molecules on adjacent cells. Epithelial cadherin is referred to as E-cadherin. Both E-cadherin and members of the nectin family represent the major transmembrane

components of epithelial AJs (Blaschuk and Rowlands, 2002). The N-terminal ectodomain

of E-cadherin contains homophilic interaction specificity and the cytoplasmic tail interacts

directly with two homologous proteins called catenin δ1 and β-catenin. Furthermore, β-

catenin interacts with actin-binding proteins such as α-catenin-1, vinculin and α-actinin,

which link E-cadherin to underlying actin filaments and regulates local actin assembly and

development of the apical perijunctional actomyosin ring (Figure 2) (Blaschuk and

Rowlands, 2002; Goto et al., 2000; Jaggi et al., 2005; Thiery et al., 2003; Wheelock and

Johnson, 2003). It is generally believed that the interaction with F-actin assembled into an

apical circumferential actin ring in polarized epithelial cells mediates the maintenance and

remodeling of the AJC (Perez-Moreno et al., 2003). AJs along with desmosomes provide the

adhesive bonds that maintain cellular proximity and also are the site of intercellular

communication. Plasma membrane localization of E-cadherin is critical for the maintenance

of epithelial cell-cell junctions and epithelium integrity (Bush et al., 2000; Goto et al., 2000;

Zabner et al., 2003). E-cadherin intracellular trafficking between plasma membrane and

cytoplasm is required for the maintenance of epithelial cell-cell junctions and functional

integrity of the paracellular barrier in the epithelium (Bush et al., 2000; Jaggi et al., 2005;

Goto et al., 2000). Loss of AJs result in a disruption of cell-cell and cell-matrix contacts,

premature apoptosis and ineffective epithelial cell polarization and differentiation

(Hermiston and Gordon, 1995). Moreover, a reduction in the adhesive properties of E-

cadherin is related to the loss of differentiation and the subsequent acquisition of a higher

motility and invasiveness of epithelial cells (Goto et al., 2000; Zabner et al., 2003; Otto et

al., 1993). Dislocation of E-cadherin in the epithelium induces epithelial shedding and

increases permeability, which leads to conditions such as chronic lung airway diseases (Goto

et al., 2000; Zabner et al., 2003). Lastly, the AJs play a pivotal role in regulating the activity

of the entire junctional complex because their establishment subsequently leads to the

formation of other cell-cell junctions (Bush et al., 2000; Chen and Gumbiner, 2006; Huntley

et al., 2002). Specifically, assembly of AJs is a prerequisite for the assembly of TJs, which

form the most exclusive aspect of the paracellular seal and function to mediate solute flux

across the paracellular space.

TJs are multi-protein complexes composed of transmembrane proteins, regulatory

molecules that include kinases and peripheral membrane proteins, which function as

scaffolds to organize the tight junction complex (Figure 2). The transmembrane proteins

physically interact with opposing partners on membranes of adjacent cells providing a

mechanical link between two plasma membranes and establishing an effective paracellular

barrier to diffusion of fluid and solutes. The transmembrane proteins of epithelial TJs

include occludin, members of the claudin family and junctional adhesion molecule (JAM)-A

(González-Mariscal et al., 2003). The most important of the transmembrane proteins are

members of the claudin family, which play significant roles in formation, integrity and

function of TJs, the epithelial permeability barrier and epithelial polarization (Turksen and

Troy, 2011). To date, 27 distinct claudins have been cloned in mammals (Angelow and Yu,

2007; Gupta and Ryan, 2010). Moreover, Claudins are expressed in a tissue-specific manner,

and mutation or deletion of individual claudin family members can have substantial effects

on organ function. The role of occludin, a transmembrane tight junction protein that interacts

directly with claudins and actin, is less understood. Occludin was the first identified TJ-

associated integral membrane protein but evidence suggests that occluding is not essential

and indeed may be dispensable as evidenced by findings showing that intestinal barrier

function remains intact in occludin-deficient mice (Saitou et al., 2000) and differentiation into polarized epithelial cells bearing tight junctions continues in occluding deficient embryonic stem cells (Saitou et al., 1998). The cytoplasmic TJ plaque has an astonishing complexity with over thirty different proteins reportedly associated with this structure (Gonzalez-Mariscale et al., 2003). The most widely studied components of the TJ cytosolic plaque are members of the zonula occludens (ZO) family, which mediate interactions between different types of transmembrane TJ proteins and/or link these transmembrane components to the actin cytoskeleton (Turner, 2009). Indeed, peripheral membrane proteins, such as ZO-1 and ZO-2, are crucial to tight junction assembly and maintenance, partly owing to the fact that that these proteins include multiple domains for interacting with other proteins, including claudins, occludin and actin.
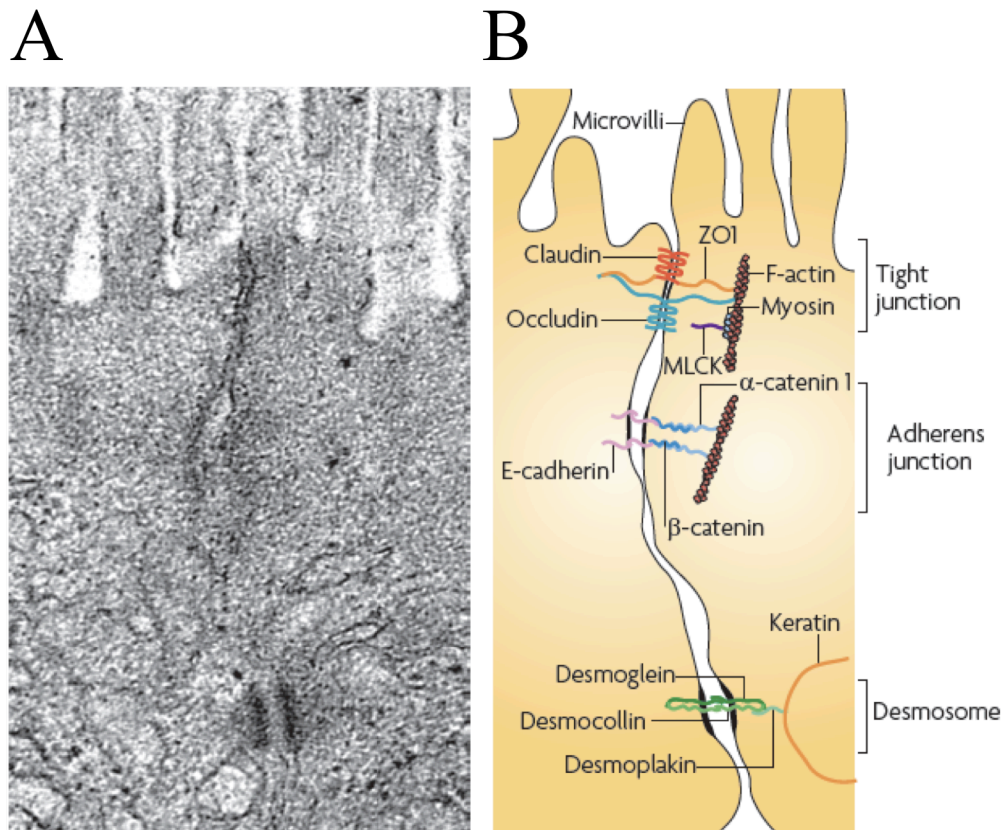
Figure 2. Epithelial barrier anatomy

An electron micrograph **(A)** and corresponding line drawing **(B)** of the apical junctional complex and desmosomes of two adjacent intestinal epithelial cells. Below the base of the microvilli, the plasma membrane of adjacent cells appear to fuse at the tight junction, where claudins, ZO-1, occluding and F-actin interact. E-cadherin, α-catenin 1, β-catenin, catenin δ1 (not shown in line drawing) and F-actin interact to form the adherens junction subjacent to the tight junction. Myosin light chain kinase (MLCK) is associated with the perijunctional actomyosin ring. Located below the apical junctional complex are the desmosomes, which are formed by interactions between desmoglein, desmocollin, desmoplakin and keratin. Reproduced with permission from Turner, 2009.

1.2.4 Barrier properties of the tight junction

Epithelial TJs are responsible for regulating the "fence and gate" function of polarized epithelial cells. Specifically, TJs provide a physical barrier at the apical end of the epithelial cell where they serve a 'gate function', which limits the free interchange of most solutes along the paracellular pathway. This paracellular pathway is generally more permeable than the transcellular pathway, which is a route of transepithelial transport that involves active or passive movement across cell membranes, usually as a result of the action of specific transport channels. Thus, the TJ is considered the rate-limiting step in transepithelial transport and the principle determinant of epithelial barrier permeability. In addition, TJs serve a 'fence function' by separating the apical end of polarized epithelial cells from the basolateral end, hence functioning as a diffusion barrier to plasma membrane lipids and proteins, and defining apical and basolateral membrane domains of polarized epithelial cells (Madara, 1988). TJs form early in development (Eckert and Fleming, 2008) and are instrumental in formation of permeability barriers that are tissue- and differentiation-specific, molecule-selective and dynamic in nature (Madara, 1990).

Via homotypic and heterotypic interactions, claudins selectively regulate the charge and size of molecules that flux through the paracellular regions of epithelial tissues (Gupta and Ryan, 2010; Angelow and Yu, 2007; Turksen and Troy, 2011). Thus, specific barrier properties of the TJ can be defined in terms of size and charge selectivity. Two routes enable transport across the TJ, and recent studies suggest the contributions of these types of paracellular transport may be regulated independently (Fihn et al., 2000; Van Itallie et al., 2008; Watson et al., 2005). The first route, which is referred to as the leak pathway, enables paracellular transport of large solutes, including limited flux of proteins and bacterial

lipopolysaccharides (Van Itallie et al., 2008; Watson et al., 2005). At present, the size at which particles are prevented from entering this pathway has not been defined. Even so, it has been established that materials as large as whole bacteria are prevented from passing through the leak pathway. This pathway does not exhibit charge selectivity, which is expected from a route that allows such large solutes to cross. Furthermore, flux across the leak pathway is significantly increased by cytokines, including interferon-γ (IFN-γ) *in vitro* and tumour necrosis factor (TNF) *in vitro* and *in vivo* (Watson et al., 2005; Wang et al., 2005; Clayburgh et al., 2006).

Small pores that are formed by TJ-associated claudin proteins characterize the second pathway. These pores are primary determinates of charge selectivity along the paracellular pathway (Amasheh et al., 2002; Colegio et al., 2003; Simon et al., 1999) and generally have a radius that excludes molecules larger than 4 Å (Van Itallie et al., 2008; Watson et al., 2005). Expression of specific claudins can vary between organs and within different regions of a single organ. Claudin expression also seems to be plastic in the context of tissue homeostasis as they respond dynamically to the needs of physiological changes in particular tissues. For example, claudin expression can be modified by external stimuli, such as cytokines (Turner, 2009). In addition, a recent study has demonstrated that LPS-induced chronic epithelial inflammation in a rat periodontitis model is associated with significant loss of claudin-1 as detected by both expression array and immunostaining (Ekuni et al., 2009) This finding was confirmed by an *in vitro* PLE cell culture experiment in which LPS-induced loss of epithelial barrier was found to correlate with loss of claudin-1 protein levels as assayed by flow cytometry (Fujita et al., 2011). Thus, TJs exhibit both size and charge

selectivity, and these properties may be mediated individually or jointly by physiological or pathophysiological stimuli.

1.2.5 Techniques to measure permselectivity of epithelial tight junctions

Depending on local transport requirements, TJs form paracellular barriers that differ in electrical conductance, ionic charge preference and level of permeability for uncharged solutes. These properties of the paracellular barrier are collectively referred to as permselectivity. An example of this is demonstrated in the renal tubule and intestine where electrical resistance is found to progressively increase as the transport of large volumes of isosmotic fluids shifts to more selective transport based on high electro-osmotic gradients (Powell, 1981). The barrier functions as if perforated by pores that exhibit both size and charge selectivity. At present, the understanding of the molecular nature of these pores is limited despite the discovery of many TJ proteins.

Paracellular permeability is commonly measured by analysis of the flux of variously sized noncharged hydrophilic tracers, such as radioactively labeled urea, inulin, mannitol and fluorescent dextrans (Ghandehari et al., 1997; Sanders et al., 1995). Studies that have employed this technique have been able to show a disproportionately larger permeability for compounds smaller than mannitol. This was demonstrated most elegantly by a study that profiled paracellular flux across monolayers of T84 and Caco-2 epithelial cells with a continuous series of noncharged polyethylene glycol oligomers (Watson et al., 2001). This study showed that paracellular permeability is biphasic, consisting of a high capacity, size-restrictive pathway and a low capacity, size-independent pathway. The high capacity pathway behaves as a system of relatively small sized pores with radii of ~4 Å. The physical

basis of the low capacity pathway is less understood and may represent fixed tricellular junctions, transient breaks or a system of large pores.

In addition to solute flux, paracellular barrier function is commonly characterized by transepithelial electrical resistance (TER). Studies have established that electrical tightness of cultured epithelial cells as measured by TER can be increased or decreased by altering the expression profiles of specific TJ proteins (Gonzalez-Mariscale et al., 2003; Schneeberger and Lynch, 2004). Significant interest has been focused on integral membrane components of the TJs, particularly claudins, occluding and JAMs as these three proteins have been shown to comprise the TJ strands that are both easily visualized by freeze fracture electron microscopy and that are the sites of the adhesive cell-cell barriers. Furthermore, studies have established that claudins can alter the TER through regulation of ionic charge selectivity (Van Itallie et al., 2001; Amasheh et al., 2002).

Although paracellular flux of noncharged solutes and electrical resistance are both measures of permeability through the paracellular pathway, their relationship sometimes is paradoxical. For instance, it has been consistently demonstrated that TER decreases at the same time that solute flux increases following treatment of T84 epithelial cell monolayers with interferon-γ (Watson et al., 2005). In contrast, there are examples where changing claudin levels alter TER levels without concomitant changes in paracellular flux of noncharged solutes (Van Itallie et al., 2001; Amasheh et al., 2002).

1.3 Regulation of Epithelial Barrier

The ability of cytokines, such as TNF and IFNγ, to regulate the function of the tight junction barrier has been previously established (Madara and Stafford, 1989). Since this discovery, increased TJ protein transcription, vesicular removal of proteins from the TJ, TJ

protein degradation, kinase activation and cytoskeletal modulation have all been proposed to mediate cytokine-induced loss of TJ barrier function. Although extensive apoptosis of epithelial cells may also induce barrier loss, the relevance of single-cell apoptosis to barrier dysfunction remains controversial owing to differing results in diverse experimental systems.

1.3.1 Tight junction regulation through the cytoskeleton

TNF and IFNγ alter TJ barrier function in intestinal (Madara and Stafford, 1989; Taylor et al., 1998), renal (Mullin et al., 1992), pulmonary (Mazzon and Cuzzocrea, 2007) and salivary gland (Baker et al., 2008) epithelia as well as between endothelial cells (Tiruppathi et al., 2001). The effects of TNF on barrier integrity have been best studied in the gut, where this cytokine has a central role in many diseases associated with intestinal epithelial barrier dysfunction, including IBD (Baert et al., 1999), intestinal ischaemia (Taylor et al., 1998; Tamion et al., 1997) and graft-versus host disease (Brown et al., 1999). For example, although the effect of therapy with TNF-specific antibodies may be largely due to the overall reduction in inflammation, it is notable that this treatment corrects barrier dysfunction in patients with Crohn's disease (Suenaert et al., 2002).

Myosin light chain kinase (MLCK) has been shown to play a central role in TNF-induced epithelial and endothelial barrier dysregulation, both *in vitro* and *in vivo* (Wang et al., 2005; Clayburgh et al., 2005; Zolotarevsky et al., 2002; Ma et al., 2005; McKenzie and Ridley, 2007). TNF-induced MLCK activation increases paracellular flux through the leak pathway (Wang et al., 2005). MLCK activation occurs as a result of increased enzymatic activity and upregulated MLCK transcription and translation, both *in vitro* and *in vivo* (Wang et al., 2005; Ma et al., 2005; Graham et al., 2006). Similarly, MLCK expression and activity are increased in intestinal epithelial cells of patients with IBD (Blair et al., 2006).

The degree to which MLCK expression and activity are increased correlates with local disease activity in these patients, suggesting that these processes are regulated by local cytokine signaling (Blair et al., 2006). MLCK also participates as an intermediate in barrier dysfunction induced by the TNF family member LIGHT (also known as TNFSF14) (Clayburgh et al., 2006; Schwarz et al. 2007), interleukin-1β (IL-1β) (Al-Sadi et al., 2008), enteropathogenic *Escherichia coli* infection (Zolotarevsky et al., 2002), *Helicobacter pylori* infection (Wroblewski et al., 2009), giardiasis (Scott et al., 2002), LPS (Moriez et al., 2005; Eutamene et al., 2005) and the ethanol metabolite acetaldehyde (Ferrier et al., 2006). Thus, MLCK activation can be viewed as a common final pathway of acute tight junction regulation in response to a broad range of infectious and immune stimuli.

Although it is clear that MLCK phosphorylates myosin II regulatory light chain (MLC) within the perijunctional actomyosin ring to activate myosin ATPase activity, the subsequent molecular events that cause increased permeability are poorly understood. Recent work suggests that ZO-1, which interacts directly with actin, occludin, claudins and other proteins, may be an essential effector of perijunctional actomyosin ring-mediated TJ regulation (Shen et al., 2006; Van Itallie et al., 2009; Scharl et al., 2009). Endocytic removal of the transmembrane protein occludin from the TJ is also common in actomyosin-dependent, cytokine-mediated TJ regulation (Clayburgh et al., 2005; Utech et al., 2005). *In vitro* studies of tight junction regulation induced by LIGHT suggest that occludin endocytosis occurs via caveolae and that inhibition of this process can prevent loss of barrier integrity despite MLCK activation (Schwarz et al., 2007). Caveolae are specialized flask-shaped invaginations of the plasma membrane that contain the protein caveolin-1 and cholesterol. These proteins mediate uptake of some extracellular materials and are involved

in cell signaling. Caveolar endocytosis of occludin has also been associated with loss of epithelial and endothelial TJ barrier function in response to actin disruption (Shen and Turner, 2005) and chemokine signaling (Stamatovic et al., 2009), respectively, *in vitro*. Nevertheless, other mechanisms of occludin removal may also be involved as *in vitro* studies have shown that IFNγ-induced occludin internalization is mediated by myosin ATPase-dependent macropinocytosis (Utech et al., 2005; Bruewer et al., 2005), and occludin cleavage may modify the barrier to enhance transepithelial migration of inflammatory cells in the lung (Chun and Prince, 2009). Further work is necessary to define the contributions of occludin and endocytosis to *in vivo* TJ regulation. This is particularly important since intestinal barrier function is intact in occludin-deficient mice, despite numerous *in vitro* studies demonstrating a role for occludin in TJ function (Saitou et al., 2000). Future analyses of the response of occludin-deficient mice to stress, with particular reference to intestinal TJ function, as well as studies of potential compensatory changes in other, perhaps undiscovered, proteins that enable these mice to avoid intestinal disease will be of interest.

Although MLCK activation is important, it is not the only means of cytoskeletal TJ regulation. Other mediators include myosin ATPase (Van Itallie et al., 2009), the activity of which is regulated by MLC phosphorylation (Amano et al., 1996); members of the Rho kinase family (McKenzie and Ridley, 2007; Van Itallie et al., 2009; Utech et al., 2005; Jou et al., 1998), which can both phosphorylate MLC directly (Amano et al., 1996) and inhibit MLC phosphatase (Kimura et al., 1996); and AMP-activated protein kinase (Scharl et al., 2009), which is activated during stress and can also directly phosphorylate MLC (Lee et al., 2007). Moreover, Rho kinases and AMP-activated protein kinase each have diverse effects

that are separate from myosin function, and it is likely that at least some of these contribute to TJ regulation.

1.3.2 Tight junction permeability and claudin expression

Regulation of perijunctional actomyosin, discussed above, provides a means of rapidly and reversibly regulating the paracellular leak pathway. In contrast, synthesis and trafficking of claudin proteins provides a means of regulating TJ pores over longer periods. The perijunctional actomyosin ring does not seem to be directly involved in this mechanism of barrier regulation, which is consistent with the fact that claudins do not interact with actin directly. Expression of specific claudin proteins changes during development, differentiation and disease and in response to stressors such as cytokines in intestinal (Heller et al., 2005), renal (Balkovetz, 2009), alveolar (Wray et al., 2009) and gingival epithelial cells (Fujita et al., 2010). In addition to affecting barrier function, altered patterns of claudin expression may have other consequences. For example, claudin proteins have been associated with control of cell and organ growth. It may be, therefore, that some changes in claudin protein expression enhance cell proliferation and regeneration, as might be necessary to compensate for cell loss in colitis. This may explain the increased claudin-1 expression by intestinal epithelial cells of patients with IBD (Weber et al., 2008). Nonetheless, claudin-1 has also been shown to enhance neoplastic transformation, tumor growth and metastasis in experimental models (Dhawan et al., 2005). Thus, changes in claudin expression likely have negative consequences.

One common change in claudin expression associated with disease that directly affects barrier function is the increased claudin-2 expression by intestinal epithelial cells in animal models of colitis and patients with IBD (Heller et al., 2005). Consistent with this, IL-

13 and IL-17, which are increased in the mucosa of patients with colitis (Heller et al., 2005; Fujino et al., 2003), reduce barrier function and increase claudin-2 expression in cultured intestinal epithelium monolayers (Heller et al., 2005; Kinugasa et al., 2000). *In vitro* studies have shown that claudin-2 expression increases the number of pores that allow paracellular flux of cations, predominantly Na+, and small molecules with radii less than 4 Å (Van Itallie et al., 2008; Yu et al., 2009), and recent analyses have provided new insight into the structure of these pores (Angelow and Yu, 2009). However, it is not clear whether increased claudin-2 expression contributes to disease progression or, as proposed above for claudin-1, is an adaptive response that promotes homeostasis.

1.3.3 Tight junctions and mucosal homeostasis

One interpretation of the available data is that the tight junction barrier integrates the relationship between luminal microbial material and mucosal immune function. In most individuals, this is a homeostatic relationship in which regulated increases in TJ permeability or transient epithelial cell damage trigger the release of pro-inflammatory cytokines, such as TNF and IFNγ, as well as immunoregulatory responses. These immunoregulatory responses may include dendritic cell conditioning by epithelial cell-derived transforming growth factor-β (TGFβ) and retinoic acid, both of which can enhance regulatory T cell differentiation (Mucida et al., 2007; Coombes et al., 2007). This precarious balance between pro-inflammatory and immunoregulatory responses can fail if there are exaggerated responses to pro-inflammatory cytokines. As a result, mucosal immune cell activation may proceed unregulated and the release of cytokines, including TNF and IL-13, may enhance barrier loss that, in turn, promotes further leakage of luminal material and perpetuates the pro-inflammatory cycle. This is clearly exemplified in IBD. Under normal circumstances,

the immense load of bacteria and associated antigens present in the lumen of the lower small intestine and colon is effectively contained by the intestinal epithelium. According to the 'leaky gut' theory of intestinal disease, an initial injury- or inflammatory-mediated insult causes disruption of TJs and increased paracellular permeability allowing entry of luminal antigens (Hollander, 1999; Clayburgh et al., 2004). The resulting immune activation triggers repeat cycles of inflammatory response and barrier disruption that establish and propagate inflammatory bowel disease.

1.3.4 Regulation of tight junctions by lipopolysaccharide

Enterohemorrhagic and enteropathogenic *Escherichia coli* can directly modify epithelial cell surface architecture and apical junctions leading to a loss of epithelial cell polarity and reduced barrier function (Guttman and Finlay, 2009; Lapointe et al., 2009) via Cdc42 (Alto et al., 2006; Dean and Kenny, 2004) and RhoA signal pathways (Arbeloa et al., 2008; Simovitch et al., 2010). Also, bacterial induction of host inflammatory mediators such as TNF-α and AR are effectors of barrier loss by causing endocytosis of TJ components such as ZO-1 (Schwarz et al, 2007; Shen et al., 2008) in a myosin light chain kinase (MLCK)-dependent manner (Al-Sadi et al., 2008; Ma et al., 2005). Recent studies that employed a rat model of LPS-induced periodontitis showed by gene expression array that the diffusible paracrine mediators TNF-α (Ekuni et al., 2009) and its downstream effector AR (Firth et al., 2011) were significantly induced at epithelial disease sites. This suggests the possibility that stromally secreted AR is diffusibly affecting epithelial behavior in chronic inflammation.

1.4 Inflammatory Mediator Signaling Pathway and Barrier Disruption

The proteolytic processing of growth factors and cytokines is a key regulatory mechanism controlling receptor-mediated signaling. In the case of membrane-anchored

growth factors, the proteolytic processing has been proposed to regulate the availability of active soluble forms, switch receptor signaling from autocrine or juxtacrine modes to paracrine or endocrine mechanisms, and/or influence the nature (e.g. duration) of the signaling event. Growth factors and cytokines that are released from membrane-anchored forms include members of the EGF superfamily, colony-stimulating factor-1, TNF-α, and the Kit ligand. The EGF superfamily includes two structurally related subfamilies: the EGF-like growth factors and the neuregulins (Sunnarborg et al., 2002). The EGF subfamily includes TGF-α, AR, HB-EGF, betacellulin, epiregulin and epigen (Pastore et al., 2008). Soluble EGF family growth factors are all derived by proteolytic cleavage of the ectodomains of integral membrane precursors.

A recent study has extensively focused on the regulation of functional epithelial barrier by LPS. This has been studied using *in vitro* cell culture approaches and by global gene array analysis using an *in vivo* rat periodontal disease model (Ekuni et al., 2009). Using Genemapp functional analysis, the laboratory recently identified that AR, an EGF family member normally sequestered at cell-cell contacts in stable epithelial barriers, was strongly induced and the corresponding EGFR signaling components were altered in disease (Firth et al., 2011).

1.4.1 Amphiregulin structure and function

The glycoprotein AR was first discovered in the concentrated conditioned medium of MCF-7 breast cancer cells treated with phorbol 12-myristate-13-acetate (PMA) (Shoyab et al., 1988). This protein was named 'amphi' due to the fact that it was stimulatory to various cells including several human fibroblast cell lines, while being inhibitory to other cells such

26

as neuroblastoma and adenocarcinoma cell lines (Shoyab et al., 1988). Notably, the inhibitory properties of AR have yet to be validated.

AR is initially synthesized as a 252 amino acid transmembrane precursor that is typically localized to the basolateral membrane domain in polarized epithelial cells such as HCA-7 and Caco-2 cells (Damstrup et al., 1999). The AR transmembrane precursor undergoes ectodomain cleavage and is released as a secreted protein (Plowman et al., 1990). As a result of proteolytic processing and posttranslational modifications, there are several forms of AR protein that vary in size both on the cell surface and for soluble forms (Johnson et al., 1993; Brown et al., 1998). Two AR soluble forms that migrate between 20 and 25 kDa on SDS-PAGE have been characterized (Shoyab et al., 1989; Plowman et al., 1990). In addition, soluble AR forms of 9.5–10, 35, and 55–60 kDa have been identified in other cell types (Culouscou et al., 1992; Johnson et al., 1993; Thorne and Plowman, 1994; Piepkorn et al., 1995; Martinez-Lacaci et al., 1996). Some of these isoforms have been found to possess biological activity but it is not known whether all forms are biologically active. Moreover, the variety of soluble AR forms implies intricacies in AR processing that have not yet been elucidated. AR can undergo substantial glycosylation but this does not appear to have an effect on its bioactivity (Plowman et al., 1990; Shoyab et al., 1989; Martinez-Lacaci et al., 1996). Thus, glycosylation may be more important for other properties of the protein such as stability, solubility, resistance to proteolysis or localization (Rademacher et al., 1988).

AR was originally demonstrated to be a ligand for EGFR because it could partially compete with ^{125}I-EGF for binding to the EGFR in A431 cells. It has now been confirmed that AR acts exclusively through the EGFR (Salomon et al., 1995; Johnson et al., 1993). AR can also be regulated by the EGFR itself and activation of EGFR has been shown to induce

AR expression in several cell types (Kansra et al., 2005; Normanno et al., 1994). For example, stimulation of EGFR in prostate stromal cells with mitogenic levels of the EGFR ligands EGF and HB-EGF increased AR expression more than 15-fold (Sorensen et al., 2000). The specific pathway leading from EGFR activation to AR transcription has not yet been elucidated. Although AR can serve as a substitute for EGFR ligands such as EGF, it acts as a much weaker growth factor compared to the other EGF family growth factors (Shoyab et al., 1989) and its only target within the ErbB family is EGFR itself (Riese and Stern, 1998).

1.4.2 AR ectodomain shedding and transactivation of the EGFR

Provided the pleiotropic effects of EGFR signaling, the strength and duration of EGFR signaling must be tightly regulated through availability of EGFR ligands. All EGFR ligands are synthesized in a proform as type I transmembrane proteins. Soluble ligands are produced via extracellular cleavage of the integral membrane precursor proteins. This cleavage event is referred to as ectodomain shedding and plays and important role in mediating ligand availability and receptor activation (Sanderson et al., 2006). A ligand may be presented to the EGFR in several ways, which include autocrine, paracrine and juxtacrine modes of signaling. Both autocrine and paracrine modes of signaling require a soluble ligand and thus require release of the membrane-anchored ligand by a protease. AR has been demonstrated to act as an autocrine factor in normal cells such as human mammary epithelial, human urothelial and human lung bronchial epithelial cells. In addition, AR has been shown to be an autocrine factor in cancer cells such as hepatocellular carcinoma, colon cancer, gastric cancer, breast cancer and pancreatic cancer cells (Funatomi et al., 1997;

Culouscou et al., 1992; Damstrup et al., 1999; Castillo et al., 2006; Akagi et al., 1995; Willmarth and Ethier, 2008).

In vitro and *in vivo* evidence points to tumor necrosis factor alpha-converting enzyme (TACE /ADAM17) as the critical convertase for AR. Mice lacking active TACE and AR knockout mice exhibit the same mammary gland branching defects (Sternlicht, 2006). TACE deficient murine fibroblasts were impaired in shedding of AR, but shedding could be rescued by transfection of wild-type TACE (Sunnarborg et al., 2002). TACE-dependent cleavage of AR has been shown to be important for EGFR phosphorylation (Schafer et al., 2004b). ADAM10 may also have small sheddase activity (Le Gall et al., 2009) so knockdowns are needed for specific identification. The mechanism of TACE activation remains unclear although ROS is implicated by several lines of evidence (Myers et al., 2009). For example exogenous H_2O_2 can stimulate shedding of various EGF members including AR (Lemjabbar et al., 2003). ROS may cause direct modifications to TACE perhaps by oxidizing a cysteine thiol group thereby relieving inhibition of its metalloprotease activity (Zhang et al., 2001).

G-protein-coupled receptor (GPCR) activation signals through EGFR (Blobel, 2005; Ohtsu et al., 2006). This communication between GPCR and EGFR signaling systems involves cell surface proteolysis of EGFR-like ligands that directly activate the EGFR. These ligands include HB-EGF, TGF-α and AR. Multiple GPCRs converge on EGFRs (Schafer et al., 2004a). Distinct members of the ADAM family regulate GPCR-induced proliferation (Schafer et al., 2004b). For example, GPCR-induced ADAM17 specific cleavage of pro-AR has been established (Gschwind et al., 2003). Studies of squamous cell carcinoma cells stimulated with the GPCR agonists lysophosphatidic acid (LPA) or carbachol specifically resulted in metalloprotease cleavage and release of AR. Moreover, AR gene silencing by

siRNA or inhibition of AR biological activity by neutralizing antibodies and heparin prevents GPCR-induced EGFR tyrosine phosphorylation, downstream mitogenic signaling events, cell proliferation, migration and activation of the survival mediator Akt/PKB (Gschwind et al., 2003). Therefore, despite some functional redundancy among EGF family ligands, a distinct and essential role for AR in GPCR-triggered cellular responses is apparent (Gschwind et al., 2003). In addition, certain GPCR agonists such as LPA can act to alter TER in pulmonary epithelial cell culture (He et al., 2009). Moreover, TACE knockdown in cell culture inhibits LPA-induced growth factor transactivation (Schafer et al., 2004b). Several signaling components have been implicated in GPCR-initiated TACE activation (Myers et al., 2009) including ROS. ROS can act as second messengers in GPCR-mediated TACE activation (Zhang et al., 2001; Forman et al., 2002). ATP stimulates mitochondrially-produced ROS to initiate P2Y family GPCR signaling resulting in EGFR phosphorylation. This pathway is inhibited both by TACE inhibitor TAPI and ROS scavenger *N*-acetylcysteine (NAC) (Myers et al., 2009). P2Y family GPCR receptors have also been linked to ROS production in eosinophils and prostate tumor cells (Ferrari et al., 2000; Sauer et al., 2001).

1.4.2.1 Oxidant-induced MMP-dependent transactivation of EGFR signaling

IBD is a chronic intestinal inflammatory disorder and its etiology remains unknown. Current models of disease pathogenesis identify as the two principal determinants of IBD pathogenesis: increased permeability of the epithelial barrier of the intestinal mucosa, which results in penetration of luminal bacterial products into the mucosa; and an abnormal immune response to these products (Farhadi et al., 2003; Clayburgh et al., 2004). Regarding intestinal hyperpermeability in IBD, two factors are thought to play critical roles: oxidant-

induced stress and pro-inflammatory cytokines, especially TNF-α and interferon-γ (Bruewer et al., 2003; Podolsky, 2002). The principal permeability pathway in IBD is the paracellular route, which is regulated by TJs between the intestinal epithelial cells that constitute the intestinal barrier (Clayburgh et al., 2004).

Several studies have identified mechanisms of oxidant-induced intestinal hyperpermeability using *in vitro*, animal, and clinical models of IBD (Keshavarzian et al., 1990; Banan et al., 2000a; Banan et al., 2000b). Using *in vitro* models of human intestinal epithelium, key roles have been identified for specific intracellular signaling pathways mediating disruption of TJ permeability by oxidative stress. These pathways involve signaling via the EGFR (Banan et al., 2000a; Banan et al., 2000b), signaling via NF-kB activation (Banan et al., 2004), and signaling via specific protein kinase C (PKC) isoforms, which are either protective or injurious, depending on the PKC isoform (Banan et al., 2001; Banan et al., 2005).

A recent study proposes an epithelial permeability model in which oxidant, H_2O_2, transactivates EGFR signaling by activation of TACE and cleavage of the precursor form of an EGFR ligand (Forsyth et al., 2007). The pathway is referred to as "metalloprotease-dependent transactivation of EGFR signaling" (Prenzel et al., 1999; Fischer et al., 2004). In this model, metalloproteases, especially from the ADAM family of membrane-bound metalloproteases, become activated by a variety of signals and cleave EGFR precursor ligands attached to the cell surface. These solubilized EGFR ligands then bind to the EGFR and initiate EGFR-mediated signaling pathways (Schafer et al., 2004a). Several studies have shown that oxidants such as H_2O_2 are one of several stimuli capable of triggering signaling via ADAM-dependent transactivation of the EGFR (Schafer et al., 2004a). The ADAM

involved in greater than 80% of all cases is the tumor necrosis factor-α convertase (TACE; ADAM-17) (Black et al., 1997; Blobel, 2005). It is known that TACE is the metalloprotease required for TNF-α cleavage and biological activity (Black et al., 1997). TNF-α is also known to stimulate TACE expression in a kind of vicious circle (Black et al., 1997). In the intestine, TACE levels are increased in the inflamed mucosa of patients with IBD, and TACE inhibitors ameliorate colitis in animal models of IBD (Colon et al., 2001; Brynskov et al., 2002). In addition, oxidant stress is known to exist in IBD epithelium, and TACE is required for TNF-α production that is important in the pathogenesis of IBD. Therefore, stimulation of TACE activity by oxidant stress could drive IBD pathogenesis by stimulation of both TNF-α production and through EGFR-mediated increased permeability resulting from TACE cleavage and activation of EGFR ligands. Finally, with oxidant stimulation TACE has been shown to be translocated to cell-cell junction areas and co-localizes with ZO-1 in proximity with the proposed EGFR ligand/EGF receptor. This data supports a model for translocation of TACE with specific pro-ligand substrates as a key regulatory mechanism of TACE specificity (Werb and Yan, 1998).

Downstream EGFR-mediated mitogen-activated protein kinase (MAPK) signaling via ERK1/2 MAPKs has been shown to be necessary for oxidant-induced intestinal hyperpermeability (Forsyth et al., 2007). Thus, another concept that emerges from this study is that ERK1/2 activation seems to be one critical pathway mediating intestinal hyperpermeability in response to oxidants through TACE-EGFR signaling. This data agrees with other studies showing tyrosine kinase and Src inhibitors block H_2O_2-induced permeability in Caco-2 monolayers (Basuroy et al., 2003). Furthermore, this result is in agreement with data from other studies showing that both TGF-α-induced hyperpermeability

in MDCK cells (Chen et al., 2000) and H_2O_2-induced endothelial hyperpermeability (Fischer et al., 2004) can be blocked with the same ERK1/2 inhibitor.

Key downstream targets of ERK appear to be critical in the regulation of paracellular permeability in many cell types. A significant downstream target is MLCK (Clayburgh et al., 2004). ERK1/2 directly phosphorylates MLCK (Nguyen et al., 1999), and MLCK activation of myosin light chain is one key mechanism regulating intestinal permeability and may play a role in IBD (Clayburgh et al., 2004). In addition, ERK1/2 can be immunoprecipitated with the TJ protein occludin in oxidant-treated IECs (Basuroy et al., 2006), suggesting phosphorylation of occludin by ERK1/2 as another mechanism for ERK1/2 regulation of TJ permeability. Finally, ERK1/2 have been shown to regulate TACE activation and phosphorylate TACE directly (Soond et al., 2005).

1.5 MAO General Introduction

MAOs belong to the protein family of flavin-containing amine oxidoreductases called flavoproteins and function to catalyze the inactivation by oxidative deamination of a range of biogenic monoamines (Edmondson et al., 2004). For example, MAOs play a vital role in inactivating catecholamine neurotransmitters that are free within the nerve terminal and not protected by storage vesicles. MAO enzymes use oxygen to remove an amine group from a molecule, resulting in the corresponding aldehyde and either ammonia (in the case of primary amines) or a substituted amine (in the case of secondary amines). H_2O_2 generation is a significant byproduct of this MAO catalyzed reaction (Magyar and Szende, 2004). H_2O_2 is also the major source of cellular ROS. Two isoenzymes of MAO, referred to as MAO-A and MAO-B, are present in most mammalian tissues and are located intracellularly in most cell types bound tightly to the outer mitochondrial membrane, however, the proportions of

MAO-A and MAO-B vary from tissue to tissue (Tipton et al., 2004; Shih et al., 1999). These isoenzymes were originally distinguished by their sensitivities to the acetylenic inhibitors clorgyline and *l*-deprenyl (Selegine), and by their substrate specificities (Johnston, 1968). Typically, MAO-A is inhibited by clorgyline at low concentrations, whereas MAO-B is inhibited by low concentrations of *l*-deprenyl. The differential substrate specificities exhibited by these isoforms include, for example, serotonin, melatonin, norepinephrine, and epinephrine being primarily broken down by MAO-A. Benzylamine and trace amines are broken down by MAO-B. MAO-B also acts on a broad spectrum of phenylethylamines including β-phenylethylamine. Common substrates exist for both types of MAO, such as tyramine and dopamine (Magyar and Szende, 2004). There is also evidence for heterogeneity in the behavior of MAO isoenzymes within the same species. For example, although MAO is known to be an imidazoline-binding enzyme in the brain and peripheral tissues, only ~10% of human liver MAO-B is capable of binding imidazolines, and human platelet MAO-B has been shown to bind imidazolines only weakly (Raddatz et al., 1995). It is not known whether this reflects tissue-specific differences in enzyme processing or results from the effects of an endogenous ligand. MAO in peripheral tissues, such as the intestine, liver, lungs and placenta, seems to protect the body by oxidizing amines from the blood or by preventing their entry into the circulation. Although the roles of MAO-A and MAO-B in terminating the actions of neurotransmitters and dietary amines have been studied extensively, less attention has been paid to the functions of the products of MAO activity. For instance, H_2O_2 formed during this reaction might have important metabolic and signaling functions in the brain (Klann and Thiels, 1999), however, at higher concentrations, H_2O_2 is toxic (Halliwell et al., 1992).

A recent study has extensively focused on the regulation of functional epithelium by the Gram-negative bacterial virulence factor LPS. This has been studied using *in vitro* cell culture approaches and by global gene array analysis using an *in vivo* rat periodontal disease model (Ekuni et al., 2009). Expression microarray analysis of healthy and diseased rat junctional epithelium found that three of the top 10 LPS-induced genes are associated with the generation of ROS signaling mediators. Notably, one of these genes was MAO-B and a weight of clinical evidence suggests that therapeutic inhibition of MAO may ameliorate the chronic inflammatory conditions found in rheumatoid arthritis and Crohn's disease (Lieb, 1983; Kast, 1998).

1.5.1 MAO inhibitors

MAO inhibitors were among the first antidepressants to be identified. The first MAO inhibitory antidepressant to be discovered was iproniazid. This compound was initially developed to treat tuberculosis. Although iproniazid was shown to be an ineffective treatment for tuberculosis, it was observed to have 'psycho energizing' effects in patients and was also found to inhibit MAO. This was followed by the development of other hydrazine derivative MAO inhibitors, such as phenelzine, as antidepressants. Nevertheless, reports of liver toxicity, hypertensive crises, haemorrhage and, in some cases, death resulted in the withdrawal of many MAO inhibitors from the clinic. Liver toxicity, which was associated specifically with hydrazine-derived inhibitors, was avoided by the development of non-hydrazine-derived inhibitors such as pargyline and tranylcypromine. Nevertheless, hypertensive crises continued to be a serious problem. This side effect, referred to as the 'cheese reaction', occurs when tyramine and other sympathomimetic amines, which are found in fermented foods such as cheese (Da Prada et al., 1988), enter the circulation and

potentiate sympathetic cardiovascular activity by releasing noradrenaline. Selective

irreversible MAO-B inhibitors, such as deprenyl (Youdim and Weinstock, 2004), have no

such tyramine potentiation effects because the intestine contains relatively low levels of

MAO-B and tyramine is effectively metabolized by intestinal MAO-A (Hasan et al., 1988).

Irreversible MAO-A inhibitors such as clorgyline possess this detrimental side effect, which

makes them undesirable for clinical use. The development of reversible MAO-A inhibitors,

such as moclobemide and lazabemide (Da Prada et al., 1990), also avoided the "cheese

reaction" side effect since reversible inhibitors can block sufficient MAO-A in the CNS to

obtain an antidepressant effect, while dietary tyramine is able to displace the inhibitor from

peripheral MAO-A, enabling its metabolism (Anderson et al., 1993).

In addition to the mechanism-based MAO inhibitors that have been developed for

clinical use as antidepressant drugs, MAO inhibitors have also been developed to treat

neurological disorders, including Parkinson's disease and Alzheimer's disease, which are

conditions associated with elevated MAO activity. Drugs such as clorgyline, deprenyl,

pargyline and others (Knoll, 2000; Mazzio et al., 1998; Raffel and Wieland, 1999) are now

utilized in pharmacological therapy as selective inhibitors of MAO for their beneficial effect

in the treatment of these neurodegenerative diseases (Youdim and Buccafusco, 2005). The

reaction catalyzed by MAOs produces, H_2O_2, which is a source of ROS hydroxyl radicals,

and MAO inhibitors might, therefore, be useful in managing the outcome of stroke and other

tissue damage associated with oxidative stress. MAO inhibitors block activity of MAOs of A

or B type thereby preventing the breakdown of monoamine neurotransmitters and increasing

their availability while decreasing intracellular H_2O_2 levels. In addition, a study has

previously demonstrated H_2O_2 scavenging by the MAO-A/B inhibitor phenelzine (Ekuni et al., 2009).

MAO inhibitors have been developed to act either on both classes of MAO or specifically inhibit type A or B isoenzymes. MAO-A inhibitors include clorgyline and moclobemide. Moclobemide has partial MAO-B inhibitory activity since this MAO inhibitor preferentially inhibits MAO-A (~80%) and to a lesser extent, MAO-B (20-30% inhibition) (Foye et al., 2008; Nair et al., 1993). MAO-B inhibitors include pargyline, (−)-deprenyl and the (−)-deprenyl derivatives selegiline and rasegiline. Phenylzine exhibits inhibitory activity against both MAO-A and MAO-B.

1.5.1.1 MAO-B inhibitor (−)-deprenyl

(−)-Deprenyl is a selective irreversible MAO-B inhibitor that has been previously used as an antidepressant and functions to increase the bioavailability of dopamine (Knoll, 2000; Matsubara et al., 2001). (−)-Deprenyl may also delay the progression of Parkinson's disease (Klegeris and McGeer, 2000; Magyar and Szende, 2004) and is utilized in the treatment of Alzheimer's disease (Birks and Flicker, 2000; Freedman et al., 1998). Moreover, (−)-deprenyl has been reported to induce a rapid increase in NO production in the brain tissue and cerebral blood vessels with a protective action on the vascular endothelium affected by the toxic effect of amyloid peptide (Thomas, 2000). The protective effects of (−)-deprenyl are lost at higher concentrations, which might even be pro-apoptotic (Magyar and Szende, 2004).

The MAO enzymes metabolize biogenic amines such as seretonine and dopamine and produces H_2O_2 as a byproduct (Magyar and Szende, 2004). The major source of cellular ROS is H_2O_2. Thus, (−)-deprenyl's effect of inhibiting the enzymes action of MAO-B serves

two roles. First, it potentiates the effect of dopamine and second, it decreases levels of ROS. Furthermore, (−)-deprenyl has been found to have antiapoptotic activities (Toronyi et al., 2002; Wadia et al., 1998; Tatton et al., 1994; Magyar et al., 1998). Although not fully understood, (−)-deprenyl protects the mitochondria (Wadia et al., 1998) and exerts its antiapoptotic effects via alterations in gene expression (i.e., (−)-deprenyl alters gene expression of the intrinsic apoptosis mediating Bcl-2 family by increasing levels of antiapoptotic Bcl-2 and Bcl-xL and decreases levels of proapoptotic BAX) (Xu et al., 1999; De Marchi et al., 2003), decreasing oxidative stress (Lee, 2006) and interfering with the action of apoptosis-mediating effector caspases such as caspase-3 (Szende et al., 2001). In rat lung microvascular endothelial cells, (−)-deprenyl attenuated BAK peptide-induced monolayer hyperpermeability, ROS formation, cytochrome c release, and caspase-3 activation (Tharakan et al., 2010). Subsequent studies have elucidated the antiapoptotic effect of (−)-deprenyl in other cells, including liver and kidney cells (De Marchi et al., 2003; Costantini et al., 1995).

Deprenyl (phenyl-isopropyl-methyl-propargylamine) was originally synthesized in 1962 by Ecseri in the Chinoin Pharmaceutical Works, Budapest, Hungary. Similar to the other MAO inhibitors, deprenyl was developed as a "psychic energizer". Deprenyl played a significant role in MAO research and has become the "golden standard" of MAO-B inhibitors. The (−)-optical isomer of deprenyl (selegiline) is more effective to inhibit MAO irreversibly, than the (+)- enantiomer (Magyar et al., 1967). (−)-Deprenyl also has been shown to not potentiate, but rather inhibit the tyramine effect on mouse vas deferens preparation (Knoll et al., 1968). The lack of tyramine potentiation may explain why (−)-deprenyl does not induce "cheese effect", which is the serious side effect that is frequently

observed in patients treated with non-selective or irreversible MAO-A selective blockers (ex. clorgyline) after ingestion of foods rich in indirectly acting sympathomimetics, such as tyramine (Youdim and Finberg, 1987; Palfreymann et al., 1988; Jarrott and Vajda, 1987). The lack of "cheese reaction" can mostly be explained by the uneven distribution of the subtypes of the MAO in the organs. The presence of MAO-A is dominant in the intestine and therefore the metabolism of tyramine is only slightly affected by MAO-B blockers. MAO-B activity is dominant in the central nervous system and it is selectively blocked by (−)-deprenyl, leading to a symptomatic improvement in Parkinsonian movement disorders (Magyar and Szende, 2004).

1.5.1.2 Pharmacology of (−)-deprenyl

(−)-Deprenyl possesses complex pharmacological properties and its mechanism of action cannot be explained solely by its selective MAO-B inhibitory potency. As a result of MAO-B inhibition, (-)-deprenyl reduces the formation of ROS by blocking the normal metabolism of biogenic amines (e.g. noradrenaline, dopamine), which results in the formation of H_2O_2, beside NH_3 and the substrate-derived aldehyde (see equation).

$$R\text{-}CH_2\text{-}NH_2 \xrightarrow[\text{H}_2\text{O}+\text{O}_2]{\text{MAO}} R\text{-}COH + NH_3 + H_2O_2$$
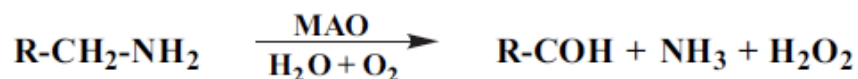
By decreasing the formation of H_2O_2, the major source of cellular ROS, (−)-deprenyl prevents or diminishes the oxidative stress in tissues. Moreover, (−)-deprenyl treatment suppresses non-enzymatic and iron-catalyzed autoxidation of dopamine, as well. Neurons rich in neuro melanine and ionized iron (Fe^{2+}) are capable of forming ROS in the presence of high concentration of H_2O_2 according to the Fenton reaction (see equation).

$$H_2O_2 + Fe^{2+} \rightarrow OH^- + {}^\circ OH + Fe^{3+}$$
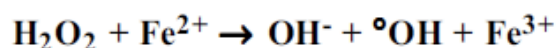
MAO-B activity increases with age, which facilitates the H_2O_2 formation. It is suggested that the over-production of H_2O_2 is not compensated by the capacity of the normal protective mechanisms of the tissues (Magyar et al., 1993). (−)-Deprenyl is able to inhibit the increased MAO-B activity in elderly patients, which might provide some protection in the treatment of patients with Parkinson's disease. In addition, chronic treatment with low concentrations of (−)-deprenyl induces antioxidant mechanisms, by enhancing processes not related to MAO-B inhibition e.g. induction of ROS scavenger functions (Magyar and Szende, 2004). (−)-Deprenyl administration at concentrations lower than needed to inhibit MAO-B activity (ex. 60 pmol and 4.2 nmol) have been shown to decrease neuronal damage due to oxidative shock (Wu et al., 1993; Chiueh et al., 1994). Long-term treatment with the drug can enhance antioxidant defense through the synthesis of Mn and Cu/Zn dependent superoxide dismutase (SOD1, SOD2) and catalase activity in experimental animals (Carrillo et al., 1991; Carrillo et al., 1992; Carrillo et al., 1993; Knoll, 1988).

1.5.1.3 MAO inhibitor transcriptional effects

(−)-Deprenyl has also been shown to affect gene expression. Using nerve growth factor-differentiated PC-12 cell line metabolic labeling of newly synthesized proteins and subsequent identification by two-dimensional gel autoradiography showed that deprenyl and other propargylamines induced *de novo* synthesis of several proteins. (−)-Deprenyl also induced neuroprotective cytokine expression. Also, when administered intraperitoneally, (−)-deprenyl enhanced the expression of nerve growth factor mRNA in intact rat cerebral cortex and protected rat cortical tissue from ischemic insult (Serkova et al., 1996). Transcriptional effects can be elicited at (−)-deprenyl concentrations below that necessary to inhibit MAO-B and therefore represent a separate mechanism. (−)-Deprenyl has been found to selectively

alter the expression of a number of mRNAs and 40 - 50 proteins in nerve and glial cells and decrease DNA fragmentation characteristic of apoptosis (Tatton et al., 1996). Of the 40-50 mRNAs and proteins whose synthesis is altered by (−)-deprenyl in nerve and glial cells the general shift in expression is interpreted to maintain mitochondrial function and decrease cytoplasmic oxidative radical levels and thereby reduce apoptosis (Tatton et al., 1997). The preponderance of (−)-deprenyl-induced proteins changes characterized to date were appropriate to antiapoptosis. These included superoxide dismutases-1 and -2, glutathione peroxidase, c-JUN and glyceraldehyde-3-phosphate dehydrognease. Also, the antiapoptotic maintenance of BCL-2/BAX ratio was found in (−)-deprenyl-treated groups. Importantly, propargylamines do not alter new protein synthesis in undamaged nerve cells (Tatton et al., 2002). Also in neuronal cells, (−)-deprenyl (and another MAO called rasagiline) protection was confirmed by the induction of pro-survival BCL-2 and neurotrophic factors. Both drugs prevented mitochondrial membrane permeabilization and loss of membrane potential. DNA array studies indicate that rasagiline increases expression of genes coding mitochondrial energy synthesis, inhibitors of apoptosis, transcription factors, kinases and components of the ubiquitin-proteasome system sequentially (Naoi et al., 2007). Similarly, (−)-deprenyl protects against MPP+-induced toxicity in mouse primary neuronal culture by inducing induction of anti-oxidant thioredoxin expression, which in turn mediates the induction of anti-oxidant mitochondrial manganese superoxide dismutase and antiapoptotic Bcl-2 (Andoh et al., 2005). Of particular interest, studies with photoaffinity labeled propargylamines bind directly to GAPDH in rat hippocampus (Kragten et al., 1998) and cultured catecholaminergic cells (Carlile et al., 2000). Drug treatment prevented GAPDH upregulation as well as nuclear accumulation associated with apoptosis (Carlile et al., 2000).

(−)-Deprenyl also significantly induced anti-oxidant heme oxygenase-1 and -2 in response to dopamine-induced oxidative stress in human neuroblastoma cell culture (Rieder et al., 2004). All studies to date have been carried out using various types of neural cells (nerve, glial, astrocyte) but none have examined (−)-deprenyl effects on gene expression in epithelial cells. We have tested for (−)-deprenyl-induced antiapoptosis in our barrier model and found that the (−)-deprenyl concentrations, which reduced TER did not reduced relative cell number suggesting TER reductions was a result of changes to junctional complexes that mediate barrier function (Figure 15). Relative cell number was reduced, however at higher concentrations of inhibitor (Figure 15). Also many of the transcriptional changes have not been characterized at either the mRNA or protein level. Of particular significance would be detected of changes involving cell-cell contacts.

1.5.1.4 Anti-inflammatory effects of MAO inhibitors

Previously it was postulated that remission of rheumatoid arthritis in patients taking MAO inhibitors may be due to inhibition of prostaglandin E2 (PGE2) synthesis (Lieb, 1983). Subsequently, two cases were described in which the MAO inhibitor phenelzine induced remission in patients with another chronic inflammatory disease, Crohn's disease (Kast, 1998). It was postulated that MAO inhibitors may inhibit these diseases by blocking TNF-α levels but no evidence was presented (Altschuler, 2000). However, further evidence begins to support this hypothesis. First, MAO-B levels are closely related to the pathogenesis of Parkinson's disease and upregulation of TNF-α and IL-6 mRNA were increased in the hippocampus of Parkinson's patients (Nagatsu and Sawada 2006; Sawada et al., 2006). MAO-B inhibitors are effective for the treatment of Parkinson's disease, both through their direct effect on MAO-B and in part by also activating multiple factors for anti-oxidative

stress including anti-inflammatory cytokines (Nagatsu and Sawada, 2006). Second, the MAO-A inhibitor moclobemide inhibited the unstimulated production of TNF-α and IL-8 in whole blood from healthy volunteers and enhanced the LPS stimulated production of the anti-inflammatory cytokine IL-10 (Lin et al., 2000). Even so, the impact MAO-B inhibitors may have on LPS-induced cytokine expression in oral tissues has not been evaluated. In an *in vivo* chronic inflammatory disease model, it was found that LPS-induced TNF-α expression was largely abrogated by inhibition of MAO-B activity (Ekuni et al., 2009). Differences in this data compared to previous reports suggest that tissue-specific differences in LPS induction of MAO-A versus MAO-B expression and regulation may exist.

1.6 Rational, Hypothesis and Objectives of this Study

Rational: Epithelial tissues play a critical role in maintaining systemic health by establishing a functional barrier that physically separates the external environment from the host to provide an innate defense against environmental insult. Loss of function of epithelial barrier that accompanies alterations of cell-cell junctional proteins is associated with a multitude of epithelial inflammatory processes typified by periodontal disease, psoriasis, chronic airway inflammatory diseases as well as gut related barrier loss seen in inflammatory bowel disease (IBD) (Fujita et al., 2010; Chung et al., 2005a; He et al., 2009; Kucharzik et al., 2001). In this regard, barrier disruption is suspected to play a central and general role in the onset of inflammatory disease. Fundamental knowledge of the underlying pathogenesis remains poorly understood. Therefore, identifying factors that mediate epithelial barrier loss is clinically relevant as it will open the possibility that novel interventional strategies may be developed to mitigate early disease-associated signaling events.

Lipopolysaccharide (LPS) is a Gram-negative bacterial virulence factor implicated in periodontal disease onset. Amphiregulin (AR) is a ligand for the epidermal growth factor receptor (EGFR) and downstream mediator of tumor necrosis factor-alpha (TNF-α) (Chokki et al., 2006) that is normally sequestered at cell-cell contacts in stable epithelial barriers. AR and corresponding signaling components modulating the EGFR pathway are altered in the oral junctional epithelium of an LPS-induced Wistar rat model of periodontal disease that exhibited concomitant altered barrier architecture (Firth et al., 2011). Expression microarray analysis of diseased junctional epithelium found that three of the top 10 LPS-induced genes are associated with the generation of ROS signaling mediators. One of these genes was monoamine oxidase-B (MAO-B). Subsequently, treatment of the LPS-induced rat periodontal disease model with MAO inhibitors was found to greatly ameliorate disease indices (Ekuni et al., 2009). In addition, a weight of clinical evidence suggests that therapeutic inhibition of MAO may ameliorate the chronic inflammatory conditions found in rheumatoid arthritis and Crohn's disease (Lieb, 1983; Kast, 1998).

Current methods for management of periodontal disease are at times unsuccessful and therefore novel approaches still need to be developed. Protection of barrier integrity may potentially reduce penetration of bacterial virulence factors and therefore represents a novel treatment modality. We will therefore examine, in cell culture, MAO effects on LPS-mediated barrier disruption.

Hypothesis: MAO inhibitors protect against LPS-mediated loss of *in vitro* epithelial cell barrier.

Objectives:

1) Develop an *in vitro* model of epithelial barrier to test the degree to which exogenous barrier mediators of interest (LPS, H_2O_2, AR and TNF-α) induce barrier loss and the degree to which MAO inhibitor treatment ameliorates this loss of barrier.

2) Employ ELISA analysis of conditioned media collected from the *in vitro* barrier model to investigate the altered secretion of AR and TNF-α in response to chronic treatment with exogenous mediators of barrier (LPS and H_2O_2) ± MAO inhibitor.

3) Perform immunostaining analysis of *in vitro* barrier model cell cultures to test the degree to which cell-cell junction markers are altered by LPS ± MAO inhibitor chronic treatment.

2 (−)-Deprenyl Attenuates Altered AR Expression and Prevents Barrier Loss Induced by Chronic LPS Challenge in a Histiotypic Model of Epithelium.

2.1 Introduction

Using a Wistar rat model of LPS-induced periodontal disease, a recent study showed that chronic inflammation of oral junctional epithelia led to altered barrier architecture and LPS penetration to underlying stroma (Ekuni et al., 2009). Gene chip analysis revealed disease-elevated MAO-B. These changes were associated with elevated ROS levels and TNF-α release. Treatment with MAO inhibitor ameliorated these disease indices (Ekuni et al., 2009). These findings were extended with gene chip analysis that showed AR, an EGFR ligand and downstream mediator of TNF-α (Chokki et al., 2006), as well as several other proteins modulating the EGFR pathway were also altered in the LPS-induced periodontal disease model (Firth et al., 2011). This project in Dr. Putnin's laboratory used an *in vitro* histiotypic model of epithelium to test the degree to which altered AR release into the conditioned media regulates LPS-induced loss of epithelial barrier. In addition, we tested the degree to which MAO inhibitor treatment modulates LPS-induced AR release to prevent loss of epithelial barrier integrity.

2.2 Material and Methods

2.2.1 Materials

Transwell™ Permeable Supports (6.5mm diameter polycarbonate membrane, 0.4μm membrane pore size), 75 cm^2 tissue culture flasks and 96 well plates were from Corning Incorporated Life Sciences (Lowell, MA). Millicell® ERS-2 (Electrical Resistance System) was from Millipore Corporation (Bedford, MA). Human amphiregulin and human TNF-α DuoSet® ELISA kits were from R&D Systems® (Minneapolis MN). CellTiter 96® AQueous Non-radioactive Cell Proliferation Assay was from Promega Corporation (Madison, WI). Amphiregulin and TNF-α were from Santa Cruz Biotechnology, INC (Santa Cruz, CA). Antibodies for mouse claudin-1, rabbit claudin-3, mouse claudin-4, rabbit claudin-7 and rabbit ZO-1 were from Invitrogen Corporation (Camarillo, CA). Bodipy FL phallocidin for cytoskeleton stain of F-actin was from Molecular Probes® (Eugene, OR). The antibody for mouse E-cadherin was from BD Biosciences (Franklin Lakes, NJ). Periodontal ligament epithelial cells (PLE) from epithelial rests of Malassez were isolated from porcine periodontal ligament and cultured as previously described (Brunette et al., 1976). Madin-Darby canine kidney-I cells (MDCK-I) at passage number 23 were generously supplied from Dr. Kevin Donato (Department of Laboratory Medicine & Pathobiology, University of Toronto). This high-barrier cell line was derived by cloning the parental cell line MDCK (CCL-34) and the source of these cells is the distal tubule of the kidney. Intestinal epithelial cells-6 (IEC-6) cell line was from the American Type Culture Collection (Manassas, VA). This cell line was derived from normal rat intestine (Quaroni et al., 1979). Lipopolysaccharides from *Escherichia coli* 055:B5, hydrogen peroxide solution 30% (w/w), R-(−)-deprenyl hydrochloride, phenelzine sulphate salt, moclobemide, N-Methyl-N-

propargyl-3-(2,4-dichlorophenoxy)propylamine hydrochloride (clorgyline) and pargyline hydrochloride were from Sigma (Oakville, Ontario). α-Minimum Essential Medium (α-MEM), antibiotic-antimycotic (anti-anti), fetal bovine serum (FBS), Dulbecco's Modified Eagle Medium (DMEM), trypsin-EDTA and Glutamax™ were from Gibco (Grand Island, NY). FBS for α-MEM was from PAA Laboratories Incorporated (Etobicoke, ON). All other chemicals were from Sigma (Oakville, Ontario).

2.2.2 Epithelial cell culture experiments

The PLE cell line was cultured in α-Minimum Essential Medium (α-MEM) containing L-glutamine, and supplemented with 1% anti-anti (10,000 units of penicillin (base), 10,000 µg of streptomycin (base), and 25 µg of amphotericin B/ml utilizing penicillin G (sodium salt), streptomycin sulfate, and amphotericin B as Fungizone® Antimycotic in 0.85% saline) and 15% FBS. The MDCK-I and IEC-6 cell lines were cultured in DMEM containing 4,500 mg/L D-glucose and sodium pyruvate and supplemented with 1% anti-anti and 10% FBS.

All cells were cultured on 75 cm^2 tissue culture flasks and were maintained at 37°C in a humidified atmosphere of 95% air 5% CO_2. To remove the confluent cells, they were treated with trypsin-EDTA (Gibco, Grand Island, NY) for 5 minutes. This was replaced with fresh trypsin for an additional 12 minutes and removed with the dislodged cells. Cells were harvested into 10 ml of medium with the corresponding concentration of supplemented serum and pelleted by centrifuging at low speed for 4 minutes. The culture medium was decanted and replaced with 10 mls of fresh medium with the corresponding concentrations of FBS and additional supplements. Cells were suspended and 100 µl of this suspension was added to 9.9 ml of Isoton-II® (Coulter Electronics of Canada, Ltd., BC) and counted three

times with a CoulterCounter$^{®}$ (Coulter Electronics of Canada, Ltd., BC). Total number of

cells and concentration of cell suspension was calculated. For the experiments, cells were

plated on Transwell™ permeable supports with polycarbonate membranes (6.5 mm diameter

and 0.4μm pore size) (Corning, Lowell, MA).
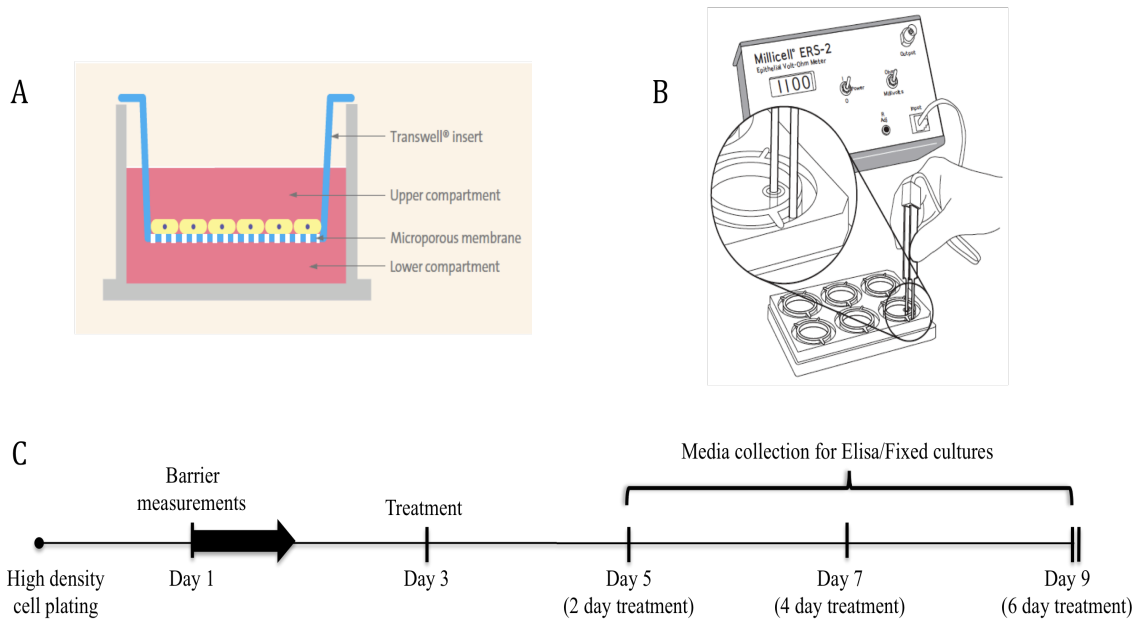
Figure 3. Experimental timeline

MDCK-I, IEC-6 and PLE epithelial cell lines were cultured in Transwell™ chambers **(A)** and transepithelial electrical resistance (TER) was monitored by a Millicell® Electrical Resistance System **(B)** as an assay of barrier formation. TER measurements on days 1, 3, 5, 7 and 9 were followed by a full media change with treatments administered at 48-hour intervals beginning on day 3 **(C)**. Media from apical and basal chambers collected at 48-hour intervals was analyzed for AR and TNF-α secretion by sandwich ELISA. Fixed cultures were immunostained for AR, zonula occludens-1 (ZO-1), actin, claudin-1, claudin-3, claudin-4 and claudin-7 and E-cadherin as markers of cell-cell junctions.

2.2.3 Assay of barrier formation

To assay changes in barrier integrity, we measured transepithelial electrical resistance (TER) of Transwell™ epithelial cell cultures, which is a commonly used technique to characterize paracellular barrier function (Gonzalez-Mariscal et al., 2003; Schneeberger and Lynch, 2004; Van Itallie et al., 2008). MDCK-I, IEC-6 and PLE epithelial cell lines were cultured in Transwell™ chambers and TER was monitored by a Millicell$^{®}$ Electrical Resistance System as an assay of barrier formation (Figure 3). Throughout the experiments, 100μl and 600μl of culture medium with or without treatments was added to the apical and basal compartments, respectively. Prior to cell plating, Transwells™ were incubated overnight in basal media supplemented with 1% anti-anti. PLE cells were plated at a high density of 8.0 x 10^4 cells and cultured in α-MEM supplemented with 15% FBS and 1% anti-anti. MDCK-I cells were plated at a density of 5.0 x 10^4 cells and cultured in DMEM supplemented with 1% FBS, 1% anti-anti. IEC-6 cells were plated at a high density of 8.0 x 10^4 cells and cultured in DMEM supplemented with 5% FBS, 1% anti-anti. When the treatments were applied at 72 hours, the serum concentration in PLE and IEC-6 culture media was reduced to 1% FBS and the MDCK-I treatment containing culture medium remained the same as the plating medium. Notably, at 72 hours post cell-plating the MAO inhibitors were applied alone in the media change for 1 hour and this was followed by the addition of the co-treatment to the apical and basal Transwell™ compartment media. Every 48 hours after this initial staggered co-treatment, both treatments were applied simultaneously in the media change. A full media change was performed at 24 hours post-cell plating. Subsequently, the medium was completely changed every 48 hours. This was done to prevent any adverse affects due to the evaporation and loss of medium that was

observable in the Transwells™ after three days of culturing. This also provided the cells with two days to recover from a consistently recorded drop in TER, likely induced by the impact of a full medium change. TER measurements were recorded in ohms with the Millicell® ERS-2 at 0, 1, 3, 5, 7 and 9 days of culturing (day 0 TER was consistently recorded as 0 ohms). Prior to taking the TER measurement, the Millicell® ERS-2 electrode was sterilized for 15 minutes in 70% ethanol (Millicell® ERS-2 User Guide). In addition, the cell cultures were allowed to cool to room temperature for 15 minutes prior to taking the TER measurements (Millicell® ERS-2 User Guide). Treatments of the cell cultures with MAO inhibitors, and/or exogenous LPS, AR, TNF-α or H_2O_2 were applied at 72 hours. This 72-hour time point was chosen as a suitable time for administering the treatments since it corresponds to a period in time where the MDCK-I cell culture TER began to increase substantially. Cell culture medium was changed immediately after the TER measurements. In addition, conditioned medium from the apical and basal compartments were reserved for later ELISA analysis. This media collection required adding 50μl of the corresponding medium to the apical compartment to account for the media loss that occurred while taking TER measurements. At day 9, Transwell™ cultures were fixed in a solution of 2% formaldehyde/PBS fix. The cells were fixed for 2 hours at room temperature followed by an overnight fix at $4^°$C before having the fix replaced with PBS.

2.2.4 Quantitation of AR and TNF-α protein secretion by ELISA analysis

MDCK-I, PLE and IEC-6 cell culture conditioned medium collected from apical and basal Transwell™ chambers at 2, 4 and 6 days of treatment (Figure 3) and immediately stored at $-80^°$C were analyzed for AR and TNF-α secretion by sandwich ELISA. Sandwich ELISA was performed according to the kit manufacturer's instructions. Briefly, 96-well

plates were coated with 100µl per well of the diluted capture antibody (2µg/ml in PBS for AR and 4µg/ml in PBS for TNF-α). These plates were then sealed and incubated overnight at room temperature. Next, each well was aspirated using vacuum suction and washed with wash buffer (0.05% Tween® 20 in PBS), repeating the process two times for a total of three washes. Plates were then blocked by adding 300µl of reagent diluent (1% BSA in PBS) to each well and incubating the plates at room temperature for 1 hour. After this incubation, the aspiration/wash step was repeated. The assay procedure began by adding 50µl per well of samples or standards in reagent diluent. To produce a standard curve, which enables the conversion of optical density to protein amount, a seven point standard curve using 2-fold serial dilutions in reagent dilution (1000-15.6pg/ml) was performed. Plates were then sealed and incubated overnight at room temperature. After this incubation, a repeat of the aspiration/wash step was performed. Next, 50µl of the detection antibody diluted in reagent diluent (100ng/ml for AR and 250ng/ml for TNF-α) was added to each well. These plates were sealed and incubated for 2 hours at room temperature. A repeat of the aspiration/wash procedure was then performed. Next, 100µl of the working dilution (1:200 dilution with reagent diluent) of Streptavidin-HRP was added to each well. The plates were covered to avoid light and incubated for 20 minutes at room temperature. After this incubation, a repeat of the aspiration/wash step was performed. Next, 100µl of substrate solution (1:1 mixture of color reagent A (H_2O_2) and color reagent B (Tetramethylbenzidine)) was added to each well. During this step, the plates were covered to avoid light. After 1 hour of incubation, 50µl of stop solution (2N H_2SO_4) was added to each well and the plates were gently tapped to ensure thorough mixing. To determine the optical density of each well, a microplate reader set to 450 nm with a 595 nm reference was immediately employed. Conversion to protein amount

in pg/ml from the optical density readings was performed using the slope of the standard curve optical density readings.

2.2.5 Immunohistochemistry

At the end of the experimental period (6 days post treatment, Figure 3C), Transwell™ cell cultures had their media removed from the apical and basolateral compartments of the Transwell™ inserts by vacuum filtration. The cultures were then washed three times in phosphate buffered saline (PBS) and the cells were fixed in a solution of 2% formaldehyde/PBS fix. The cells were fixed at room temperature for 2 hours and then fixed at 4°C overnight. The following day, the fix solution was rinsed three times in PBS. Next, all the PBS was vacuum suctioned and the Transwell™ inserts were removed from the 24 well tray and flipped upside down so that the membrane could be carefully removed with a fresh scalpel. This was done quickly to prevent the membranes from drying. The membranes, once removed, were placed onto the well of a 24 well plastic tray with the cells facing upwards. Next, 0.5% Triton X-100 (50μl Triton X-100/10ml PBS) was administered to each membrane for exactly 4 minutes. This was followed by five washes with PBS for a 10-minute period each on a shaker system set at medium-low shaker level. Next, free aldehyde groups were quenched with a 0.05% $NaBH_4$/PBS solution (.005g/10ml PBS) for 10 minutes. The 0.05% $NaBH_4$/PBS solution was vacuum suctioned and this was followed by administration of block solution (Glycine/PBS/Block (30 mg/ml BSA(V)/10mg/ml glycine/0.1% NaN_3)) to eliminate any potential non-specific binding. This block solution remained on the cultures for 1 hour. Next, the primary antibodies were prepared with block solution and 10μl total solution was applied per membrane. This solution was comprised of a dilution (1:50) of block/primary antibody. Next, the block buffer was removed by vacuum

suction. The membranes were then positioned in the center of the well in order to prevent the

antibody solution from running off of the membrane. 10μl of the antibody solution was then

pipetted into the center of each membrane. The primary antibody solution was left for 1 hour

and checked periodically for any loss of antibody solution. If primary antibody solution was

lost, more of the solution was added. The cultures were left overnight in 250μl of this

primary antibody solution, which was a volume that completely submersed the membranes.

Next, a wash buffer was prepared by making a dilution (1:30) of the block/buffer/glycine

solution with PBS and Bodipy FL Phallocidin cytoskeleton stain of F- actin was

administered in a dilution (1:300) of reagent and wash buffer solution (1:300 dilution of

6.6μM Bodipy FL Phallocidin is 22nM) for 10 minutes. Subsequently, the wash buffer alone

was applied 5 times for 10 minutes each. Next, the secondary antibody was added in a

PBS/block solution (1:100) and the samples were incubated at room temperature in the dark

for 1 hour. Next, the samples were washed 3 times for 5 minutes in PBS in the dark. Lastly,

the membranes were mounted on glass microscope slides with Invitrogen Prolong® Gold

Antifade with DAPI reagent (Invitrogen Molecular Probes® Eugene, OR, P-36931). Imaging

of the samples was performed immediately with a Nikon Confocal Microscope C1 with Q

Imaging Retiga 2000R (Melville, NY). Filters used were ND16, ND8 and ND4. The laser

and detector configuration was as follows: Laser 1 was a 408nm UV Laser for blue

fluorescence, laser 2 was a 488nm blue laser for green fluorescence and laser 3 was a 543nm

green laser for red fluorescence.

Representative confocal images from IEC-6 and MDCK-I Transwell™ cultures were

processed to display scale bars and separated RGB channels using Nikon EZ-C1 software.

Image J64 image-processing software was used to reconstruct z-axis images of MDCK-I

cultures on Transwell™ membranes. As shown by z-axis images, ZO-1 immunostaining was localized at the apical region of polarized MDCK-I Transwell barrier model cultures, which is consistent with the literature (Turner, 2009). As a result, confocal imaging of x,y-axis images was restricted to this apical region. All other confocal imaging of cell-cell markers in the x,y-axis was restricted to cellular regions near the middle of the DAPI nuclear staining to maintain consistency between sample images and to image junctional regions containing adherens junctions, which are typically located subjacent to the tight junctions (Figure 2) (Turner, 2009). Lastly, for each experiment, RGB gain structures were established using Nikon EZ-C1 software. These gain structures were maintained throughout the image collecting process to enable direct comparisons between samples of the various treatment groups. By doing this, protein expression of the molecules of interest could be inferred by observing the corresponding immunostaining fluorescence intensity.

2.2.6 Proliferation assay

MDCK-I cultures were grown on Transwell™ polycarbonate membranes in DMEM supplemented with 1% FBS and 1% anti-anti. Cells were treated after 72 hours of cell plating and chronic treatments continued every 48 hours as outlined in the barrier model protocol (Figure 3C). The CellTiter 96® AQueous Non-Radioactive Cell Proliferation Assay was performed directly on these cultures at day 6 of treatment. For every 100μl of conditioned media, 20μl of MTS/PMS solution was added as per the manufacturers instructions (Promega, Technical Bulletin No. 169). Next, plates were incubated for 1-hour at $37^{\circ}C$ in a humidified, 5% CO_2 atmosphere. After a 1-hour incubation period, the conditioned media/MTS/PMS solution from the apical and basal compartments of the Transwell™ cell cultures were pooled and mixed. Lastly, the absorbance of formazan was

immediately recorded from the cell culture plates at 490nm using an ELISA plate reader. Absorbance was expressed as relative cell number.

2.2.7 Statistical analysis

Data analysis was performed using a statistical program called "A calculating companion for Brunette's Critical Thinking". This program is available at the following website: http://www.dmbru.net/Calculating_Companion/tests.php (Website and all applets copyright © 2008, DM Brunette). All results were subjected to statistical analysis using one-way analysis of variance (ANOVA) and analyzed for comparisons between the groups by Tukey's test. Data were expressed as means ± S.D. of triplicate samples and the level of significance was taken to * p < 0.05 and **p<0.01.

2.3 Results

2.3.1 Exogenous mediators of epithelial barrier model

The high barrier forming MDCK-I cell line is considered a gold standard for studies of epithelial barrier formation as measured by TER (Gonzalez-Mariscale et al., 2003; Schneeberger and Lynch, 2004). This cell line was employed in a pilot experiment (n=1) (Figure 4A) designed to investigate exogenous mediators of an *in vitro* epithelial barrier model. These mediators included the bacterial virulence factor LPS, TNF-α, and inhibitors of MAO-A/B and MAO-B, which became of interest for this barrier study because of previous data collected using an *in vitro* rat periodontitis disease model (Ekuni et al., 2009). Previous studies showed that proinflammatory cytokines such as TNF-α decrease TER and increase paracellular permeability to ions and normally impermeable molecules in intestinal (Bruewer et al., 2003; Fish et al., 1999; Francoeur et al., 2004; Li et al., 2007; Rodriguez et al., 1999)

and airway epithelia (Coyne et al., 2002). Dr Putnins' laboratory employed gene chip

analysis of epithelial tissues from a rat LPS-induced periodontal disease model, which

showed amphiregulin (AR), an epidermal growth factor receptor (EGFR) ligand and

downstream mediator of TNF-α (Chokki et al., 2006), as well as several associated proteins

that modulate the EGFR pathway were also altered in the LPS-induced periodontal disease

model (Firth et al., 2011). Thus, AR became of interest as a potential significant mediator of

the *in vitro* barrier model. Changes in Transwell™ MDCK-I cell culture TER were measured

by a Millicell® ERS-2 at 48, 96 and 144 hours of treatment. Chronic treatment of the model

at 72 hours post-cell plating with the MAO-A/B inhibitor phenelzine at $50\mu M + 5\mu g/ml$

LPS-induced increases in TER, suggesting MAO-A/B inhibitor-mediated enhancement of

epithelial barrier integrity can occur in an LPS-rich environment (Figure 4A). Treatment

with 5μg/ml LPS, 10ng/ml AR and 10ng/ml TNF-α-induced reduced epithelial barrier

formation (Figure 4A). TNF-α chronic treatment was the most effective at reducing TER,

followed by AR and last LPS (Figure 4A). Further experiments that employed exogenous

AR and TNF-α treatments were carrier out with this MDCK-I barrier model (Figure 4B, C).

This study employed larger sample sizes (n=3) and a concentration range of exogenous AR

and TNF-α treatments. Both treatments reduced TER in a concentration dependent manner

and confirmed that chronic TNF-α treatment induced greater reduction in TER in

comparison to chronic AR treatment at the same concentrations (Figure 4B,C).
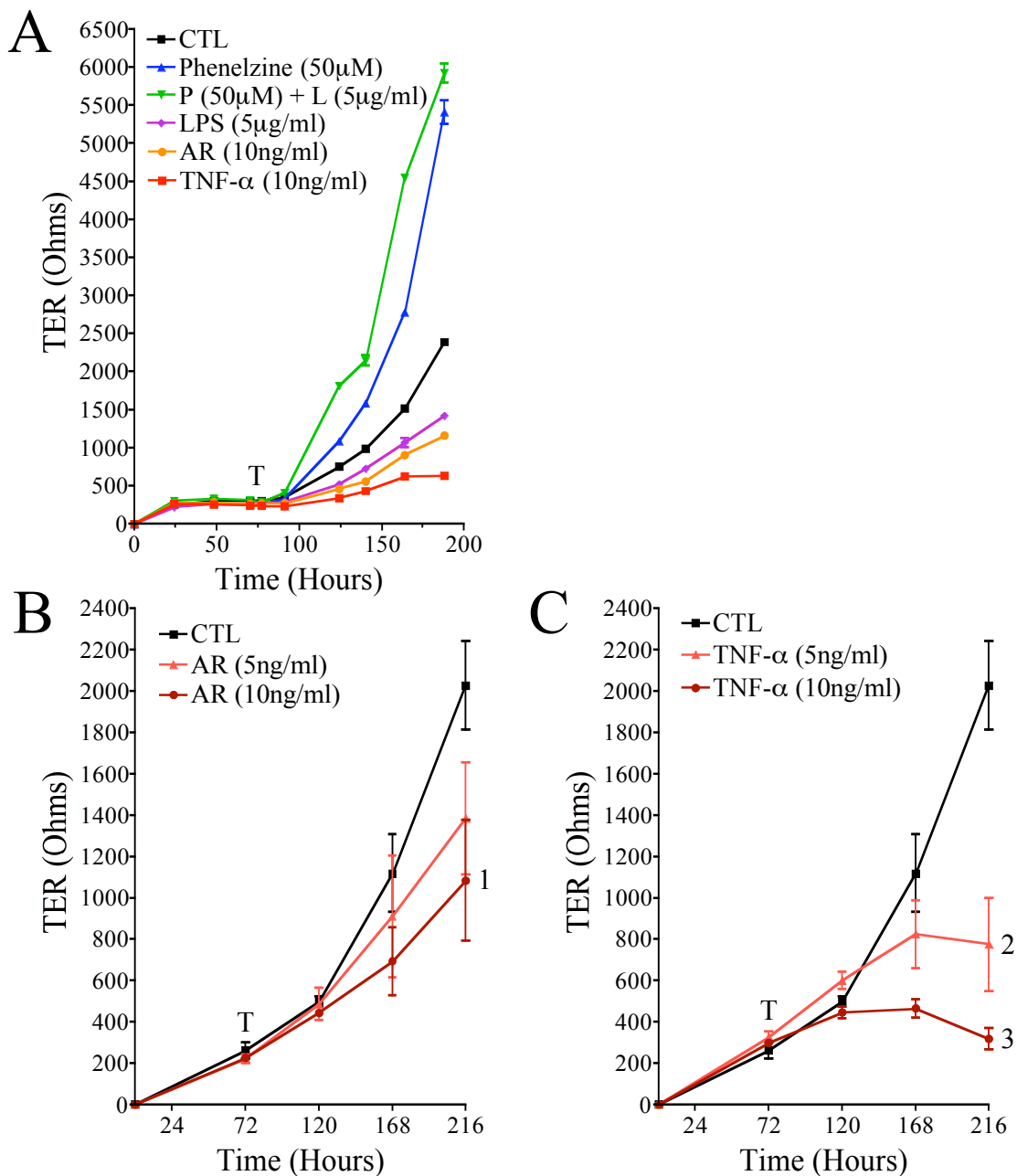
Figure 4. Exogenous mediators of *in vitro* MDCK-I barrier model

Pilot experiment (n=1) using the MDCK-I barrier model treated at 72 hours **(T)** post-cell plating with the MAO-A/B inhibitor phenelzine (P) ± LPS (L), LPS alone, AR and TNF-α **(A)**. Changes in TER were measured with the Millicell® ERS-2 at 48, 96 and 144 hours of treatment. Exogenous AR **(B)** and TNF-α **(C)** treatment of MDCK-I barrier model and assay of barrier formation by TER. Data are presented as mean ± SD; n = 3. Analysis of 144-hour TER using One-way ANOVA with Tukey's test found notable significant differences between (1) Control (CTL) and AR (10ng/ml) at $p<0.05$, (2) CTL and TNF-α (5ng/ml) at $p<0.01$ and (3) TNF-α (5ng/ml) and TNF-α (10ng/ml) at $p<0.05$.

2.3.2 Treatment of the MDCK-I barrier model with MAO-A/B, MAO-B and MAO-A inhibitor classes

Previously it was demonstrated that chronic treatment with the MAO-A/B inhibitor phenelzine induced increases in the MDCK-I barrier model TER (Figure 4A). To further determine the effect of MAO inhibition in the barrier model TER, MDCK-Is were chronically treated with a concentration range of MAO-A/B, MAO-B and MAO-A over a 6 day time period as defined in the experimental protocol (Figure 3C). MAO-A/B and MAO-B inhibitor treatment induced concentration dependent increases in TER (Figure 5A). MAO-A inhibitor treatment negatively affected barrier formation as measured by TER (Figure 5A). At 96 hours of treatment, reduction of TNF-α and AR protein secretion was noted in the MAO-A/B and MAO-B inhibitor treated groups. In contrast, increased AR and TNF-α protein secretion was noted at 96 hours of MAO-A inhibitor and LPS treatment (Figure 5B,C).

An interesting finding, was that chronic treatment of the barrier model with the low concentration (5μM) treatment of the MAO-A inhibitor moclobemide, resulted in a significant ($p < 0.01$) increase in TER above the control (Figure 5A). In addition, this increase in TER was associated with reduced TNF-α and AR secretion at 96 hours of treatment (Figure 5B,C). These findings contradict the results from the other MAO-A inhibitor treatments, which include clorgyline (5μM and 40μM) and moclobemide (at the higher treatment concentration of 40μM). These treatments induced decreases in TER below the control measurements. This discrepancy can be explained by the fact that moclobemide preferentially inhibits MAO-A (~80%) and to a lesser extent, MAO-B (20-30% inhibition) (Foye et al., 2008; Nair et al., 1993). The partial inhibition of MAO-B by the low

concentration treatment of moclobemide may be the factor that is inducing an increase in barrier formation as assessed by TER. Furthermore, higher concentrations of moclobemide would likely introduce an increased amount of MAO-A inhibition that could override the increase in TER due that may be caused by the partial inhibition of MAO-B.
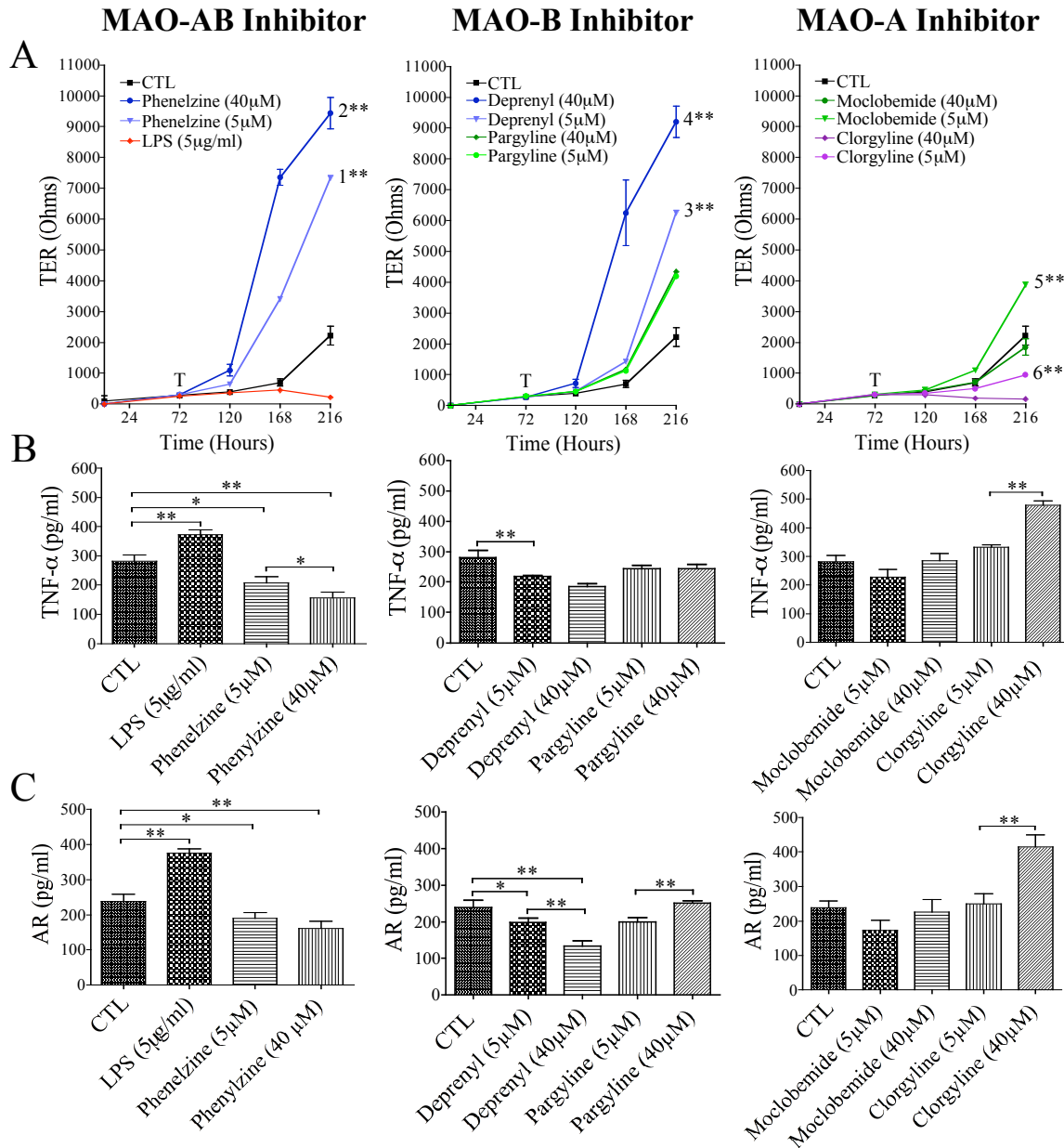
Figure 5. Treatment of the MDCK-I barrier model with MAO-A/B, MAO-B and MAO-A inhibitor classes

(A) MDCK-I cultures grown on Transwell™ membranes were treated at 72 hours **(T)** post-cell plating with a concentration range of MAO inhibitors and LPS alone. Analysis of 144-hour TER using One-way ANOVA with Tukey's test found notable significant differences between 1) Control (CTL) and 5μM phenelzine (P), 2) 5μM P and 10μM P, 3) 5μM deprenyl (D) and CTL, 4) 5μM D and 40μM D, 5) 5μM moclobemide and CTL and 6) 5μM clorgyline and CTL. **(B, C)** At 96 hours of treatment, total TNF-α and AR protein secretion was assayed by ELISA analysis of pooled and mixed apical and basal conditioned media. Significant difference between groups numbered and groups bordering bars (*p <0.05, **p<0.01). Data are presented as mean ± SD; n = 3.

2.3.3 Treatment of PLE, IEC-6 and MDCK-I barrier models with (−)-deprenyl ± LPS

Treatment of PLE, IEC-6 and MDCK-I barrier models with (−)-deprenyl induces increases in TER in an LPS conditioned environment, demonstrating a potential protective role against LPS-induced reduction in TER (Figure 6A). Furthermore, ELISA analysis of the conditioned media showed inhibition of LPS-induced TNF-α protein secretion in the presence of (−)-deprenyl (Figure 6B,C). TNF-α secretion was most highly active at the early assay time point (48hrs) and induction decreased progressively at the 96 and 144-hour assay time points (Figure 6C). This finding of a temporal TNF-α activation pattern in several cell types is consistent with literature findings that have established TNF-α as an acute inflammatory mediator in many epithelial tissues (Noti et al., 2010; Ulich et al., 1995). Furthermore, the finding of a consistent pattern between the three epithelial cell lines of LPS reduction in TER and protection by (−)-deprenyl co treatment and a temporal pattern of TNF-α secretion suggests that these signaling mechanisms represent an epithelial phenomenon that may be consistent among all epithelial cell types.

A summary of the *in vitro* assays (Table 1A,B and C) highlights that LPS reduced barrier and increased TNF-α and AR expression. Subsequently, the effect of a variety of MAO inhibitors was tested using these *in vitro* assays. MAO-A/B was effective at reconstituting the barrier that was reduced by LPS and also reduced LPS‑mediated TNF‑α and AR expression. The MAO-B (−)-deprenyl was as effective as the tested MAO-A/B inhibitor. The MAO-A inhibitors tended to work in an opposite manner. *In vivo* rat periodontal disease model experiments that were conducted previously in Dr. Putnin's laboratory are summarized in Table 1D (Ekuni et al., 2009). Only MAO-A/B inhibitor was tested for reduction in disease and this was effective.
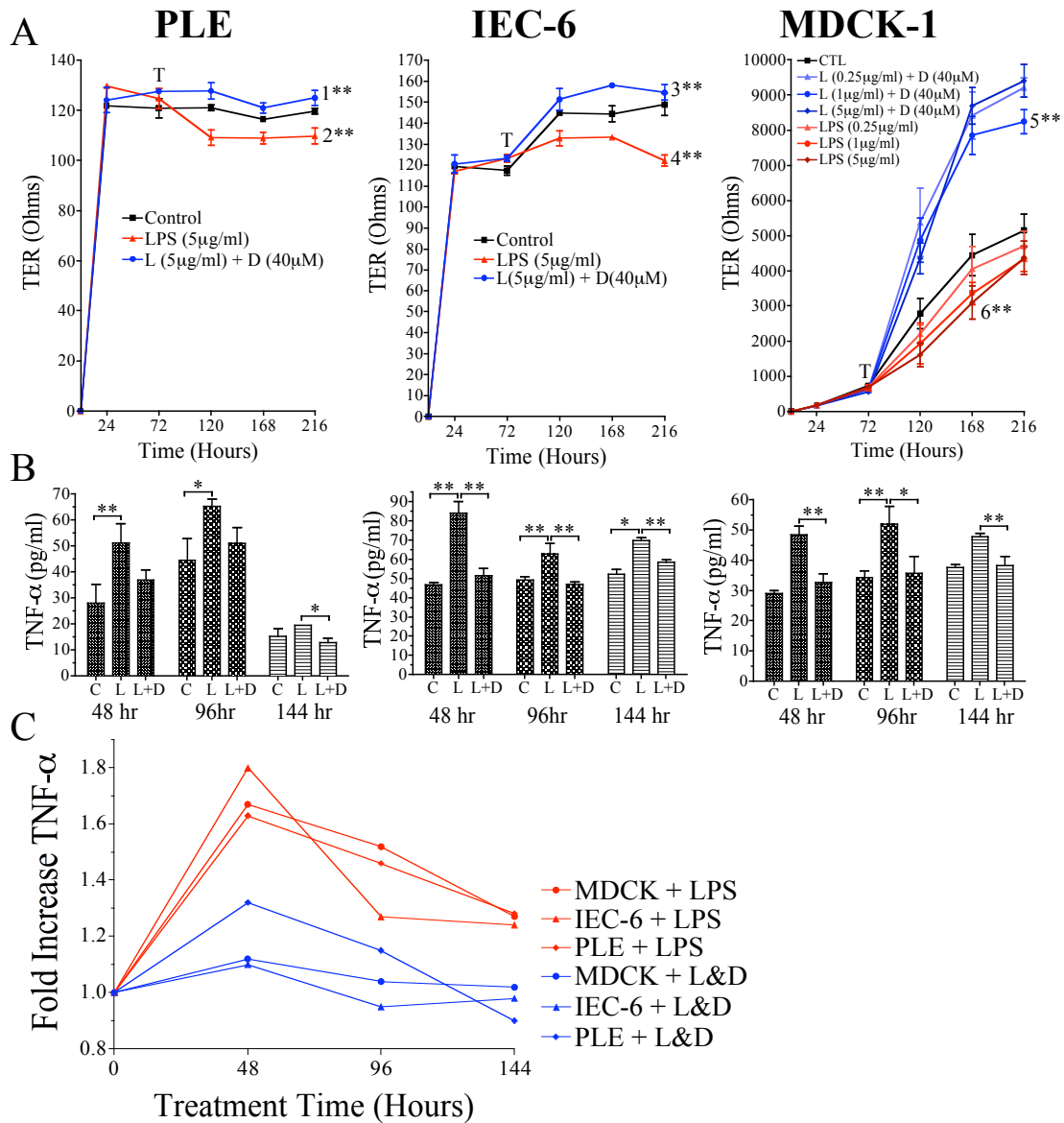
Figure 6. PLE, IEC-6 and MDCK-I barrier model treatment with (−)-deprenyl ± LPS

(A) PLE and IEC-6 were challenged at 72 hours **(T)** with LPS (L) ± (−)-deprenyl (D). MDCK-I cultures were treated with a concentration range of L ± D. TER changes were measured at 48, 96 and 144 hours of treatment. Analysis using One-way ANOVA with Tukey's test found notable significant differences between LPS 5μg/ml and L (5μg/ml) + D (40μM) (1**), LPS (2**) 5μg/ml and CTL, LPS 5μg/ml and L (5μg/ml) + D (40μM) (3**), L (5μg/ml) (4**) and CTL, LPS 1μg/ml and L (1μg/ml) + D (40μM) (5**) and LPS 5μg/ml (6**) and CTL. **(B)** Total TNF-α protein secretion was assayed by ELISA analysis of pooled and mixed apical and basal conditioned media. Significant difference between groups numbered and groups bordering bars (*p <0.05, **p<0.01). Data are presented as mean ± SD; n = 3. **(C)** Relative protein expression of TNF-α assayed in the conditioned media is presented as mean; n =3 of fold change over untreated controls.

64

Table 1. MAO inhibitor *in vitro* and *in vivo* effects

	In vitro Transwell™ MDCK-I culture			*In vivo* animal
	A. Barrier Effect	B. TNF-α Expression	C. AR Expression	D. Periodontal Disease
MAO-A/B				
Phenelzine	++	--	-	reduced
MAO-B				
Deprenyl	++	--	---	nd
Pargyline	+	-	-	nd
MAO-A				
Clorgyline	--	++	++	nd
Moclobemide (partial MAO-B inhibitor activity)	-/+ (higher concentration)	nd	nd	nd

In vitro Assays **(A, B and C)**: LPS reduced barrier formation as measured by TER and increased TNF-α and AR expression. Subsequently, the effect of a variety of MAO inhibitors was tested using these *in vitro* assays. MAO-A/B was effective at reconstituting the barrier that was reduced by LPS and also reduced LPS-mediated TNF-α and AR expression. The MAO-B (−)-deprenyl was as effective as the tested MAO-A/B inhibitor. The MAO-A inhibitors tended to work in an antagonistic manner. *In vivo* Disease Model **(D)**: Dr. Putnin's laboratory previously tested the change in disease using an *in vivo* rat periodontal disease model (Ekuni et al., 2009). Only MAO-A/B inhibitor was tested for reduction in disease and this was effective.

2.3.4 (−)-Deprenyl prevents LPS-induced loss of actin and E-cadherin at cell-cell junctions

As loss of E-cadherin-mediated adherence junctions is involved in epithelial barrier dysfunction (Goto et al., 2000; Zabner et al., 2003), the next experiment investigated the effect of LPS ± (−)-deprenyl on E-cadherin localization in the MDCK-I barrier model Transwell™ cultures. E-cadherin localization was determined by immunocytochemistry with antibody specificity to the extracellular domain of E-cadherin. After 6 days of chronic LPS ± (−)-deprenyl treatments, immunostaining of barrier model MDCK-I cultures grown on Transwell™ membranes showed that (−)-deprenyl prevented LPS-induced loss of intercellular E-cadherin at cell-cell contacts (Figure 7).

The cytoplasmic tail of E-cadherin, interacts directly with β-catenin. Furthermore, β-catenin interacts with α-catenin-1, which regulates local actin assembly and plays a significant role in the development of the perijunctional actomyosin ring. Thus, actin staining was performed on these cells to assess this important indirect interaction with E-cadheren. Actin immunostaining was localized at cell-cell junctions and remained stable after 6 days of LPS challenge (Figure 7). This suggests that LPS-induces loss of specific cell-cell junctions proteins, in this case E-cadherin and not actin. This finding also suggests that the cells were still viable and that the LPS concentration used (5μg/ml) to induce reduced TER and loss of E-cadherin cell-cell staining in these Transwell™ cultures was not inducing cellular apoptosis. This was confirmed in a corresponding cell proliferation assay of conditioned media collected from Transwell™ barrier model cultures at day 6 of treatment, which showed no difference in relative cell number between the treatment groups (Figure. 16A).
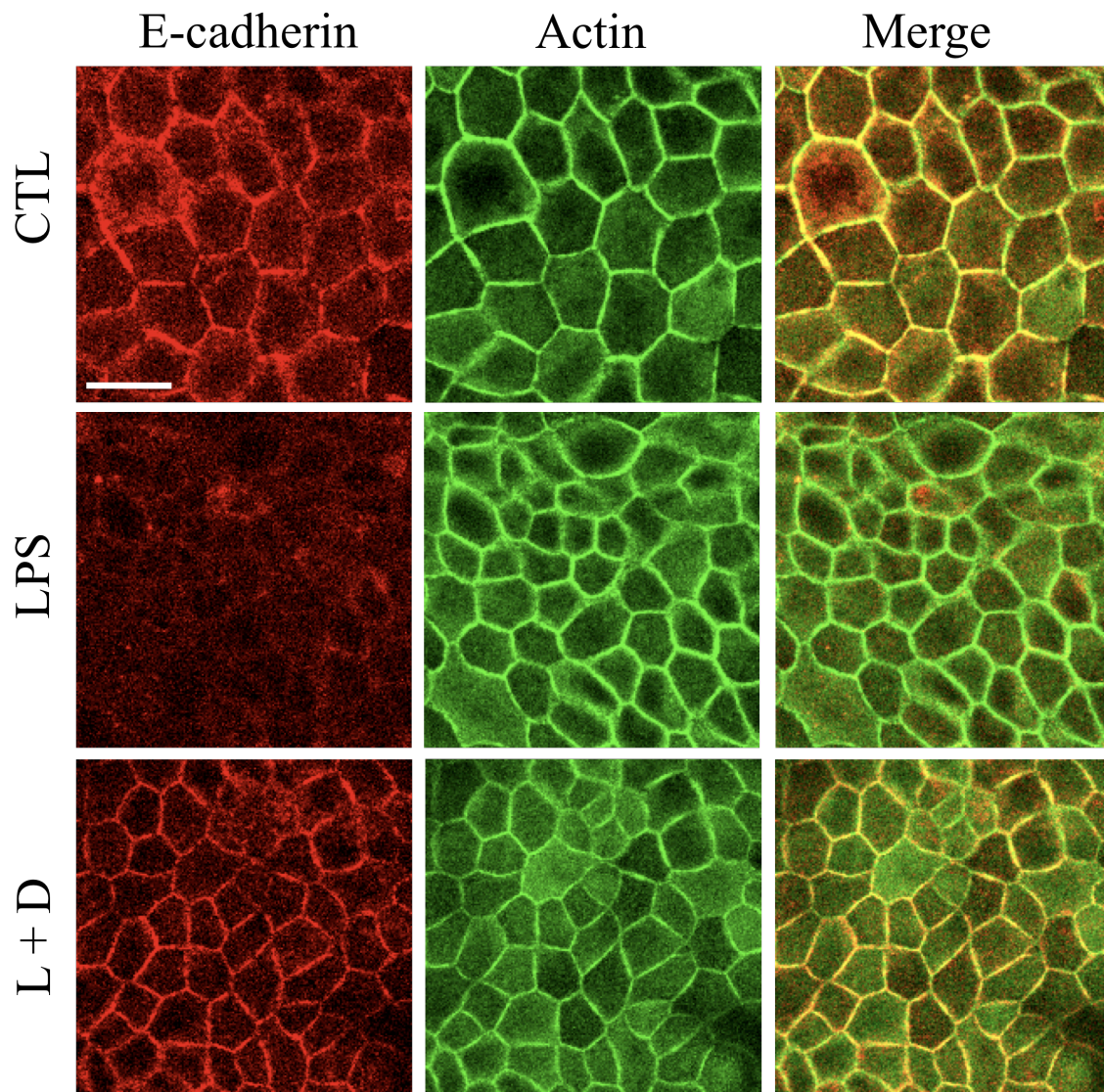
Figure 7. E-cadherin and actin immunostaining of MDCK-I barrier model cultures

Cells were fixed and immunostained at the final day 6 treatment time point of the epithelial barrier model. MDCK-I cultures were treated at 72 hours post cell plating with LPS (L) at 5μg/ml ± 40μM (−)-deprenyl (D) and chronic treatments continued every 48 hours as outlined in the barrier model protocol (Figure 3C). Bar = 50μm.

2.3.5 (−)-Deprenyl prevents LPS-induced loss of ZO-1 at tight junctions and increased ZO-1 immunostaining at these cell contact sites

ZO-1 was studied because this peripheral membrane component, plays a significant role in organizing tight junction assembly and maintenance, partly owing to the fact that this protein includes multiple domains for interacting with other proteins, including the transmembrane proteins claudin and occludin and cytoskeleton-associated actin (Turner, 2009). Immunostaining of MDCK-I cultures grown on Transwell™ membranes showed that at 6 days of chronic treatment, (−)-deprenyl prevented LPS-induced loss of ZO-1 and increased protein expression at apical tight junction contacts (Figure 8C). In addition, ZO-1 immunostaining was exclusively localized in the apical regions of the cell as shown in the z-axis images, suggesting that these MDCK-I cultures were polarized on these Transwell™ membranes (Figure 8C, z-axis images). These images are consistent with the results of the TER barrier experiment in Figure 6A from which these samples were collected. Comparing the TER data that corresponds to these immunostaining results suggests that disruption of ZO-1 immunostaining by LPS is associated with reduced TER. The finding that (−)-deprenyl increased ZO-1 immunostaining intensity at tight junction contact sites suggests that the increased TER measured in theses samples may be influenced by either upregulated ZO-1 protein expression at these sites or inhibition of the normal level of endocytotic cycling of ZO-1 away from tight junctions.
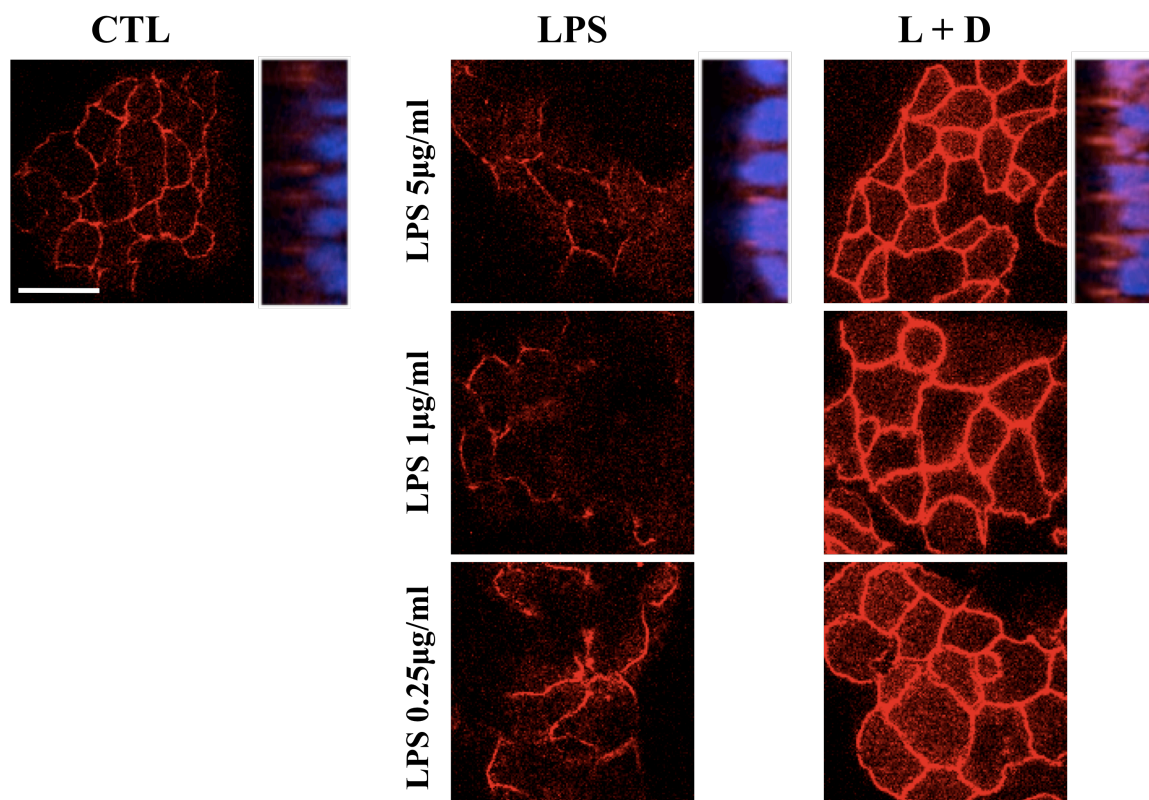
Figure 8. ZO-1 immunostaining of MDCK-I barrier model cultures

MDCK-Is were fixed and immunostained at day 6 of chronic treatment as outlined in the barrier model protocol (Figure 3C). Representative z-axis images of the control (CTL), LPS alone and LPS + (−)-deprenyl (L+D) treatment groups are presented alongside their corresponding x,y axis image. MDCK-I cultures were treated 72 hours after cell plating with a concentration range of LPS ± (−)-deprenyl and chronic treatments continued every 48 hours as outlined in the barrier model protocol (Figure 3C). Bar = 50μm.

2.3.6 Claudin immunostaining of MDCK-I and IEC-6 barrier model cultures at day 6 of chronic (−)-deprenyl ± LPS treatment

Claudins are transmembrane proteins associated with the epithelial tight junction and are important because they determine the extent of barrier. Different epithelial cell sheets have their own unique set of claudin species, and this compositional heterogeneity is now believed to explain the diversified barrier properties of tight junctions (Goodenough, 1999; Morita et al., 1999). Claudin proteins can exert a unique barrier property in terms of charge selectivity and size selectivity and that the combination and mixing ratios of claudins in a given cell type determine the overall barrier properties of its tight junctions.

MDCKs have most often been reported to express claudin 1 and 4 (Table 2). Thus, these proteins were analyzed by immunocytochemistry. Immunostaining of MDCK-I cultures grown on Transwell™ membranes showed that at 6 days of chronic treatment, (−)-deprenyl prevented LPS-induced loss of claudin-1 and -4 and increased claudin positive staining at pericellular and intracellular locations (Figure 9). Both pericelluar and intracellular claudin positive staining was increased in the (−)-deprenyl + LPS co-treatment samples relative to the other treatment groups (Figure 9). Despite this, our pericellular and intracellular claudin immunostaining results do not appear consistent with immunostaining results from previous studies, which show defined localization of claudins at cell-cell junctions (Wisner et al., 2008; Wang et al., 2009). Even so, the overall increase in claudin protein expression associated with chronic (−)-deprenyl treatment suggests an important area for future research. In particular, a future area of investigation may include screening of additional claudin proteins.

Rat colon epithelium is reported to express a multitude of different claudin proteins with claudin-1, -3 and -7 showing importance to barrier function in colonocytes (Table 2). As a result, immunocytochemistry was performed to analyze the expression of these tight junction proteins in the IEC-6 *in vitro* barrier model. Immunostaining of IEC-6 cultures grown on Transwell™ membranes showed that at 6 days of chronic treatment, (−)-deprenyl prevented LPS-induced loss of claudin-1, claudin-3 and claudin-4 and increased claudin positive staining (Figure 10). Similar to the MDCK-I samples, both pericellular and intracellular claudin positive immunostaining was increased in the (−)-deprenyl + LPS co-treatment samples relative to the other treatment groups (Figure 10). Lastly, the claudin distributions were again found to be inconsistent with previous reports of claudin immunostaining in IEC-6 cultures.
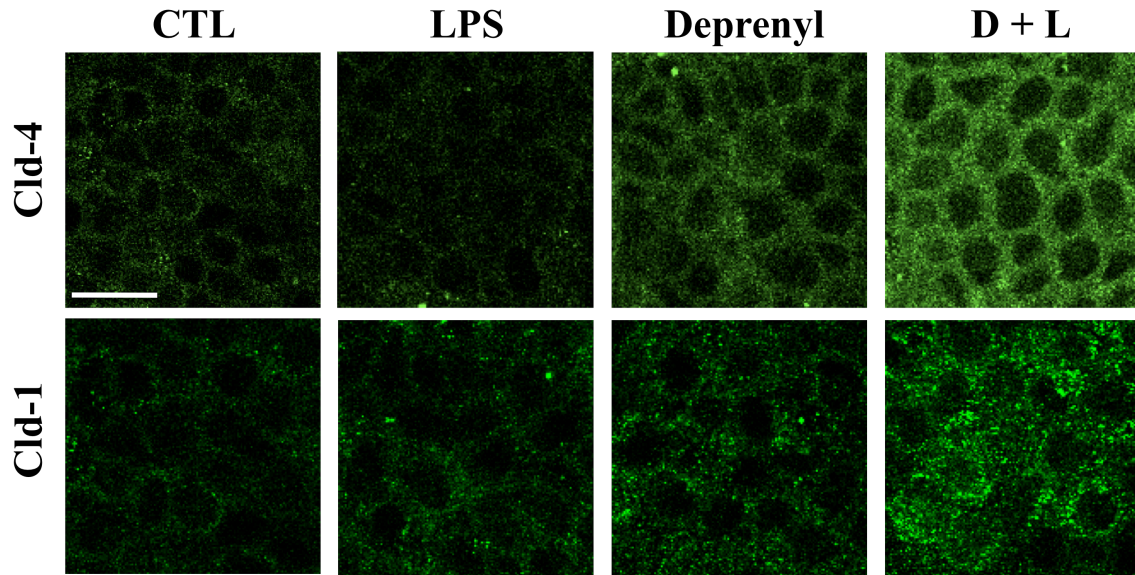
Figure 9. Claudin-1 and claudin-4 immunostaining of MDCK-I barrier model cultures

MDCK-Is were fixed and immunostained for claudin-1 (cld-1) and claudin-4 (cld-4) at day 6 of chronic treatment. The cultures were initially treated after 72 hours of cell plating with LPS (L) at 10μg/ml ± 10μM (−)-deprenyl (D) and chronic treatments continued every 48 hours as outlined in the barrier model protocol (Figure 3C). Bar = 50μm.
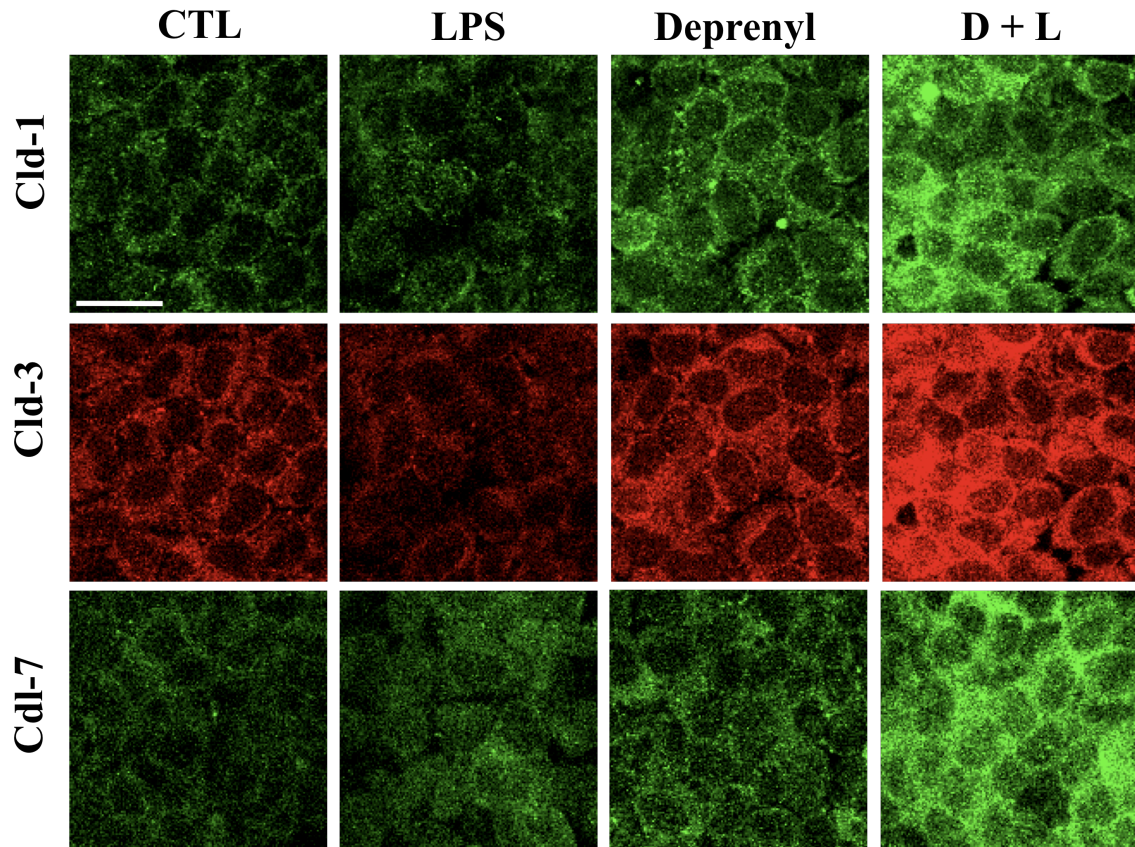
Figure 10. Claudin-1, claudin-3 and claudin-4 immunostaining of IEC-6 barrier model cultures

IEC-6s were fixed and immunostained for claudin-1 (cld-1), claudin-3 (cld-3) and claudin-7 (cld-7) at day 6 of chronic treatment. IEC-6 cultures were initially treated at 72 hours post cell plating with LPS (L) at 10μg/ml ± 10μM (−)-deprenyl (D) and chronic treatments continued every 48 hours as outlined in the barrier model protocol (Figure 3C). Bar = 50μm.

Table 2. Distribution of claudins expressed in different epithelial cell lines and tissues

Table reproduced with permission from Turksen and Troy, 2004.

Epithelial Cell Lines	Known Claudin Expression	Reference
IEC-6 (Rat intestinal epithelial cell line-6)	1, 2, 4	Poritz et al., 2004; Guo et al., 2003; Wang et al., 2009
MDCK (Madin-Darby canine Kidney)	1	Ohkubo and Ozawa, 2004
MDCK-I (Madin-Darby canine Kidney-1)	1, 4	Furuse et al., 2001; Sonoda et al., 1999
MDCK-II (Madin-Darby canine Kidney-II)	1, 2, 3, 4	Furuse et al., 2001; Singh and Harris, 2004
Caco-2 (Human colorectal adenocarcinoma-2)	1	Dorkoosh et al., 2004
T84 (Human colonic adenocarcinoma cell line)	1, 4	Bruewer et al., 2003
HMEC (Human mammary epithelial cells)	1	Swisshelm et al., 1999
Human retinal pigment epithelium	1, 3	Abe et al., 2003; Rajasekaran et al., 2003
COMMA-1D (Mouse epithelial mammary cells)	1	Stelwagen and Callaghan, 2003
HaCat (Human keratinocyte cells)	1, 3	Tebbe et al., 2002
Epithelial Tissues		
Skin epidermis	1, 2, 3, 4, 6, 8, 12, 17	Brandner et al., 2002 (human); Furuse et al., 2002 (mouse); Tebbe et al., 2002 (human); Turksen and Troy 2002 (mouse)
Human cornea epithelium	1, 2, 3, 7, 9, 14	Ban et al., 2003
Rat pancreatic duct epithelia	2, 3, 4	Rahner et al., 2001
Kidney distal tubule	1, 3, 8	Kiuchi-Saishin et al., 2002 (mouse); Reyes et al., 2002 (rabbit)
Kidney collecting duct	1, 3, 4, 8	Kiuchi-Saishin et al., 2002 (mouse); Reyes et al., 2002 (rabbit)

Table 2. Distribution of claudins expressed in different epithelial cell lines and tissues

Epithelial Tissues	Known Claudin Expression	Reference
Kidney proximal tubule	2, 10, 11	Kiuchi-Saishin et al., 2002 (mouse); Reyes et al., 2002 (rabbit)
Mouse vestibule sensory epithelium	1, 3, 9, 12, 14, 18	Kitajiri et al., 2004
Rat uterus epithelium	1	Orchard and Murphy, 2002
Human gut gastrointestinal mucosa	4	Nichols et al., 2004
Rat colon epithelium (colonocytes)	1, 2, 3, 4, 5, 7	Rahner et al., 2001; Zeissig et al., 2004; Guttman et al., 2006

2.3.7 AR immunostaining of MDCK-I and IEC-6 barrier model cultures at day 6 of chronic (−)-deprenyl ± LPS treatment

Immunostaining of AR in MDCK-I and IEC-6 Transwell™ barrier model cultures at day 6 of chronic (−)-deprenyl ± LPS treatment showed that (−)-deprenyl prevented LPS-induced loss of AR at locations normally localized pericellularly and increased protein expression at these sites (Figure 11). These results suggest that chronic LPS treatment either induces the release of AR from its attachment to the cell membrane and/or reduces the amount of AR expressed at these pericellular locations. This finding is consistent with previous literature demonstrating that LPS-induces AR release from epithelial cells (Brandl et al., 2010). Co-treatment with (−)-deprenyl may prevent this LPS-induced AR release from its cell attachment and/or upregulate the amount of AR expressed at these pericellular sites. In representative MDCK-I control samples, immunostaining of AR was localized pericellularly and displayed what appears to be intense localized intracellular staining. The pericellular and intracellular immunostaining of AR in (−)-deprenyl and (−)-deprenyl + LPS treated cultures was more prevalent in the representative samples in comparison to control samples. AR immunostaining in MDCK-I barrier model cultures was dramatically reduced with chronic LPS treatment over 6 days. IEC-6 AR immunostaining showed a similar pattern to the MDCK-I samples. In control samples, AR showed pericellular localization in the IEC-6 samples and in (−)-deprenyl and (−)-deprenyl + LPS treated cultures this staining pattern was more prevalent in the cells. Again, AR immunostaining was significantly lost with chronic LPS treatment over 6 days. These results suggest that AR protein expression may be upregulated in (−)-deprenyl treated cells or that the release of AR from its cell attachment is reduced by (−)-deprenyl treatment.
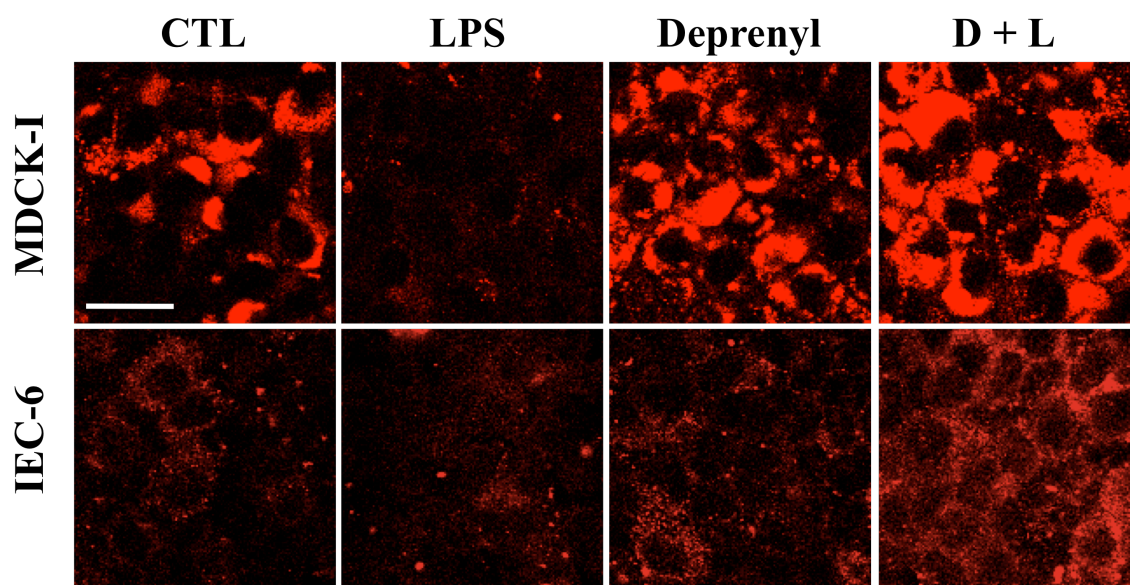
Figure 11. AR immunostaining of MDCK-I and IEC-6 barrier model cultures

MDCK-Is and IEC-6s were fixed and immunostained for AR at day 6 of chronic treatment. Cultures were initially treated after 72 hours of cell plating with 10μg/ml of LPS (L) ± 10μM (−)-deprenyl (D) and chronic treatments continued every 48 hours as outlined in the barrier model protocol (Figure 3C). Bar = 50μm.

2.3.8 AR and TNF-α ELISA analysis of conditioned media collected from MDCK-I barrier model cultures at day 2, 4 and 6 of LPS ± (−)-deprenyl chronic treatment

ELISA analysis of MDCK-I conditioned media collected from apical and basal Transwell™ chambers at 2, 4 and 6 days of LPS challenge was performed to investigate the release of AR and TNF-α in response to LPS ± (−)-deprenyl treatment (Figure 12 and Figure 13). LPS-treated MDCK-I cultures showed a concentration dependent total increase in AR protein secretion into the conditioned media, which was significantly induced ($p<0.05$) by 17% on day 2, 66% on day 4 and 105% on day 6 (Figure 12). In relation to AR protein secretion, a smaller but significant ($p<0.05$) total increase in TNF-α secretion into the conditioned media was induced by 34% on day 2 and 36% on day 4 but induction diminished to 18% above control by day 6 (Figure 13). This temporal pattern of LPS-induced TNF-α and AR secretion is consistent with previous studies that established TNF-α as an acute inflammatory mediator and AR as a chronic inflammatory mediator (Noti et al., 2010; Ulich et al., 1995; Nakagome and Nagata, 2011; Ungaro et al., 2009). Increasing LPS concentration and treatment duration correlated to both the extent of barrier loss (Figure 6A-MDCK-I barrier model) and total AR secretion (Figure 12). Co-treatment of LPS with (−)-deprenyl reduced the level of TNF-α secreted into the conditioned media (shown as percent reduction of amount induced by LPS) although the level reduced secretion was not significantly below the amount induced by LPS alone (Figure 13). Co-treatment of LPS with (−)-deprenyl also reduced the level of AR secreted into the conditioned media (Figure 12). Notably, this reduction in AR expression was more pronounced in comparison to (−)-deprenyl-induced TNF-α reduction in expression and was found to have protein expression significantly below control levels at all assay time points (Figure 12). LPS-induced AR was

predominantly secreted into the basal culture chamber whereas induced TNF-α secretion was more equally distributed between apical and basal directions (Figure 12 and Figure 13). Lastly, AR and TNF-α were both predominantly expressed in the basal compartment and (−)-deprenyl-associated reduction in both of these barrier mediators was far greater in the basal direction (Figure 12 and Figure 13). This finding that AR is predominately secreted in to the basal medium in MDCK-I cells is supported by previous studies of epithelial cells grown on Transwell™ membranes, which showed both AR cell-surface protein expression localized predominately in the basolateral domain of polarized epithelial cells and secretion of AR directed predominately towards the basal Transwell™ compartment (Damstrup et al., 1999; Brown et al., 1998). Furthermore, this pattern of accentuated AR secretion towards the basolateral Transwell™ compartment is supported by studies showing that the putative receptor for AR, called EGFR, is localized primarily in the basolateral domain of polarized epithelial cells (Rumelhard et al., 2007; Mascia et al., 2003) and the metalloprotease called TACE, which is responsible for cleaving and release of pro-AR into the active soluble form of AR, is also predominately localized basolateraly in polarized epithelial cultures (Merchant et al., 2008).
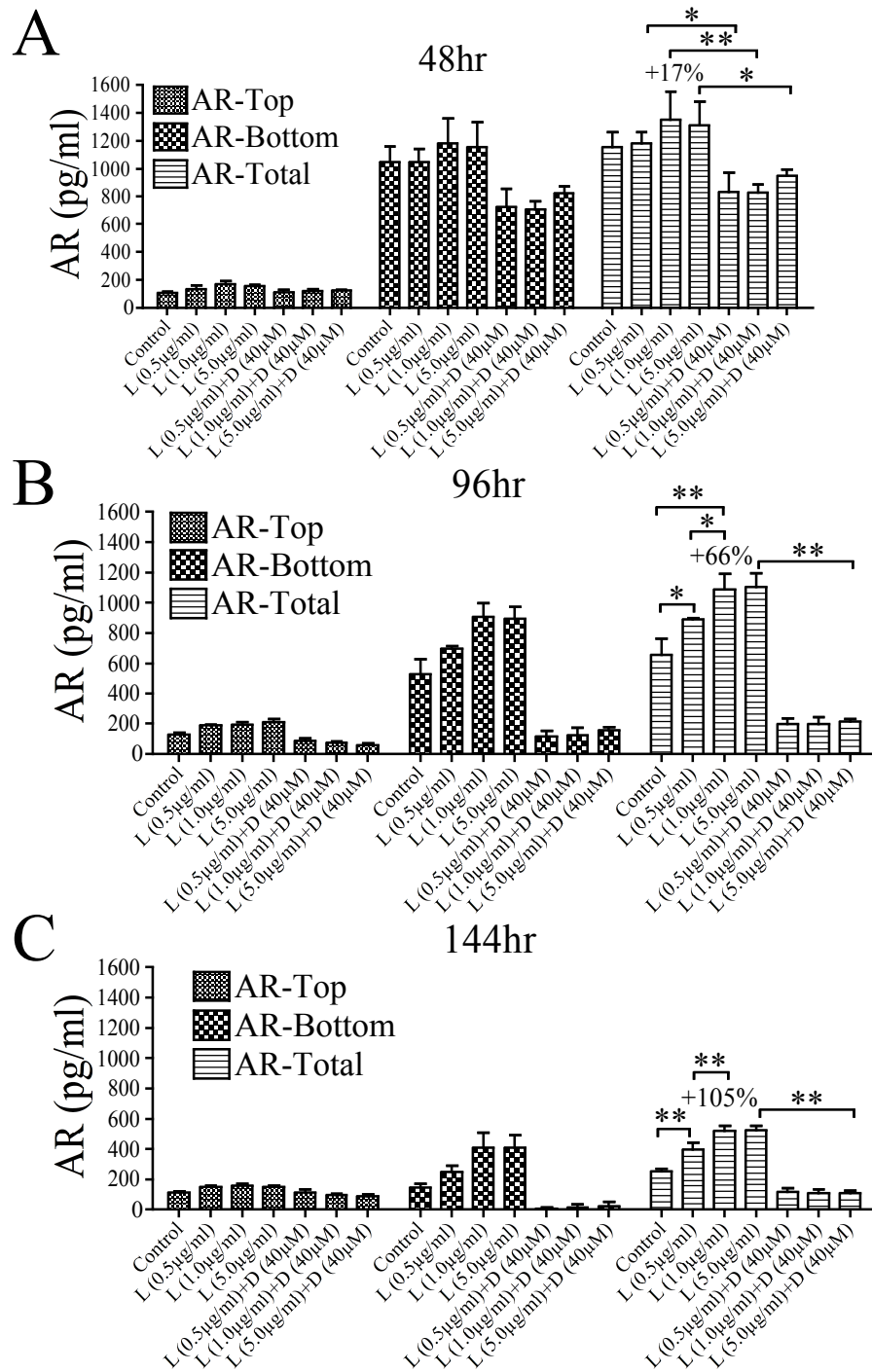
Figure 12. AR ELISA of LPS ± (−)-deprenyl treated MDCK-I barrier model

Conditioned media collected from apical and basal Transwell™ chambers at 2 **(A)**, 4 **(B)** and 6 **(C)** days of LPS (L) ± (−)-deprenyl (D) treatment. Percentage increase shown relative to control. One-way ANOVA with Tukey's test (* p<0.05, ** p<0.01).
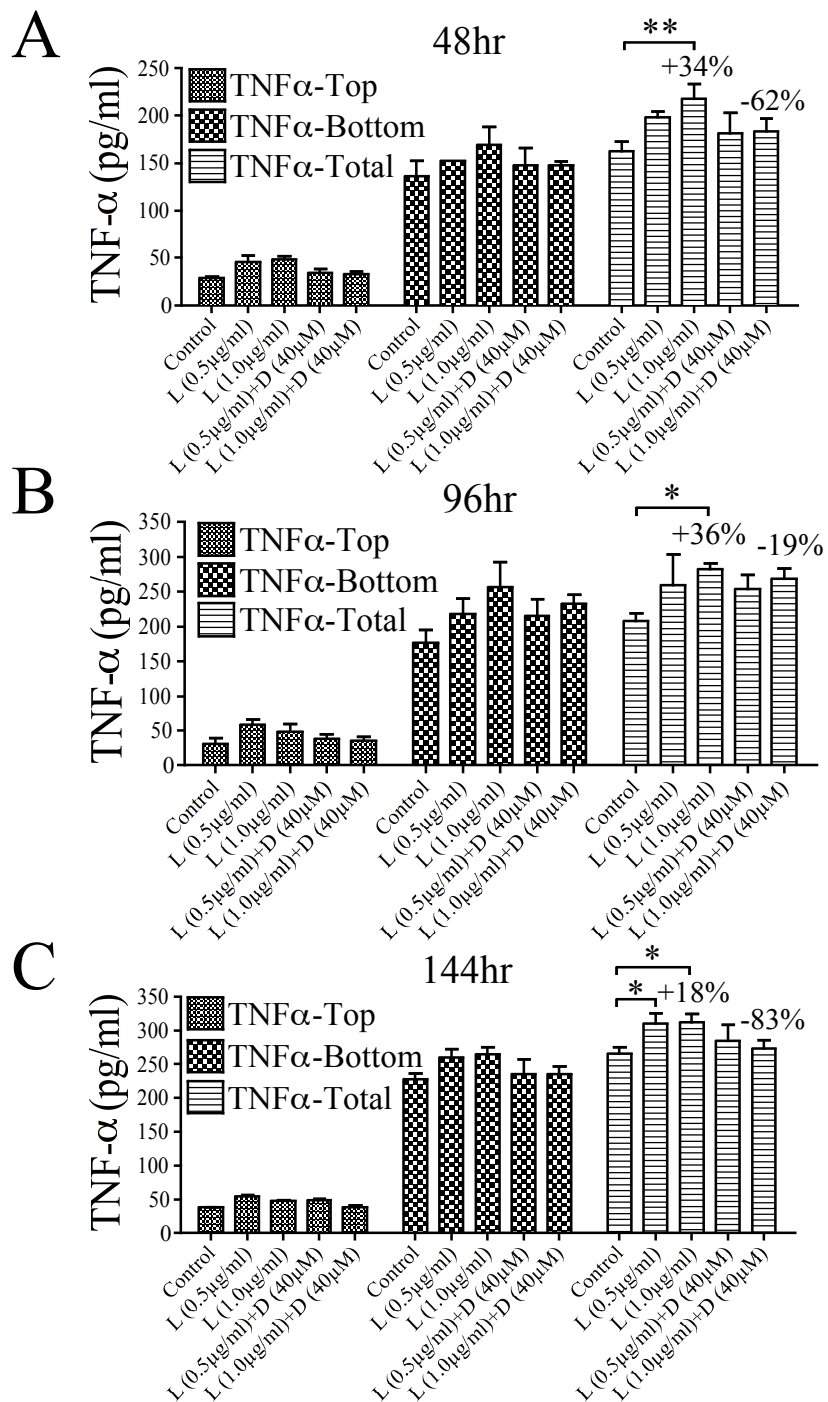
**Figure 13. TNF-α ELISA of LPS ± (−)-deprenyl treated MDCK-I barrier model**

Conditioned media collected from apical and basal Transwell™ chambers at 2 **(A)**, 4 **(B)** and 6 **(C)** days of treatment with a range of LPS (L) concentrations ± (−)-deprenyl (D). Percentage increase shown relative to control. Percentage decrease of amount induced shown. One-way ANOVA with Tukey's test (* p<0.05, ** p<0.01).

2.3.9 Exogenous mediators of *in vitro* barrier model ± (−)-deprenyl co-treatment

The next set of experiments was designed to study mediators of *in vitro* barrier, specifically AR and H_2O_2, which are proposed to act downstream in the epithelial response to LPS challenge. The previously established (−)-deprenyl-induced increase in MDCK-I TER (Figure 5A and Figure 6A) was attenuated by co-treatment of exogenous AR in a concentration dependent manner (Figure 14). Challenging the MDCK-I barrier model alone with exogenous AR resulted in a concentration dependent reduction barrier formation as measured by TER at 144 hours of treatment (Figure 14). In comparison to the AR treatments, TNF-α treatments produced dramatic reductions in TER (data not shown) that were significantly more pronounced in comparison to the previous barrier experiment that challenge barrier formation with these concentrations (Figure 4C). This was likely a result of employing a new stock solution of TNF-α that may of had greater TNF-α activity in comparison to the previous 'older' stock solution of TNF-α that was used in the previous TER experiment outlined in Figure 4C. With increasing concentration of AR, the (−)-deprenyl-induced increases in MDCK-I TER at 144 hours of treatment was progressively reduced suggesting that AR was able to override the induction of increased barrier by (−)-deprenyl treatment (Figure 14). This finding suggests that AR is a significant mediator of *in vitro* barrier integrity as measured by TER and that AR likely acts downstream of (−)-deprenyl.

We wanted to next investigate the impact on epithelial barrier TER caused by treatment with the proposed ROS signaling mediator H_2O_2 that induces the activation of downstream mediators of *in vitro* barrier, AR and TNF-α. H_2O_2-induced TER reduction in the MDCK-I barrier model with concomitant altered AR secretion was prevented by (−)-

deprenyl co-treatment (Figure 15). This finding suggests that (−)-deprenyl may inhibit the release of AR caused by H_2O_2 dependent mechanism. The concentration of H_2O_2 used in the study by Forsyth et al., 2007 is consistent with the 200 to 500 μM concentration used by other investigators in the initial discovery of oxidant-induced EGFR transactivation (Prenzel et al., 1999) as well as more recent intestinal epithelial cell studies by others (Song et al., 2006). We have found in this study and in previous studies this concentration does not affect cell viability (Figure 16D) (Banan et al., 2000a, Banan et al., 2000b).
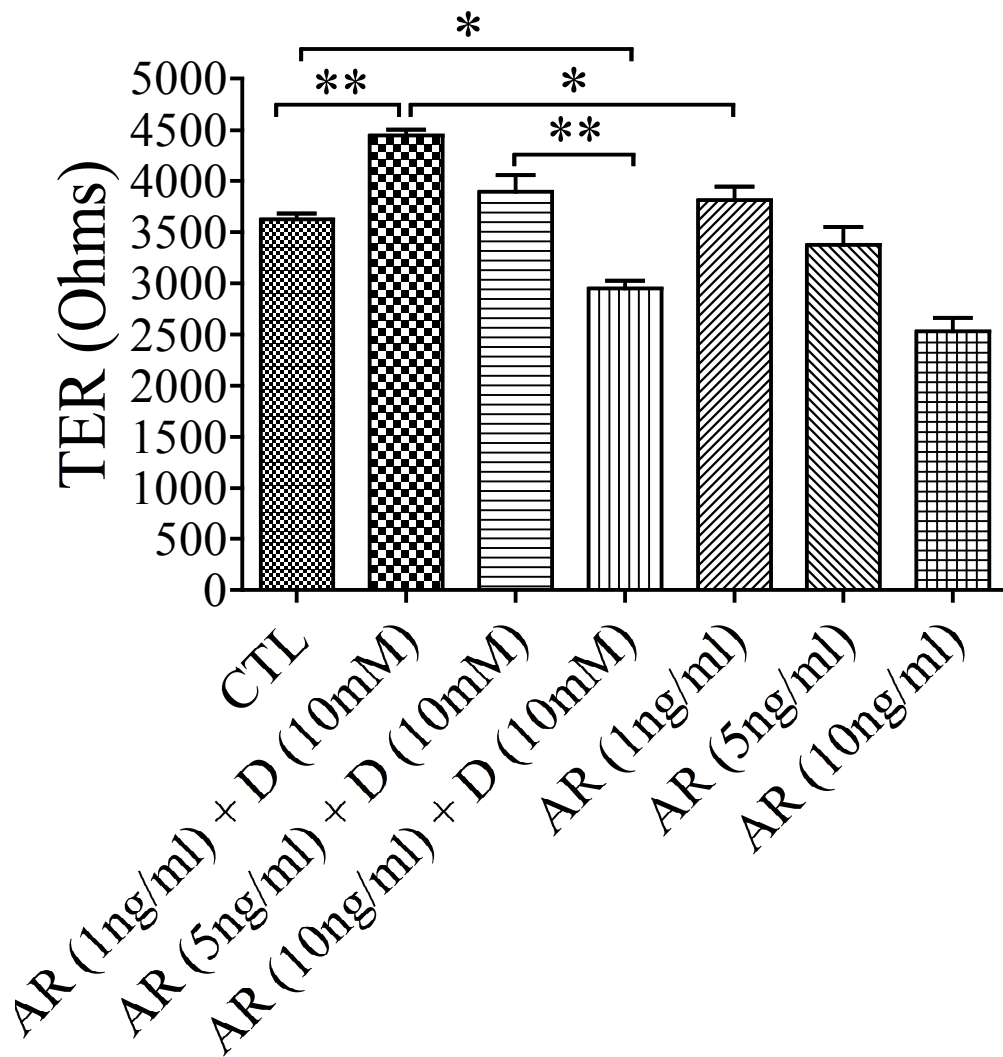
Figure 14. (−)-Deprenyl-induced increases in MDCK-I barrier model TER are attenuated by co-treatment of exogenous AR in a concentration dependent manner

MDCK-Is grown on Transwell™ membranes were challenged at 72 hours with a concentration range of AR ± (−)-deprenyl. Analysis of TER after 144 hours of treatment using One-way ANOVA with Tukey's test found notable significant differences between groups bordering bars (*p <0.05, **p<0.01). Data are presented as mean ± SD; n = 3.
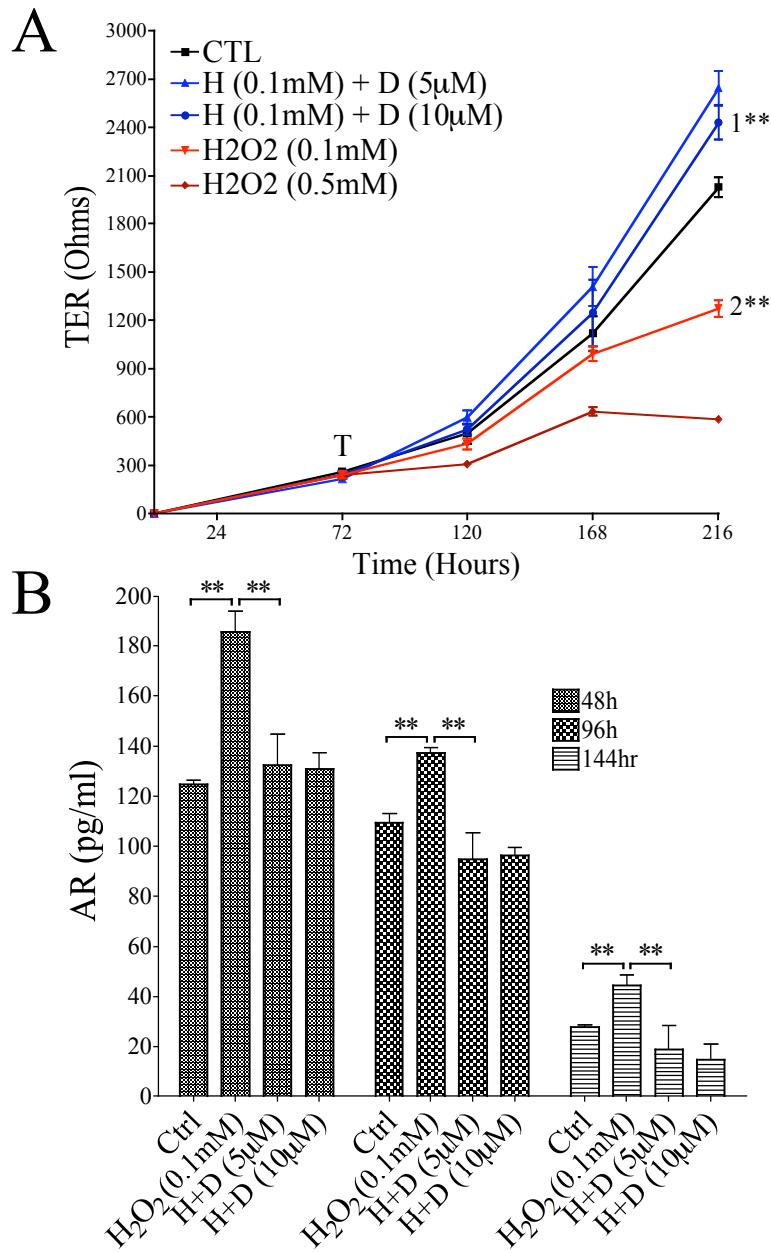
Figure 15. H_2O_2-induced TER reduction in the MDCK-I barrier model with associated increases in AR secretion was prevented by (−)-deprenyl co-treatment

MDCK-I Transwell™ barrier model cultures were treated at 72 hours **(T)** with various concentrations of H_2O_2 alone and 0.1mM H_2O_2 ± a range of (−)-deprenyl (D) concentrations. Analysis of 144-hour TER **(A)** using One-way ANOVA with Tukey's test found notable significant differences between 1) Control (CTL) and 10µM D + 0.1mM H_2O_2, 2) CTL and 0.1mM H_2O_2. AR secretion into the basal Transwell™ compartment was assayed by ELISA **(B)**. Significant difference between groups bordering bars and numbered (**p<0.01). Data are presented as mean ± SD; *n* = 3.

2.3.10 Proliferation assays of MDCK-I barrier model challenged with exogenous mediators of *in vitro* barrier model ± (−)-deprenyl co-treatment

MDCK-Is grown on Transwells™ membranes and treated at 72 hours with (A) LPS ± (−)-deprenyl showed differences in the level of cellular proliferation in the (−)-deprenyl alone and (−)-deprenyl + LPS treated groups (Figure 16A). This minor increase in relative cell number in (−)-deprenyl treated cells is consistent with literature that has established (−)-deprenyl as an anti-apoptotic agent (Toronyi et al., 2002; Wadia et al., 1998; Tatton et al., 1994; Magyar et al., 1998). Nonetheless, these differences were minor and do not appear sufficient to account for the dramatic increased in TER found in (−)-deprenyl treatment of the MDCK-I barrier model (Figure. 5A and Figure 6A). A concentration range of exogenous AR treatment induced no significant difference in the level of cellular proliferation (Figure 16B). Likewise, a concentration range of TNF-α and H_2O_2-induced no significant difference in cellular proliferation at lower concentrations but did exhibit a significant reduction at the higher treatment concentration (Figure 16C and D). These results suggest that the corresponding TER experiments (Figure 4B,C and Figure 15A) (corresponding LPS ± (−)-deprenyl TER experiment not shown), which showed a concentration dependent reduction in TER at these concentrations of *in vitro* barrier mediators, were not influenced by cellular apoptosis. Furthermore, these results suggest that the cells were viable at these treatment concentrations and the reduction of TER was largely a result of changes in the junctional components that mediate barrier function.
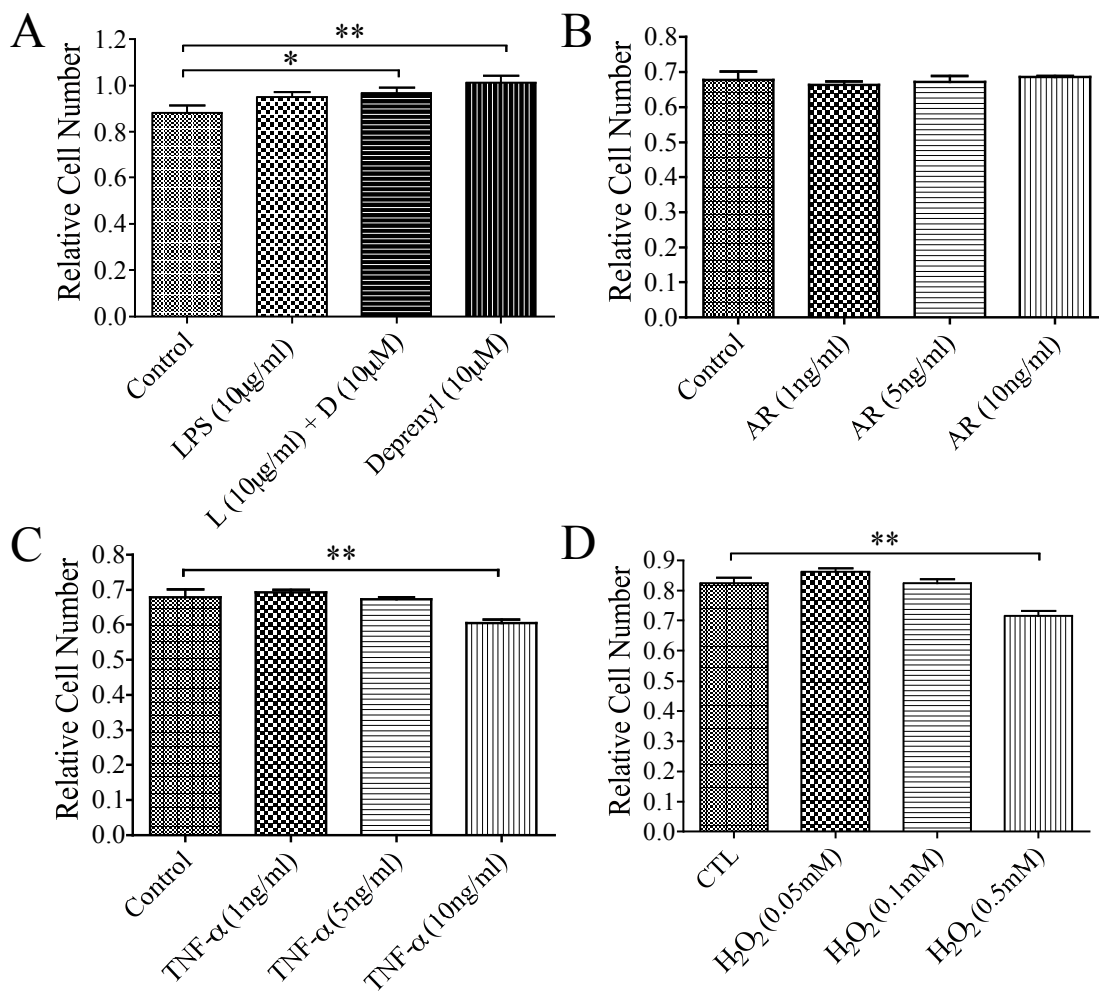
Figure 16. Cell proliferation assays of MDCK-I barrier model experiments

Transwell™ barrier model cultures of MDCK-Is were treated at 72 hours post cell plating with **(A)** LPS ± (−)-deprenyl (D) and a concentration range of exogenous AR **(B)**, TNF-α **(C)** and H_2O_2 **(D)**. At day 6 of chronic treatment, conditioned media from the apical and basal Transwell™ compartments were pooled, mixed and assayed. The absorbance at 490nm was measured directly from 96-well assay plates and is expressed as relative cell number. Significant differences between groups bordering bars (*$p < 0.05$, **$p < 0.01$). Data are presented as mean ± SD; $n = 3$.

3 Discussion

3.1 Background and Design of Epithelial Barrier Model

Onset of epithelial barrier disease is associated with a multitude of chronic inflammatory disorders (Fujita et al., 2010; Chung et al., 2005a; He et al., 2009; Kucharzik et al., 2001; Xavier and Podolsky, 2007; Sartor, 2006; Runswick et al., 2007; Balkovetz, 2009; Wine et al., 2009). Using an *in vivo* rat model of LPS-induced periodontal disease it has been demonstrated that chronic inflammation of oral junctional epithelia, which may be associated with barrier disruption, leads to LPS penetration to underlying stroma (Ekuni et al., 2009). Further support for this was provided in a recent immunostaining analysis of tight junction components that mediate epithelial barrier function in periodontal epithelium. This study showed loss of claudin-1 immunostaining in LPS-treated junctional epithelia (Fujita et al., 2011). Gene chip analysis of the junctional epithelia revealed disease-elevated MAO-B. These changes were associated with elevated ROS (H_2O_2) and TNF-α immunostaining *in vivo* and increased TNF-α release into the conditioned media of an *in vitro* PLE culture model of the junctional epithelium (Ekuni et al., 2009). Treatment with MAO inhibitor greatly ameliorated these disease indices (Ekuni et al., 2009). These findings were extended with gene chip analysis that showed AR, an EGFR ligand and downstream mediator of TNF-α (Chokki et al., 2006), as well as several other proteins modulating the EGFR pathway were altered in the LPS-induced periodontal disease model (Firth et al., 2011).

To study epithelial barrier responses to chronic LPS-induced inflammatory challenge, my project employed a timed epithelial cell culture model (Figure 3C), which offered several experimental advantages. 1) Application of LPS or inflammatory mediators TNF-α, AR or ROS mediator H_2O_2 every 48 hours for up to 216 hours (9 days) modeled loss

of barrier associated with chronic inflammation. 2) Concurrent application of MAO-A/B and MAO-B inhibitors was found to both protect against this loss of barrier and enhance barrier. Progression of the loss of a functional barrier could be monitored over many days of chronic challenge with barrier mediators of interest by analyzing TER changes in the Transwell™ epithelial cultures, altered secretion of endogenous mediators of epithelial barrier and alteration of the localization and accumulation of critical junctional markers of barrier integrity. This *in vitro* barrier model design permitted precise analysis of barrier formation specific to healthy and diseased epithelium. It also revealed the potential of MAO inhibitor treatment for therapeutic management of epithelial barrier diseases.

MDCK-I cells were employed in this study because they form cell culture barriers with high TER and, thus, are considered a 'Gold Standard' for analysis of TER responses to mediators of *in vitro* epithelial barrier. In this study, high TER was confirmed in cell culture experiments that compared the MDCK-I, PLE and IEC-6 barrier model responses to chronic LPS ± (−)-deprenyl treatment. PLE and IEC-6 barrier models exhibited significantly lower TER when compared to barriers produced by MDCK-Is, however, the impact of LPS ± (−)-deprenyl treatment on changes in both TER and TNF-α secretion was similar among these cell lines, suggesting that the epithelial responses to LPS ± (−)-deprenyl represent an epithelial-wide phenomenon. Further experiments in this study were restricted to using the MDCK-I barrier model since the TER effect sizes were considerably greater than that those found in the PLE and IEC-6 barrier models.

3.2 Epithelial Barrier Model Responses to MAO Inhibitor Treatment

To determine the effect of MAO inhibition in epithelial barrier TER, MDCK-I barrier model cultures were treated with the three classes of MAO inhibitors (MAO-A/B, MAO-B and MAO-A). These experiments showed that MAO-A/B and MAO-B inhibitor treatment of the epithelial barrier model induced dramatic increases in epithelial barrier formation as measured by TER. Associated with these increases in TER, was a significant reduction in the amounts of TNF-α and AR protein secreted by the barrier model cell cultures into the conditioned media. In contrast, MAO-A inhibitor treatment negatively affected barrier formation as measured by TER and this was associated with a significant concomitant increase in both TNF-α and AR protein secretion into the conditioned media (Figure 5B, C). Selective MAO-A inhibitors possess a detrimental side effect referred to as tyramine syndrome, which makes MAO-A inhibitors undesirable for clinical use (Youdim and Finberg, 1987; Palfreymann et al., 1988; Jarrott and Vajda, 1987). This side effect, also referred to as the 'cheese reaction', occurs when tyramine and other sympathomimetic amines, which are found in fermented foods such as cheese (Da Prada et al., 1988), enter the circulation and potentiate sympathetic cardiovascular activity by releasing noradrenaline. Selective irreversible MAO-B inhibitors, such as (−)-deprenyl, do not exhibit tyramine potentiation effects because the intestine contains relatively low levels of MAO-B and tyramine is effectively metabolized by intestinal MAO-A (Hasan et al., 1988). Since MAO-B inhibitors do not exhibit this negative side effect and because the selective MAO-B inhibitor (−)-deprenyl was shown to produce enhanced barrier formation as measured by increases in TER similar to treatment with the MAO-A/B inhibitor phenelzine, this study focused on the role of MAO-B inhibition by (−)-deprenyl in mediating *in vitro* epithelial

90

barrier. Further analysis was focused to validate (−)-deprenyl-induced increases in the epithelial barrier model TER by investigating cell-cell markers of functional tight junctions and adherens junctions and endogenous mediators of *in vitro* epithelial barrier function.

Treatment of the *in vitro* barrier model with (−)-deprenyl enhanced epithelial barrier integrity both by itself and by negating the reduction in barrier TER induced by chronic LPS, AR and H_2O_2 challenge. Associated with this (−)-deprenyl-induced barrier enhancement was a reduction in the level of endogenous protein secretion of critical downstream regulators of barrier integrity. Specifically, (−)-deprenyl-induced increases in MDCK-I barrier model TER were associated with both attenuated H_2O_2-induced AR protein secretion and attenuated LPS-induced AR and TNF-α protein secretion. In addition, this study employed histiotypic models of PLE, IEC-6 and MDCK-I epithelial barriers to demonstrate that (−)-deprenyl treatment enhanced barrier and prevented both LPS-induced barrier loss as measured by TER and LPS-induced TNF-α secretion in multiple epithelial cell types. This suggests that (−)-deprenyl increased TER and attenuated release of inflammatory cytokines may be an epithelial phenomenon. These findings are supported by a previous study that showed LPS-induced TNF-α was significantly reduced by co-treatment with the MAO-A/B inhibitor phenelzine in an *in vivo* rat periodontal disease model and this was associated with less inflammation and reduction in disease indices (Ekuni et al., 2009). Lastly, these findings clarify previously described protective effects of (−)-deprenyl in inhibiting vascular endothelial cell hyperpermeabilty after both hemorrhagic shock (Tharakan et al., 2010) and burn injury (Whaley et al., 2009). Notably, protective effects of (−)-deprenyl have been shown to be lost at higher treatment concentrations and these concentrations may be pro-apoptotic (Magyar and Szende, 2004). This study supports the possibility of (−)-deprenyl-

induced pro-apoptosis at higher concentrations by showing that *in vitro* epithelial barrier model TER was reduced in a concentration dependent manner at concentrations of ($-$)-deprenyl treatment greater than 40μM (data not shown).

The mechanism by which MAO up-regulation and subsequent therapeutic inhibition may mediate chronic inflammatory disease progression and prevention, respectively, is significant. It was previously suggested that remission of rheumatoid arthritis in patients taking MAO inhibitors was a result of inhibition of the synthesis of prostaglandin E_2 (Lieb, 1983). Two cases were described in which the MAO-A/B inhibitor phenelzine induced remission in patients exhibiting Crohn's disease, another chronic inflammatory disorder (Kast, 1998). It was postulated that MAO inhibitors may induce remission in these diseases by reducing TNF levels, but no evidence was produced (Altschuler, 2000). Even so, further evidence supports this hypothesis. For example, MAO-B levels are related to the pathogenesis of Parkinson's disease and up-regulation of TNF-α and interleukin-6 mRNA was elevated in the hippocampus of Parkinson's patients (Nagatsu and Sawada, 2006; Sawada et al., 2006). MAO-B inhibitors are effective for the treatment of Parkinson's disease, both through their direct effect on MAO-B and in part by activating multiple factors for anti-oxidative stress including anti-inflammatory cytokines (Nagatsu and Sawada, 2006).

3.3 Inflammatory Mediator Signaling Pathway and Barrier Disruption

Engagement of TLR4 with LPS induces dimerization by bringing together two signaling domains, which subsequently serve as a platform for the recruitment of various intracellular adaptor molecules. MyD88 is an adaptor used by TLR4 and functions to activate mitogen-activated protein kinases (MAPKs) and the transcription factors NF-κB, AP-1, IRF-5. These transcription factors induce expression of pro-inflammatory cytokine

genes (Lu et al., 2008) (Figure 17). The immune responses elicited by LPS-induced TLR4 activation represent a double-edged sword. In the context of local acute infection, TLR4-induced events are critical to immune defense and the survival of the host by functioning to provoke the innate immune response and enhance adaptive immunity against infection. Despite this, TLR4 activation by LPS often is debilitating, and sometimes fatal, in the context of systemic inflammation leading to sepsis, or in the setting of chronic inflammatory disease resulting in tissue damage (Zuany-Amorim et al., 2002). This study employed histiotypic models of PLE, IEC-6 and MDCK-I epithelial barriers to demonstrate that chronic treatment with LPS-induced barrier loss as measured by TER in multiple epithelial cell types. This suggests that LPS-induced loss of barrier may be an epithelial phenomenon.

LPS-induced loss of barrier model TER was associated with a concomitant increase in TNF-α and AR protein secretion into the conditioned medium. This finding is significant since metalloprotease-dependent AR release is understood to mediate TNF-α-induced IL-8 secretion in the human airway epithelial cell line NCI-H292, suggesting that TNF-α is an upstream mediator of AR activation (Chokki et al., 2006). It is possible that LPS binding to its putative TLR4 receptor on the surface of epithelial cells is eliciting a signaling cascade involving TNF-α-induced AR activation (Figure 17). Additionally, LPS induced a significant reduction of the immunostaining of AR protein accumulation at pericellular locations, which is consistent with established literature that suggests pro-AR may be released from its cell attachment into its diffusible active form by external stimuli such as LPS (Willmarth and Ethier, 2008). Co-treatment of the barrier model with LPS and the MAO-B inhibitor (−)-deprenyl prevented this LPS-induced loss in TER, attenuated the induction of AR secretion into the conditioned medium and prevented the LPS-induced loss of pericellular AR

immunostaining in barrier model cultures. This study addresses the underlying mechanism by which (−)-deprenyl mediates a protective role against bacterial virulence factor-induced disruption of epithelial barrier and points to a significant role for AR as a central mediator of barrier integrity.

It has been previously shown that H_2O_2 was elevated in diseased junctional epithelial tissues in a LPS-treated cell culture model of chronic inflammatory periodontitis (Ekuni et al., 2009). Moreover, H_2O_2 along with other ROS participate in cell signaling and/or injury (Thannickal et al., 2000). Consistent with these findings, chronic exogenous H_2O_2 treatment of our MDCK-I barrier model reduced TER in a concentration dependent manner and was associated with concomitant upregulation of AR release into the conditioned media. Co-treatment of the barrier model with the MAO-B inhibitor (−)-deprenyl prevented this H_2O_2-induced loss in TER and attenuated the induction of AR secretion into the conditioned medium. This increase in AR protein secretion induced by chronic ROS (H_2O_2) treatment is supported by previous studies of EGFR signal transactivation that have showed ROS mediate the activity of TACE, which in turn cleave membrane-anchored AR proligand into a soluble ligand that binds the EGFR leading to receptor dimerization and activation (Shao and Nadel, 2005; Singh et al., 2009). In addition, studies of smoke triggered EGFR transactivation in lung epithelial cells have provided evidence for a signaling mechanism in lung epithelial cells that includes generation of oxygen radicals (including H_2O_2) by smoke particles and associated stimulants such as LPS, which in turn stimulate TACE to cleave transmembrane AR, which in turn promotes binding of soluble AR to the EGFR that leads to upregulated cell proliferation (Lemjabbar et al., 2003; Baginski et al., 2006). The NOX family of NADPH oxidases participates in the production of ROS (Bedard and Krause,

2007). Nox enzymes share the capacity to transport electrons across the plasma membrane and to generate superoxide and other downstream ROS. The core component of Nox is the catalytic subunit glycoprotein p91^{phox}, and several homologs have been identified in various cell types (Cheng et al., 2001; Lambeth, 2002). Activation of TLR4 by LPS generates ROS (Asehnoune et al., 2004) and a study by Park et al., 2004 reported that TLR4 has a direct interaction with Nox enzymes. This interaction is essential for LPS-induced ROS production and activation of NF-κB (Figure 17). Recently, a homolog of the gp91^{phox}, Duox1, was identified in epithelial cells and was found to be involved in the LPS-induced generation of H_2O_2 through a PKC-αβ dependent signaling mechanism (Geiszt et al., 2003; Koff et al., 2009) (Figure 17). In support of a role for PKC in LPS-induced barrier loss, it has been shown that MAO-A and MAO-B genes exhibit difference in their core promoter regions, which is suggested to account for the varying effects of some specific ligands on the differential expression of the *MAO-A* and *MAO-B* genes. Interestingly, expression of MAO-B, but not MAO-A, is specifically regulated by a mitogen-activated protein kinase (MAPK) pathway that includes PKC (Shih et al., 1999; Zhu et al., 1994; Wong et al., 2002). In addition, a previous microarray analysis has shown that LPS-induced periodontal disease is associated with significant MAO-B upregulation and not MAO-A upregulation in diseased epithelial tissues (Ekuni et al., 2009). These findings are consistent with an LPS-induced barrier loss may be mediated by a PKC-dependent upregulation of MAO-B activity (Figure 17). Furthermore, a recent study that employed a gastric epithelial cell line supports the involvement of PKC in the ROS-mediated metalloprotease activation and sequential ectodomain shedding of AR (Kishida et al., 2005). These findings are supported in our barrier model study, which clearly showed that MAO-B inhibition by (−)-deprenyl reduced

both H_2O_2 and LPS-induced AR activation and associated epithelial barrier loss induced by H_2O_2 and LPS.

TNF-α and oxidants such as H_2O_2 are widely acknowledged as key pro-inflammatory factors involved in mediating tissue alterations associated with chronic inflammatory diseases such ulcerative colitis and Crohn's disease (Podolsky, 2002; Farhadi et al., 2003). Indeed, anti-TNF-α (Zeissig et al., 2004) or antioxidant (Keshavarzian et al., 1992) therapies have been shown to be effective in the treatment of IBD. A previous study employed a cell culture model of the junctional epithelium to demonstrate that H_2O_2 induces TNF-α protein expression in a concentration-dependant manner, and it can be effectively inhibited by treatment with the H_2O_2 antagonist catalase and the ROS scavenger *N*-acetylcysteine (Ekuni et al., 2009). In addition, in lung epithelial cells, a smoke triggered cell proliferation mechanism has been demonstrated that includes generation of oxygen radicals (including H_2O_2), which in turn stimulate TACE to cleave transmembrane AR to enable binding of AR to the EGFR and induced epithelial cell proliferation (Lemjabbar et al., 2003). Moreover, it has been established that LPS-induced ROS coordinates TNF-α production through IκB kinase complex regulation of transcription factor NF-κB (Figure 17) (Sanlioglu et al., 2001). Increased TNF-α activity during inflammation may be due to post-translational activation of the pro-hormone rather than transcriptional upregulation. Indeed, a previous study demonstrated that neither microarray nor RT-qPCR data revealed any significant changes in *Tnfa* transcription in a LPS-induced rat periodontal disease model (Ekuni et al., 2009). Among candidates for LPS-induced TNF-α converting enzyme function in mouse myeloid cells *in vivo* is primarily ADAM 17 (TACE), although ADAM 10 and ADAM 19, matrix metalloproteinase 7 and proteinase 3 are also TNF-α converting enzyme candidates

(Horiuchi et al., 2007). TNF-α is also known to stimulate TACE expression in a kind of vicious circle (Black et al., 1997). A previous microarray of a rat periodontal disease model showed moderate increase in ADAM 10 (1.82-fold) and ADAM 17 (1.16-fold) (Ekuni et al., 2009). The elucidation of TNF-α and AR activation by ADAMs in our *in vitro* epithelial barrier model remains a subject for further enquiry. Lastly, A recent study provided the novel finding that oxidant-induced barrier hyperpermeability and tissue injury in chronic inflammatory disease is partly dependent on TACE metalloproteinase-mediated transactivation of EGFR signaling (Forsyth et al., 2007).

This study addresses, for the first time, the underlying mechanism by which (−)-deprenyl mediates a protective role against bacterial virulence factor-induced epithelial barrier disruption and points to a significant role for AR as a central mediator of barrier integrity. The data from this study provides evidence for AR acting as the critical EGFR ligand that mediates loss of epithelial barrier. The key points of this proposed model are summarized in Figure 17. The model begins with LPS-induced oxidant stress (1), resulting in activation of the metalloproteinase TACE (2). Activated TACE then cleaves membrane AR to a soluble form (3) that binds to the EGFR. EGFR activation then results in downstream MAPK/ERK1/2 activation (4). ERK1/2 signaling (5) then results in increased intestinal permeability (6) by pathways that have yet to be identified.
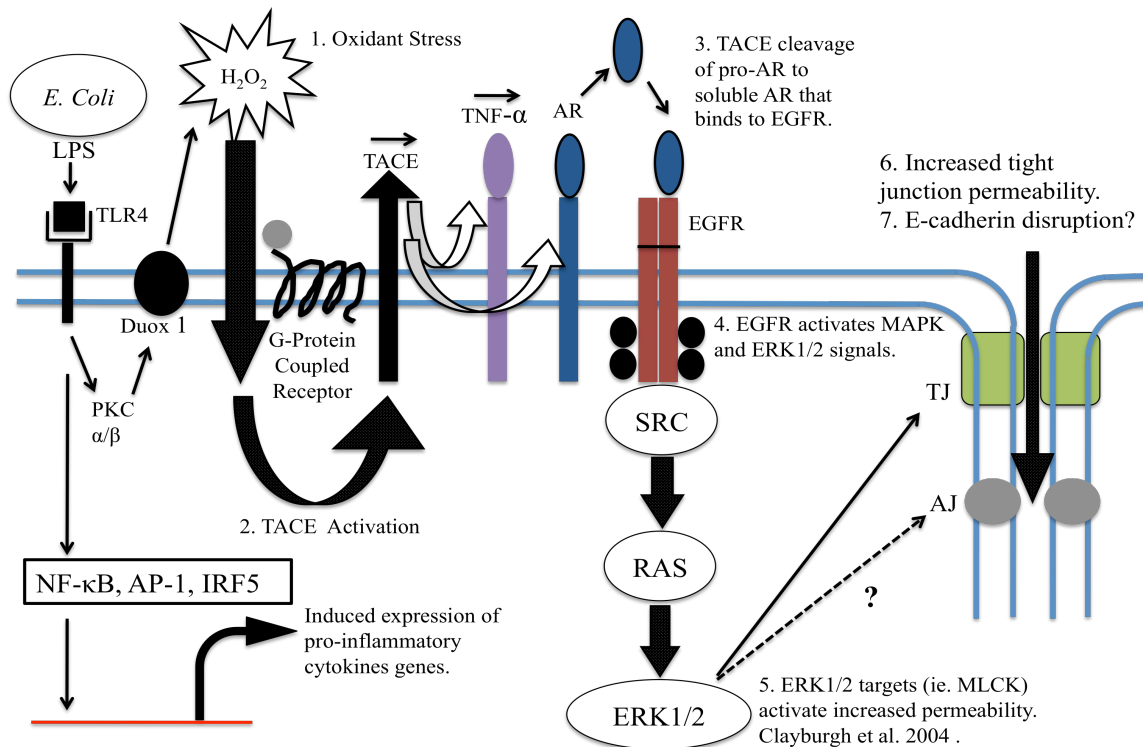
Figure 17. Proposed signaling model for AR-mediated EGFR regulation of epithelial barrier permeability in response to LPS-induced oxidant stress

The schematic depicts the elements proposed in a mechanism for epithelial barrier hyperpermeability induced by LPS-mediated oxidant stress (Reproduced with permission from Forsyth et al., 2007). Proposed steps are numbered in order of occurrence. **1)** The process begins with LPS-induced H_2O_2 (oxidant stress) via a Nox enzyme called Duox-1. This initiates both cell-surface signals through TACE activation (Koff et al., 2006) and induces pro-inflammatory gene expression by activation of the transcription factors NF-κB, AP-1 and IRF-5 (Lu et al., 2008) **2)** TACE activation. **3)** TACE activation results in translocation to cell-cell contact zones where it cleaves AR pro-ligand to form soluble AR that is able to bind to the EGFR. TACE also mediates TNF-α activation, which has been previously demonstrated to be an upstream signaling event involved in AR activation (Chokki et al., 2006) **4)** EGFR becomes phosphorylated and activates downstream MAPK signals including ERK1/2. **5)** Activated ERK1/2 then phosphorylate cellular targets that mediate barrier permeability. **6)** These ERK1/2 targets then mediate changes in intestinal permeability. **7)** Activation of the EGFR has also been shown to disrupt E-cadherin expression and localization, which affects cell-cell adhesion and further potentiating the loss of tight junction-mediated barrier function (Chung et al., 2005a; Chung et al., 2005b).

3.4 Analysis of Epithelial Junction Proteins Involved in Barrier Function

Immunostaining analysis of integral markers of tights junctions and adherens junctions in barrier model cell cultures suggested that (−)-deprenyl treatment might enhance barrier integrity by mediating ZO-1 and E-cadherin protection from LPS-induced disruption at cell-cell junctions. In addition, LPS-induced alteration of the immunostaining of AR and claudin protein accumulation at pericellular locations was attenuated by (−)-deprenyl co-treatment. This study addresses the underlying mechanism by which (−)-deprenyl mediates a protective role against bacterial virulence factor-induced disruption of key tight junction and adherens junctions components and points to a significant role for AR as a central mediator of barrier integrity.

A previous study employed an AR expressing transgenic mouse model (INV-AR mouse) to investigate the contribution of upregulated AR in altering the integrity of cell–cell junctions associated with pathogenesis of the chronic inflammatory condition psoriasis. This study showed that components of adherens junctions (E-cadherin, P-cadherin, α- and β-catenin) and tight junctions (ZO-1 and ZO-2) were downregulated in the involved skin of the INV-AR mouse compared with site-matched skin taken from a non-transgenic littermate (Chung et al., 2005a). Our study supports this finding of downregulation of tight junction and adherens junction components by AR. Immunostaining analysis of integral markers of tight junctions and adherens junctions in our MDCK-I barrier model cell cultures showed that LPS-mediated reduction in TER was associated with disruption of ZO-1 and E-cadherin accumulation at cell-cell junctions and this was also associated with increased TNF-α and AR secretion into the conditioned media. In addition, LPS-induced a significant reduction of the immunostaining of AR protein accumulation at pericellular locations, which is consistent

with established literature that suggests pro-AR may be released from its cell attachment into its diffusible active form by external stimuli such as LPS (Willmarth and Ethier, 2008).

Several studies have suggested that AR might have a unique effect on E-cadherin expression and localization. In support of this, our study found that chronic LPS treatment of the MDCK-I barrier model reduced E-cadherin immunostaining at cell-cell junctions and this was associated with increased AR secretion into the conditioned media. In addition, (−)-deprenyl co-treatment ameliorated this loss of E-cadherin and this was associated with significant reduction in AR secretion. E-cadherin is a structural protein that mediates cell-cell adhesion and supports development of tight junctions. E-cadherin expression was found to be down regulated in keratinocytes of mice that over express AR (INV-AR mice) and AR was involved in processing E-cadherin to an 80kDa form in psoriatic lesions of these mice. In addition, treatment of MDCK cells with AR stimulated their motility up to two-fold more than another EGFR ligand called TGF-α due to a relocalization and downregulation of E-cadherin (Chung et al., 2005a). Treatment of MDCK cells with AR-induced a spindle-like morphology that was associated with relocalization of E-cadherin at sites of cell-cell contact (Chung et al., 2005b).

Tight junctions and adherens junctions regulate cell–cell adhesion and barrier function of simple polarized epithelia. These junctions are positioned in the apical end of the lateral plasma membrane and form the so-called apical junctional complex (AJC). In this study, immunostaining analysis of the MDCK-I barrier model cultures confirmed this localized apical staining of the peripheral-associated tight junction ZO-1 (Figure 8). Studies on the molecular mechanisms that regulate tight junctions have shown that actomyosin contraction, which is mediated by myosin II regulatory light chain (MLC) phosphorylation

through MLCK, is a primary force that regulates acute tight junctions under physiological conditions (Shen, 2009). Studies have also indicated that pro-inflammatory cytokines such as TNF-α and IL-1β induce tight junction dysfunction in an MLCK-dependent manner in both cultured epithelial cells and mouse intestines (Al-Sadi et al., 2008; Ma et al., 2005). Furthermore, MLCK activation has been implicated in human diseases such as IBD based on clinical evidence showing patients' samples have increased MLC phosphorylation and MLCK expression. These findings suggest that MLCK-mediated breaching of cell-cell junctions is a significant pathogenic element in chronic inflammatory disease progression. In my study, it is possible, although no experiments were performed, that MLCK is involved in the alteration of barrier integrity induced by mediators of *in vitro* barrier. Future analysis is required to assess the role of MLCK in mediating the barrier integrity of our epithelial model as assessed by both changes in TER, mediators of *in vitro* barrier and markers of functional tight junctions and adherens junctions. For instance, future studies should investigate the role of MLCK activation in (−)-deprenyl treated epithelial barrier models and its relevance to the dramatic increases in TER.

The AJC is a highly dynamic entity, undergoing rapid remodeling during normal epithelial morphogenesis and under pathologic conditions. There is growing evidence that remodeling of the AJC is mediated by internalization of junctional proteins (Ivanov et al., 2005). For example, live-cell fluorescence imaging and analyses of frozen jejunum sections from mice revealed that occludin and ZO-1 concentrate at tight junctions but are dynamically internalized from these cell-cell junctions upon treatment with TNF-α (Schwarz et al., 2007; Shen et al., 2008). Disruption of epithelial barrier properties and cell–cell adhesion by various pathogenic stimuli including cytokines, growth factors, oxidative stress

and bacterial and viral toxins has been shown to result in endocytosis of adherens junction and tight junction proteins. For example, oxidative stress triggers internalization of endothelial VE-cadherin (Kevil et al., 1998) and epithelial E-cadherin (Rao et al., 2002) as well as internalization of epithelial tight junction proteins, occludin and ZO-1 (Basuroy et al., 2003) Furthermore, internalization of the AJC components has been described as a result of bacterial or viral invasion of epithelial monolayers. Examples include cytosolic translocation of adherens junction proteins by *Listeria innocula* (Lecuit et al., 2000; Sousa et al., 2004) as well as internalization of occludin induced by *Escherichia coli* or *Clostridial* toxins, (McNamara et al., 2001; Nusrat et al., 2002) rotavirus (Obert et al., 2000) and dengue virus (Talavera et al., 2004). In my study, immunostaining of chronically treated MDCK-I barrier model cultures showed significant disruption of E-cadherin, ZO-1 and claudins, which supports these previous findings.

Several mechanisms can mediate disassembly of the epithelial AJC. The first mechanism implies expressional downregulation of junctional proteins. Another mechanism suitable for rapid disassembly of the AJC involves endocytosis of tight junction and adherens junction proteins. In this study, immunostaining analysis of the MDCK-I barrier model cultures showed that the peripheral-associated tight junction protein ZO-1 was disrupted at the apical tight junction and (−)-deprenyl treatment by itself or with co-treatment of LPS ameliorated this disruption. In addition, (−)-deprenyl treatment induced a significant increase in the immunostaining of ZO-1 at the apical tight junction. This suggests that (−)-deprenyl is suppressing the normal downregulation of this junctional protein and/or that (−)-deprenyl treatment is disrupting normal endocytosis and is effectively trapping ZO-1 at the apical tight junction. Further studies must be conducted to determine the mechanism

causing this (−)-deprenyl-induced increase in ZO-1 staining at the apical tight junction, especially since this is associated with a dramatic increase in the level of TER and may be a principle event that is inducing this dramatic TER increase since ZO-1 functions as an integral scaffolding protein which organizes and thus mediates the barrier function of the tight junction.

Claudins are transmembrane proteins associated with the epithelial tight junction and play a significant role in establishing the extent of epithelial barrier integrity. Different epithelial cell sheets have their own unique set of claudin species, and this compositional heterogeneity is believed to explain the diversified barrier properties of tight junctions (Goodenough, 1999; Morita et al., 1999). Claudin proteins can exert a unique barrier property in terms of charge selectivity and size selectivity and the combination and mixing ratios of claudins in a given cell type determine the overall barrier properties of its tight junctions. In this study, fixed IEC-6 and MDCK-I barrier model cultures were immunostained for specific claudin proteins that were previously determined to be highly expressed and confer barrier function in these particular cell lines and corresponding epithelial tissue types (Table 2). In both cell lines, (−)-deprenyl treatment induced increases in intracellular and pericellular claudin protein expression, suggesting that the increased TER associated with these cultures may be a result of increased transmembrane claudin expression producing enhanced sealing of the paracellular flux pathway. Pores that are formed by tight junction-associated claudin proteins are primary determinates of charge selectivity along the paracellular pathway (Amasheh et al., 2002; Colegio et al., 2003; Simon et al., 1999) and based on our immunostaining results, it is possible that an increase in claudin expression is altering the pore structure and thus influencing paracellular flux. Our

pericellular and intracellular claudin immunostaining results do not appear consistent with

immunostaining results from previous studies (Wisner et al., 2008; Wang et al., 2009),

which show highly defined localization of claudins at cell-cell junctions. Even so, the overall

increase in claudin protein expression associated with chronic (−)-deprenyl treatment

suggests an important area for future research. Studies of claudin upregulated expression

using epithelial cell lines do have their limitations. Specifically, upregulation of exogenous

claudins affects the expression and function of endogenous claudins (Yu et al., 2003) and the

effects of exogenous claudins on tight junction permeability are dependent on the types of

claudin endogenously expressed in the analyzed cells (Van Itallie et al., 2003). Nevertheless,

taking the results of these types of study together, it seems that each claudin can exert a

unique barrier property in terms of charge selectivity and size selectivity and that the

combination and mixing ratios of claudins in a given cell type determine the overall barrier

properties of its tight junctions (Furuse and Tsukita, 2006).

3.5 Conclusions

In conclusion, this study provides evidence that both MAO-B inhibition by (−)-

deprenyl and MAO-A/B inhibition by phenelzine induces dramatic increases in epithelial

barrier integrity as measured by TER. (−)-Deprenyl-induced increases in MDCK-I TER

were associated with concomitant reduction in TNF-α and AR protein secretion into the

conditioned media, increased immunostaining of ZO-1 at tight junctions and increased

pericellular immunostaining of endogenous AR and claudin proteins. Progression of MDCK-

I barrier loss induced by exogenous treatment of LPS and downstream signaling mediators

H_2O_2 and AR could be prevented or reduced by (−)-deprenyl co-treatment. (−)-Deprenyl co-

treatment also prevented LPS-induced loss of E-cadherin and ZO-1 immunostaining at cell-

cell junctions and AR and cluadin-1 immunostaining at pericellular locations. MAO-A inhibitor treatment was found to negatively impact MDCK-I barrier model TER with concomitant increases in AR and TNF-α protein secretion. Since selective MAO-A inhibitors are associated with the negative side effect called tyramine syndrome, this barrier model data supports the focused development of MAO-B inhibitors as a potential clinical treatment for barrier disease. The mechanism by which (−)-deprenyl alleviates the symptoms of chronic inflammatory diseases may largely be a reduction in the levels of MAO-B produced ROS molecules (in this case H_2O_2) that can induce expression of both pro-inflammatory cytokines and downstream barrier mediators. In particular, (−)-deprenyl-mediated attenuation of LPS- and H_2O_2-induced AR release appears to significantly regulate barrier, however, other mechanisms mat be involved. In summary, this study proposes a model in which MAO-B inhibition by (−)-deprenyl mediates AR-dependent EGFR transactivation in response to LPS and H_2O_2. This may be an important mechanism mediating epithelial barrier loss in chronic inflammatory disease.

3.6 Future Directions

Clinical use of MAO-B inhibitors is currently limited to anti-depression and Parkinson's therapy and their use for epithelial barrier protection requires modification to reduce or eliminate access across the blood-brain barrier. The global aim of future research is the development of enhanced MAO-B inhibitors that may provide an effective clinical treatment for epithelial barrier disease.

1. Future studies could perform animal testing of novel MAO inhibitors as a step towards the development of a clinical treatment for epithelial barrier disease. These experiments could

use an established mouse model of intestinal barrier disease to test the *in vivo* effectiveness of novel MAO inhibitors in re-establishing epithelial barrier. These studies could further characterize the novel drugs for reductions to crossing the blood-brain barrier, optimal doses and possible toxicity and side effects.

2. The functional examination of the epithelial barrier can be accomplished through a variety of means. One of the most common involves the use of TER. Although this is a relatively simple method to examine electrical conductivity between epithelial compartments, its specificity in accurately examining the integrity of the tight junctions has come into question, as TER does not always correspond to tight junction porosity (Stevenson et al., 1988; Gonzàlez-Mariscal et al., 1989). Despite this, TER remains an important tool as a preliminary indicator of barrier function.

This project provides preliminary evidence that ($-$)-deprenyl treatment induced increases in TER in an epithelial barrier model (Figure 5 and Figure 6). As a confirmation of the barrier maintenance, a future study should utilize molecular tracers to visually examine the integrity of the barrier. This may be performed by adding FITC conjugated 10kD dextran (Invitrogen) to the apical compartment of the monolayers, fixing the samples and examining the permeation of the dextran between the cells that form the monolayer (Umeda et al., 2006; Furuse et al., 2001). Once examined, these experiments can also be performed in conjunction with claudin or ZO-1 antibody localization.

3.To follow up on the results of this study, which established that MAO inhibitors attenuate LPS-induced TNF-α and AR protein levels and re-establishes control cell-cell contacts,

future studies could employ an *in vitro* model of epithelial barrier to determine the precise mechanism and point of action of MAO inhibitors on suppression of the inflammatory pathways associated with supporting barrier function at the levels of gene transcription, protein function and intercellular signaling pathways.

4. Future studies could use the knowledge gained from determining the precise mechanism of MAO inhibitors to develop novel MAO inhibitors designed specifically for the treatment of inflammatory epithelial barrier disease. Novel MAO inhibitors will be designed and synthesized to target specific molecular determinants of epithelial barrier loss and will also incorporate modifications that reduce or eliminate the drug from crossing the blood-brain barrier.

References

Actis GC, Rosina F, Mackay IR. Inflammatory bowel disease: beyond the boundaries of the bowel. *Expert. Rev. Gastroenterol. Hepatol*. 2011; **5**(3): 401-10.

Akagi M, Yokozaki H, Kitadai Y, Ito R, Yasui W, Haruma K, et al. Expression of amphiregulin in human gastric cancer cell lines. *Cancer* 1995; **75**(6 Suppl):1460–1466.

Akalın FA, Baltacıoğlu E, Alver A, Karabulut E. Lipid peroxidation levels and total oxidant status in serum, saliva and gingival crevicular fluid in patients with chronic periodontitis. *J. Clin. Periodontol.* 2007; **34**:558–565.

Akira S, Uematsu S, Takeuchi O. Pathogen recognition and innate immunity. *Cell* 2006; **124**:783-801.

Al-Sadi R, Ye D, Doklandy K, Ma TY. Mechanism of IL-1beta-induced increase in intestinal epithelial tight junction permeability. *J. Immunol.* 2008; **180**:5653-5661.

Alto NM, Shao F, Lazar CS, Brost RL, Chua G, Mattoo S, McMahon SA, Ghosh P, Hughes TR, Boone C, Dixon JE. Identification of a bacterial type III effector family with G protein mimicry functions. *Cell* 2006; **124**:133-145.

Altschuler EL. Monoamine oxidase inhibitors in rheumatoid arthritis— anti-tumor necrosis factor? *Int. J. Immunopharmacol.* 2000; **5**:353–357.

Amano M, Ito M, Kimura K, Fukata Y, Chihara K, Nakano T, Matsuura Y, Kaibuchi K. Phosphorylation and activation of myosin by Rho-associated kinase (Rho-kinase). *J. Biol. Chem.* 1996; **271**(34):20246–20249.

Amasheh S, Meiri N, Gitter AH, Schoneberg T, Mankertz J, Schulzke JD, Fromm M. Claudin-2 expression induces cation-selective channels in tight junctions of epithelial cells. *J. Cell Sci.* 2002; **115**:4969-4976.

Anderson MC, Hasan F, McCrodden JM, Tipton KF. Monoamine oxidase inhibitors and the cheese effect. *Neurochem. Res.* 1993; **18**:1145-1149.

Andoh T, Chock PB, Murphy DL, Chiueh CC. Role of the redox protein thioredoxin in cytoprotective mechanism evoked by (-)-deprenyl. *Mol. Pharmacol.* 2005; **68**(5):1408-1414.

Angelow S, Yu AS. Claudins and paracellular transport: an update. *Curr. Opin. Nephrol. Hypertens.* 2007; **16**:459-464.

Angelow S, Yu AS. Structure-function studies of claudin extracellular domains by cysteine-scanning mutagenesis. *J. Biol. Chem.* 2009; **284**:29205–29217.

Arbeloa A, Bulgin, RR, MacKenzie G, Shaw RK, Pallen MJ, Crepin VF, Berger CN, Frankel G. Subversion of actin dynamics by EspM effectors of attaching and effacing bacterial pathogens. *Cell. Microbiol.* 2008; **10**:1429–1441.

Arrieta MC, Madsen K, Doyle J, Meddings JB. Reducing small intestinal permeability attenuates colitis in the IL-10 gene-deficient mouse. *Gut* 2008; **58**:41–48.

Asehnoune K, Strassheim D, Mitra S, Kim JY, Abraham E. Involvement of reactive oxygen species in Toll-like receptor 4-dependent activation of NF-B. *J. Immunol.* 2004; **172**:2522–2529.

Baert FJ, D'Haens GR, Peeters M, Hiele MI, Schaible TF, Shealy D, Geboes K, Rutgeerts PJ. Tumour necrosis factor α antibody (infliximab) therapy profoundly downregulates the inflammation in Crohn's ileocolitis. *Gastroenterology* 1999; **116**(1):22–28.

Baginski TK, Dabbagh K, Satjawatcharaphong C, Swinney DC. Cigarete smoke synergistically enhances respiratory mucin induction by proinflammatory stimuli. *Am. J. of Respir. Cell Mol. Biol.* 2006; **35**:165-174.

Baker OJ, Camden JM, Redman RS, Jones JE, Seye CI, Erb L, Weisman GA.
Proinflammatory cytokines tumour necrosis factor-α and interferon-γ alter tight
junction structure and function in the rat parotid gland Par-C10 cell line. *Am. J.
Physiol. Cell Physiol.* 2008; **295**(5):C1191–C1201.

Balkovetz DF. Tight junction claudins and the kidney in sickness and in health. *Biochim
Biophys. Acta*. 2009; **1788**(4):858-863.

Banan A, Zhang Y, Losurdo J, Keshavarzian A. Carbonylation and disassembly of the F-
actin cytoskeleton in oxidant induced barrier dysfunction and its prevention by
epidermal growth factor and transforming growth factor alpha in a human colonic cell
line. *Gut* 2000a; **46**(6):830-837.

Banan A, Choudhary S, Zhang Y, Fields JZ, Keshavarzian A. Oxidant-induced intestinal
barrier disruption and its prevention by growth factors in a human colonic cell line:
role of the microtubule cytoskeleton. *Free Radic. Biol. Med.* 2000b; **28**(5):727-738.

Banan A, Fields JZ, Zhang Y, Keshavarzian A. Key role of PKC and Ca2+ in EGF
protection of microtubules and intestinal barrier against oxidants. *Am. J. Physiol.
Gastrointest. Liver Physiol.* 2001; **280**(5):G828-843.

Banan A, Zhang LJ, Farhadi A, Fields JZ, Shaikh M, Keshavarzian A. PKC-beta1 isoform
activation is required for EGF-induced NF-kappaB inactivation and IkappaBalpha
stabilization and protection of F-actin assembly and barrier function in enterocyte
monolayers. *Am. J. Physiol. Cell Physiol.* 2004; **286**(3):C723-738.

Banan A, Zhang LJ, Farhadi A, Fields JZ, Shaikh M, Forsyth CB, Choudhary S,
Keshavarzian A. Critical role of the atypical {lambda} isoform of protein kinase C
(PKC-{lambda}) in oxidant-induced disruption of the microtubule cytoskeleton and

barrier function of intestinal epithelium. *J. Pharmacol. Exp. Ther.* 2005; **312**(2):458-471.

Basuroy S, Sheth P, Kuppuswamy D, Balasubramanian S, Ray RM, et al. Expression of kinase-inactive c-Src delays oxidative stress-induced disassembly and accelerates calcium-mediated reassembly of tight junctions in the Caco-2 cell monolayer. *J. Biol. Chem.* 2003; **278**:11916–11924.

Basuroy S, Seth A, Elias B, Anjaparavanda P, Naren A, Rao R. MAP kinase interacts with occludin and mediates EGF-induced prevention of tight junction disruption by hydrogen peroxide. *Biochem. J.* 2006; **393**:69–77.

Bedard K, Krause KH. The NOX family of ROS-generating NADPH oxidases: physiology and pathophysiology. *Physiol. Rev.* 2007; **87**(1):245-313.

Bibiloni R, Fedorak RN, Tannock GW, Madsen KL, Gionchetti P, et al. 2005. VSL#3 probiotic-mixture induces remission in patients with active ulcerative colitis. *Am. J. Gastroenterol.* 2005; **100**:1539–46.

Birks J, Flicker L. Selegiline for Alzheimer's disease. *Cochrane Database Syst. Rev.* 2000; **2**: CD000442.

Black RA, Rauch CT, Kozlosky CJ, Peschon JJ, Slack JL, Wolfson MF, Castner BJ, Stocking KL, Reddy P, Srinivasan S, et al. A metalloproteinase disintegrin that releases tumor-necrosis factor-alpha from cells. *Nature (Lond)* 1997; **385:**729–733.

Blair SA, Kane SV, Clayburgh DR, Turner JR. Epithelial myosin light chain kinase expression and activity are upregulated in inflammatory bowel disease. *Lab. Invest.* 2006; **86**:191-201.

Blaschuk OW, Rowlands TM. Plasma membrane components of adherens junctions. *Mol. Membr. Biol.* 2002; **19**:75–80.

Blobel CP. ADAMs: key components in EGFR signalling and development. *Nat. Rev. Mol. Cell Biol.* 2005; **6**:32– 43.

Bosshardt DD, Lang NP. The junctional epithelium: from health to disease. *J. Dent. Res.* 2005; **84**:9-20.

Brandl K, Sun L, Neppl C, Siggs OM, Le Gall SM, Tomisato W, Li W, Du X, Maennel DN, Blobel CP, Beutler B. MyD88 signaling in nonhematopoietic cells protects mice against indued colitis by regulating specific EGF receptor ligands. *PNAS* 2010; **107**(46):19967-19972.

Brown CL, Meise KS, Plowman GD, Coffey RJ, Dempsey PJ. Cell surface ectodomain cleavage of human amphiregulin precursor sensitive to a metalloprotease inhibitor. Release of a predominant N-glycosylated 43-kDa soluble form. *J. Biol. Chem.* 1998; **273**(27):17258-17268.

Brown GR, Lindberg G, Meddings J, Silva M, Beutler B, Thiele D. Tumor necrosis factor inhibitor ameliorates murine intestinal graft-versus-host disease. *Gastroenterology* 1999; **116**:593–601.

Brown SL, Riehl TE, Walker MR, Geske MJ, Doherty JM, Stenson WF, Thaddeus S. Stappenbeck TS. Myd88-dependent positioning of Ptgs2-expressing stromal cells maintains colonic epithelial proliferation during injury. *J. Clin. Invest.* 2007; **117**:258-269.

Bruewer M, Luegering A, Kucharzik T, Parkos CA, Madara JL, Hopkins AM, Nusrat A. Proinflammatory cytokines disrupt epithelial barrier function by apoptosis-independent mechanisms. *J. Immunol.* 2003; **171**:6164–6172.

Bruewer M, Utech M, Ivanov AI, Hopkins AM, Parkos CA, Nusrat A. Interferon-γ induces internalization of epithelial tight junction proteins via a macropinocytosis-like process. *FASEB J.* 2005; **19**(8):923–933.

Brunette DM, Melcher AH, Moe HK. Culture and origin of epithelium-like and fibroblast – like cells from porcine periodontal ligament explants and cell suspensions. *Archs. Oral Biol*. 1976; **21**:393-400.

Brynskov J, Foegh P, Pedersen G, Ellervik C, Kirkegaard T, Bingham A, Saermark T. Tumour necrosis factor alpha converting enzyme (TACE) activity in the colonic mucosa of patients with inflammatory bowel disease. *Gut* 2002; **51**(1):37-43.

Bush KT, Tsukamoto T, Nigam SK. Selective degradation of E-cadherin and dissolution of E-cadherin-catenin complexes in epithelial ischemia *Am. J. Physiol. Renal Physiol*. 2000; **278**(5):F847–F852.

Carlile GW, Chalmers-Redman RM, Tatton NA, Pong A, Borden KE, Tatton WG. Reduced apoptosis after nerve growth factor and serum withdrawal: conversion of tetrameric glyceraldehyde-3 phosphate dehydrogenase to a dimer. *Mol. Pharmacol.* 2000; **57**: 2-12.

Carrillo MC, Kanai S, Nokubo M, Kitani K. (-) deprenyl induces activities of both superoxide dismutase and catalase but not of glutathione peroxidase in the striatum of young male rats. *Life Sci.* 1991; **48**(6):517-521.

Carrillo MC, Kitani K, Kanai S, Sato Y, Ivy GO. The ability of (-)deprenyl to increase

superoxide dismutase activities in the rat is tissue and brain region selective. *Life Sci.* 1992; **50**(25):1985-1992.

Carrillo MC, Kanai S, Sato Y, Nokubo M, Ivy GO, Kitani K. The optimal dosage of (-) deprenyl for increasing superoxide dismutase activities in several brain regions decreases with age in male Fischer 344 rats. *Life Sci.* 1993; **52**(24):1925-1934.

Castillo J, Erroba E, Perugorria MJ, Santamaria M, Lee DC, Prieto J, et al. Amphiregulin contributes to the transformed phenotype of human hepatocellular carcinoma cells. *Cancer Res.* 2006; **66**(12):6129–6138.

Chapple IL, Brock GR, Milward MR, Ling N, Matthews JB: Compromised GCF total antioxidant capacity in periodontitis: cause or effect? *J. Clin. Periodontol.* 2007; **34**:103-110.

Chen Y, Lu Q, Schneeberger EE, Goodenough DA. Restoration of tight junction structure and barrier function by down-regulation of the mitogenactivated protein kinase pathway in Ras-transformed Madin-Darby canine kidney cells. *Mol. Biol. Cell* 2000; **11**:849–862.

Chen X, Gumbiner BM. Crosstalk between different adhesion molecules. *Curr. Opin. Cell Biol.* 2006; **18**(5):572–578.

Cheng G, Cao Z, Xu X, van Meir EG, Lambeth JD. Homologs of gp91*phox*: cloning and tissue expression of Nox3, Nox4, and Nox5. *Gene* 2001; **269**:131–140.

Chiueh CC, Huang SJ, Murphy DL. Suppression of hydroxyl radical formation by MAO inhibitors: a novel possible neuroprotective mechanism in dopaminergic neurotoxicity. *J. Neural. Transm.* Suppl. 1994; **41**:189-196.

Chokki M, Mitsuhashi H, Kamimura T. Metalloprotease-dependent amphiregulin release

mediates tumor necrosis factor-α-indued IL-8 secretion in the human airway epithelial

cell line NCI-H292. *Life Science* 2006; **78**:3051-3057.

Chun J, Prince A. TLR2-induced calpain cleavage of epithelial junctional proteins facilitates

leukocyte transmigration. *Cell Host Microbe* 2009; **5**:47–58.

Chung E, Cook PW, Parkos CA, Park YK, Pittelkow MR, Coffey RJ. Amphiregulin causes

functional downregulation of adherens junctions in psoriasis. *J. Invest. Dermatol.*

2005a; **124**:1134-1140.

Chung E, Graves-Deal R, Franklin JL, Coffey GJ. Differential effects of amphiregulin and

TGF-alpha on the morphology of MDCK cells. *Exp. Cell. Res.* 2005b; **309**(1):149-160.

Clayburgh DR, Shen L, Turner JR. A porous defense: the leaky epithelial barrier in intestinal

disease. *Lab. Investig.* 2004; **84**:282–291.

Clayburgh DR, Barrett TA, Tang Y, Meddings JB, Van Eldik LJ, Watterson DM, Clarke LL,

Mrsny RJ, Turner JR. Epithelial myosin light chain kinase-dependent barrier

dysfunction mediates T cell activation-induced diarrhea *in vivo*. *J. Clin. Invest.* 2005;

115:2702–2715.

Clayburgh DR, Musch MW, Leitges M, Fu YX, Turner JR. Coordinated epithelial NHE3

inhibition and barrier dysfunction are required for TNF-mediated diarrhea *in vivo*. *J.

Clin. Invest.* 2006; **116**:2682-2694.

Colegio OR, Van Itallie C, Rahner C, Anderson JM. Claudin extracellular domains

determine paracellular charge selectivity and resistance but not tight junction fibril

architecture. *Am. J. Physiol.* 2003; **284**:C1346-C1354.

Colon AL, Menchen LA, Hurtado O, De Cristobal J, Lizasoain I, Leza JC, Lorenzo P, Moro MA. Implication of TNF-alpha convertase (TACE/ADAM17) in inducible nitric oxide synthase expression and inflammation in an experimental model of colitis. *Cytokine* 2001; **16**(6):220-226.

Coombes JL, Siddiqui KR, Arancibia-Carcamo CV, Hall J, Sun CM, Belkaid Y, Powrie F. A functionally specialized population of mucosal CD103+ DCs induces Foxp3+ regulatory T cells via a TGF-β and retinoic acid-dependent mechanism. *J. Exp. Med.* 2007; **204**(8):1757–1764.

Costantini P, Chernyak BV, Petronilli V, Bernardi P. Selective inhibition of the mitochondrial permeability transition port at the oxidation-reduction sensitive dithiol by monobromobimane. *FEBS Lett.* 1995; **362**:239-242.

Culouscou J, Remacle-Bonnet M, Carlton G, Plowman G, Shoyab M. Colorectum cell-derived growth factor (CRDGF) is homologous to amphiregulin, a member of the epidermal growth factor family. *Growth Factors* 1992; **7**(3):195–205.

Coyne CB, Vanhook MK, Gambling TM, Carson JL, Boucher RC, Johnson LG. Regulation of airway tight junctions by proinflammatory cytokines. *Mol. Biol. Cell* 2002; **13**:3218–3234.

D'Haens G, Van Deventer S, Van Hogezand R, Chalmers D, Kothe C, et al. Endoscopic and histological healing with infliximab antitumor necrosis factor antibodies in Crohn's disease: a European multicenter trial. *Gastroenterology* 1999; **116**:1029–1034.

Damstrup L, Kuwada SK, Dempsey PJ, Brown CL, Hawkey CJ, Poulsen HS, Wiley HS, RJ Coffey RJ Jr. Amphiregulin acts as an autocrine growth factor in two human polarizing

colon cancer lines that exhibit domain selective EGF receptor mitogenesis. *British Journal of Cancer* 1999; **80**(7):1012–1019.

Da Prada M, Zürcher G, Würthrich I, Haefely WE. On tyramine, food beverages and the reversible MAO inhibitor moclobemide. *J. Nerual. Transm.* 1988; **26**(Suppl.):33-56.

Da Prada M, Kettler R, Keller HH, Cesura AM, Richards JG, Saura Marti J, Muggli-Maniglio D, Wyss PC, Kyburz E, Imhof R. From moclobemide to Ro 19-6327 and Ro 41-1049: the development of a new class of reversible, selective MAO-A and MAO-B inhibitors. *J. Neural. Transm.* 1990; **29**(Suppl.):279-292.

De Marchi U, Pietrangeli P, Marcocci L, Mondovi B, Toninello A. L-Deprenyl as an inhibitor of menadione-induced permeability transition in liver mitochondrial. *Biochem. Pharmacol.* 2003; **66**:1749-1754.

Dean P, Kenny B. Intestinal barrier dysfunction by enteropathogenic Escherichia coli is mediated by two effector molecules and a bacterial surface protein. *Mol. Microbiol.* 2004; **54**:665-675.

Dhawan P, Singh AB, Deane NG, No Y, Shiou SR, Schmidt C, Neff J, Washington MK, Beauchamp RD. Claudin-1 regulates cellular transformation and metastatic behavior in colon cancer. *J. Clin. Invest.* 2005; **115**(7):1765–1776.

Dunford PJ, O`Donnell N, Riley JP, Williams KN, Karlsson L, Thurmond RL. The histamine H4 receptor mediates allergic airway inflammation by regulating the activation of CD4+ T cells. *J. Immunol.* 2006; **176**:7062–7070.

Ebersole JL, Stevens J, Steffen MJ, Dawson D III, Novak MJ. Systemic endotoxin levels in chronic indolent periodontal infections. *J. Periodont. Res.* 2010; **45**:1–7.

Eckert JJ, Fleming TP. Tight junction biogenesis during early development. *Biochim. Biophys. Acta.* 2008; **1778**:717-728.

Edmondson DE, Mattevi A, Binda C, Li M, Hubalek F. Structure and Mechanism of Monoamine Oxidase. *Current Medicinal Chemistry* 2004; **11**:1983-1993.

Ekuni D, Firth JD, Nayer T, Tomofuji T, Sanbe T, Irie K, Yamamoto T, Oka T, Liu Z, Vielkind J, Putnins EE. Lipopolysaccharide-Induced Epithelial Monoamine Oxidase Mediates Alveolar Bone Loss in a Rat Chronic Wound Model *Am. J. Pathol.* 2009; **175**:1398-1409.

Eutamene H, Theodorou V, Schmidlin F, Tondereau V, Garcia-Villar R, Salvador-Cartier C, Chovet M, Bertrand C, Bueno L. LPS-induced lung inflammation is linked to increased epithelial permeability: role of MLCK. *Eur. Respir. J.* 2005; **25**(5):789–796.

Farhadi A, Banan A, Fields J, and Keshavarzian A. Intestinal barrier: an interface between health and disease. *J. Gastroenterol. Hepatol.* 2003; **18:**479–487.

Ferrari D, Idzko M, Dichmann S, Purlis D, Virchow C, Norgauer J, Chiozzi P, Di Virgilio F, Luttmann W. P2 purinergic receptors of human eosinophils: characterization and coupling to oxygen radical production. *FEBS Lett.* 2000; **486**:217–224.

Ferrier L, Berard F, Debrauwer L, Chabo C, Langella P, Bueno L, Fioramonti J. Impairment of the intestinal barrier by ethanol involves enteric microflora and mast cell activation in rodents. *Am. J. Pathol.* 2006; **168**(4):1148–1154.

Fihn BM, Sjoqvist A, Jodal M. Permeability of the rat small intestinal epithelium along the villus-crypt axis: effects of glucose transport. *Gastroenterology* 2000; **119**:1029-1036.

Firth JD, Ekuni D, Irie K, Tomofuji T, Morita M. Putnins EE. Stromal-Epithelial Cross-talk in Lipopolysaccharide-Induced Chronic Inflammation. *Clinical and Vaccine Immunology*. Manuscript submitted 2011.

Fischer OM, Hart S, Gschwind A, Prenzel N, Ullrich A. Oxidative and osmotic stress signaling in tumor cells is mediated by ADAM proteases and heparin-binding epidermal growth factor. *Mol. Cell. Biol.* 2004; **24**:5172–5183.

Fish SM, Proujansky R, Reenstra WW. Synergistic effects of interferon gamma and tumour necrosis factor alpha on T84 cell function. *Gut* 1999; **45**:191–198.

Fisher SA, Tremelling M, Anderson CA, Gwilliam R, Bumpstead S, et al. Genetic determinants of ulcerative colitis include the ECM1 locus and five loci implicated in Crohn's disease. *Nat. Genet.* 2008; **40**:710–12.

Forman HJ, Torres M, Fukuto J. Redox signaling. *Mol. Cell Biochem*. 2002; **234**:49-62.

Forsyth CB, Banan A, Farhadi A, Fields JZ, Tang Y, Shaikh M, Zhang LJ, Engen PA, Keshavarzian A. Regulation of oxidant-induced intestinal permeability by metalloprotease-dependent epidermal growth factor receptor signaling. *J. Pharmacol. Exp. Therap.* 2007; **321**(1):84-97.

Foye WO, Lemke TL, Williams DA. Foye's principles of medicinal chemistry (6th edition). *Lippincott Williams & Wilkins, a Wolters Kluwer buisness*. 2008; 6th edition:1377.

Francoeur C, Escaffit F, Vachon PH, Beaulieu JF. Proinflammatory cytokines TNF-α and IFN-γ alter laminin expression under an apoptosisindependent mechanism in human intestinal epithelial cells. *Am. J. Physiol. Gastrointest. Liver Physiol.* 2004; **287**:G592–G598.

Freedman M, Rewilak D, Xerri T, Cohen S, Gordon AS, Shandling M, Logan AG. L-deprenyl in Alzheimer's disease: cognitive and behavioral effects. *Neurology* 1998; **50**(3):660-668.

Fujino S, Andoh A, Bamba S, Ogawa A, Hata K, Araki Y, Bamba T, Fujiyama Y. Increased expression of interleukin 17 in inflammatory bowel disease. *Gut* 2003; **52**(1):65–70.

Fujita T, Hayashida K, Shiba H, Kishimoto A, Matsuda S, Takeda K, Kawaguchi H, Kurihara H. The expression of claudin-1 and E-cadherin in junctional epithelium. *J. Periodont. Res.* 2010; **45**:579-582.

Fujita T, Firth JD, Kittaka M, Ekuni D, Kurihara H, Putnins EE. Loss of claudin-1 in lipopolysaccharide-treated periodontal epithelium. *Clinical and Vaccine Immunology*. Manuscript submitted 2011.

Fukata M, Michelsen KS, Eri R, Thomas LS, Hu B, Lukasek K, Nast CC, Lechago J, Xu R, Naiki Y, Soliman A, Arditi M, Abreu MT. Toll-like receptor-4 is required for intestinal response to epithelial injury and limiting bacterial translocation in murine model of acute colitis. *Am. J. Physiol. Gastrointest. Liver Physiol.* 2005; **288**:1055-1065.

Funatomi H, Itakura J, Ishiwata T, Pastan I, Thompson SA, Johnson GR, et al. Amphiregulin antisense oligonucleotide inhibits the growth of T3M4 human pancreatic cancer cells and sensitizes the cells to EGF receptor-targeted therapy. *Int. J. Cancer.* 1997; **72**(3):512 517.

Furuse M, Furuse K, Sasaki H, Tsukita S. Conversion of *zonulae occludentes* from tight to leaky strand type by introducing claudin-2 into Madin-Darby canine kidney I cells. *J. Cell Biol.* 2001; **153**:263-272.

Furuse M, Tsukita S. Claudins in occluding junctions of humans and flies. *Trends Cell Biol.* 2006; **16**(4):181-188.

Ghandehari H, Smith PL, Ellens H, Yeh PY, Kopecek J. Size-dependent permeability permeability of hydrophilic probes across rabbit colonic epithelium. *J. Pharmacol. Exp.* 1997; **280**:747-753.

Geiszt M, Witta J, Baffi J, Lekstrom K, Leto TL. Dual oxidases represent novel hydrogen peroxide sources supporting mucosal surface host defense. *FASEB J.* 2003; **17**:1502–1504.

González-Mariscal L, Chaves de Ramirez B, Lazaro A, Cereijido M. Establishment of tight junctions between cells from different animal species and different sealing capacities. *J. Membr. Biol.* 1989; **107**:43-56.

González-Mariscal L, Betanzos A, Nava P, Jaramillo BE. Tight junction proteins. *Prog. Biophys. Mol. Biol.* 2003; **81**(1):1-44.

Goodenough DA. Plugging the leaks. *Proc. Natl. Acad. Sci. U.S. A.* 1999; **96**: 319–321.

Goto Y, Uchida Y, Nomura A, Sakamoto T, Ishii Y, Morishima Y, Masuyama K, Sekizawa K. *Am. J. Respir. Cell. Mol. Biol.* 2000; **23**:712–718.

Graham WV, Wang F, Clayburgh DR, Cheng JX, Yoon B, et al. Tumor necrosis factor–induced long myosin light chain kinase transcription is regulated by differentiation-dependent signaling events. Characterization of the human long myosin light chain kinase promoter. *J. Biol. Chem.* 2006; **281**:26205–26215.

Gschwind A, Hart S, Fischer OM, Ullrich A. TACE cleavage of proamphiregulin regulates GPCR-induced proliferation and motility of cancer cells. *EMBO J.* 2003; **22**:2411–2421.

Gupta IR, Ryan AK. Claudins: unlocking the code to tight junction function during embryogenesis and in disease. *Clin. Genet.* 2010; **77**:314-325.

Guttman JA, Finlay BB. Tight junctions as targets of infectious agents. *Biochimica et Biophysica. Acta.* 2009; **1788**:832–841.

Haapamäkia J, Roineb RP, Turunena U, Färkkiläa MA, Arkkilaa P. Increased risk for coronary heart disease, asthma, and connective tissue diseases in inflammatory bowel disease. *Journal of Crohn's and Colitis* 2011; **5**(1):41-47.

Halliwell B. Reactive oxygen species and the central nervous system. *J. Neurochem.* 1992; **59**:1609–1623.

Hasan F, McCrodden JM, Kennedy NP, Tipton KF. The involvement of intestinal monoamine oxidase in the transport and metabolism of tyramine. *J. Neural. Transm.* 1988; **26**(Suppl.):1-9.

Hanson PJ, Moran AP, Butler K. Paracellular permeability is increased by basal lipopolysaccharide in a primary culture of colonic epithelial cells; an effect prevented by an activator of Toll-like receptor-2. *Innate Immunity* 2011; **17**(3):269-282.

He D, Su Y, Usatyuk PV, Spannhake EW, Kogut P, Solway J, Natarajan V, Zhao Y. Lysophosphatidic acid enhances pulmonary epithelial barrier integrity and protects endotoxin-induced epithelial barrier disruption and lung injury. *J. Biol. Chem.* 2009; **284**:24123-24132.

Heller F, Florian P, Bojarski C, Richter J, Christ M, Hillenbrand B, Mankertz J, Gitter AH, Burgel N, Fromm M, Zeitz M, Fuss I, Strober W, Schulzke JD. Interleukin-13 is the key effector Th2 cytokine in ulcerative colitis that affects epithelial tight junctions, apoptosis, and cell restitution. *Gastroenterology* 2005; **129**(2):550–564.

Hermiston ML, Gordon JI. *In vivo* analysis of cadherin function in the mouse intestinal epithelium: essential roles in adhesion, maintenance of differentiation, and regulation of programmed cell death. *J. Cell Biol.* 1995; **129**:489–506.

Hollander D. Intestinal permeability, leaky gut, and intestinal disorders. *Curr. Gastroenterol. Rep.* 1999; **1**:410-416.

Horiuchi K, Kimura T, Miyamoto T, Takashi H, Lkada Y, Toyama Y, Blobel CP. Cutting edge: TNF-α-converting enzyme (TACE/ADAM17) inactivation in mouse myeloid cells prevents lethality from endotoxin shock. *J. Immunol.* 2007; **179**:2686–2689.

Huntley GW, Gil O, Bozdagi O. The cadherin family of cell adhesion molecules: multiple roles in synaptic plasticity *Neuroscientist* 2002; **8**(3):221–233.

Ivanov AI, Nusrat A, Parkos CA. Endocytosis of the apical junctional complex: mechanisms and possible roles in regulation of epithelial barriers. *BioEssays* 2005; **27**:356-365.

Jaggi M, Rao PS, Smith DJ, Wheelock MJ, Johnson KR, Hemstreet GP, Balaji KC. E-Cadherin Phosphorylation by Protein Kinase D1/Protein Kinase Cμ is Associated with Altered Cellular Aggregation and Motility in Prostate Cancer *Cancer Res*. 2005; **65**(2):483–492.

Jarrott B, Vajda FJ. The current status of monoamine oxidase and its inhibitors *Med. J. Aust.* 1987; **146**(12):634-638.

Jarry A, Bossard C, Bou-Hanna C, Masson D, Espaze E, et al. Mucosal IL-10 and TGF-β play crucial roles in preventing LPS-driven, IFN-γ-mediated epithelial damage in human colon explants. *J. Clin. Investig.* 2008; **118**:1132–42.

Johnson GR, Prigent SA, Gullick WJ, Stromberg K. Characterization of high and low molecular weight forms of amphiregulin that differ in glycoslylation and peptide core

length. Evidence that the NH2-terminal region is not critical for bioactivity. *J. Biol. Chem.* 1993; **268**(25):18835-18843.

Johnston JP. Some observations upon a new inhibitor of monoamine oxidase in brain tissue *Biochem. Pharmacol.* 1968; **17**:1285-1297.

Jou TS, Schneeberger EE, Nelson JW. Structural and functional regulation of tight junctions by rhoA and rac1 small GTPases. *J. Cell Biol.* 1998; **142**:101–115.

Kansra S, Stoll SW, Johnson JL, Elder JT. Src family kinase inhibitors block amphiregulin-mediated autocrine ErbB signaling in normal human keratinocytes. *Mol. Pharmacol.* 2005; **67**(4):1145-1157.

Kast RE. Crohn's disease remission with phenelzine treatment. *Gastroenterology* 1998; **115**:1034-1035.

Kenny EF, O'Neill LA. Signaling adaptors used by Toll-like receptors: an update. *Cytokine* 2008; **43**:342–349.

Keshavarzian A, Morgan G, Sedghi S, Gordon JH, Doria M. Role of reactive oxygen metabolites in experimental colitis. *Gut* 1990; **31**(7):786-790.

Keshavarzian A, Haydek J, Zabihi R, Doria M, D'Astice M, and Sorenson JR. Agents capable of eliminating reactive oxygen species, catalase, WR-2721, or Cu(II)2(3,5-DIPS)4 decrease experimental colitis. *Dig. Dis. Sci.* 1992; **37**:1866–1873.

Kevil CG, Ohno N, Gute DC, Okayama N, Robinson SA, Chaney E, Alexander JS. Role of cadherin internalization in hydrogen peroxide-mediated endothelial permeability. *Free Radic. Biol. Med.* 1998; **24**(6):1015-1022.

Kimura K, Ito M, Amano M, Chihara K, Fukata Y, Nakafuku M, Yamamori B, Feng J, Nakano T, Okawa K, Iwamatsu A, Kaibuchi K. Regulation of myosin phosphatase by Rho and Rho-associated kinase (Rho-kinase). *Science* 1996; **273**(5272):245–248.

Kinugasa T, Sakaguchi T, Gu X, Reinecker HC. Claudins regulate the intestinal barrier in response to immune mediators. *Gastroenterology* 2000; **118**:1001–1011.

Kishida O, Miyazaki Y, Murayama Y, Ogasa M, Miyazaki T, Yamamoto T, Watabe K, Tsutsui S, Kiyohara T, Shimomura I, Shinomura Y. Gefitinib (Iressa, ZD1839) inhibits SN38-triggered EGF signals and IL-8 production in gastric cancer cells. *Cancer Chemother. Pharmacol.* 2005; **55**:584-594.

Klann E, Thiels E. Modulation of protein kinases and protein phosphatases by reactive oxygen species: implications for hippocampal synaptic plasticity. *Prog. Neuropsychopharmacol. Biol. Psychiatry* 1999; **23**:359–376.

Klegeris A, McGeer PL. R-(-)-Deprenyl inhibits monocytic THP-1 cell neurotoxicity independently of monoamine oxidase inhibition. *Exp. Neurol.* 2000; **166**(2):458-464.

Knoll J, Vizi ES, Somogyi G. Phenylisopropylmethylpropinylamine (E-250), a monoamine oxidase inhibitor antagonizing the effects of tyramine. *Arzn.-Forsch.,* 1968; **18**:109-112.

Knoll J. The striatal dopamine dependency of life span in male rats. Longevity study with (-) deprenyl. *Mech. Ageing Dev.* 1988; **46**(1-3):237-262.

Knoll J. (-)Deprenyl (Selegiline): past, present and future. *Neurobiology (Bp)* 2000; **8**(2):179-199.

Koff JL, Shao MX, Kim S, Ueki IF, Nadel JA. Pseudomonas lipopolysacharide accelerates wound repair via activation of a novel epithelial cell signaling cascade. *J. Immunology*

2006; **177**(12):8693-8700.

Kragten E, Lalande I, Zimmermann K, Roggo S, Schindler P, Muller D, van Oostrum J, Waldmeier P, Furst P. Glyceraldehyde-3-phosphate dehydrogenase, the putative target of the antiapoptotic compounds CGP 3466 and R-(-)-deprenyl. *J. Biol. Chem*. 1998; **273**(10):5821-5828.

Kuboniwa M, Hasegawa Y, Mao S, Shizukuishi S, Amano A, Lamont RJ, Yilmaz O. P. gingivalis accelerates gingival epithelial cell progression through the cell cycle. *Microbes. Infect*. 2007; **10**:122-128.

Kucharzik T, Walsh SV, Chen J, Parkos CA, Nusrat A. Neutrophil transmigration in inflammatory bowel syndrom is associated with differential expression of epithelial intercellular junctional proteins. *Am. J. Pathol.* 2001; **159**:2001-2009.

Lambeth JD. Nox/Duox family of nicotinamide adenine dinucleotide (phosphate) oxidases. *Curr. Opin. Hematol.* 2002; **9**:11–17.

Lapointe TK, O'Connor PM, Buret AG. The role of epithelial malfunction in the pathogenesis of enteropathogenic E.coli-induced diarrhea. *Lab. Invest.* 2009; **89**:964-970.

Lecuit M, Hurme R, Pizarro-Cerda J, Ohayon H, Geiger B, Cossart P. A role for alpha- and beta-catenins in bacterial uptake. *Proc. Natl. Acad. Sci. USA* 2000; **97**(18):10008-10013.

Le Gall SM, Bobe P, Reiss K, Horiuchi K, Niu XD, Lundell D, Gibb DR, Conrad D, Saftig P, Blobel CP. ADAMs 10 and 17 represent differentially regulated components of a general shedding machinery for membrane proteins such as transforming growth factor and tumor necrosis factor *Mol. Biol. Cell.* 2009; **20**:1785–1794.

Lee CS. Monoamine oxidase inhibitors attenuate cytotoxicity of 1-methyl-4-phenylpyridinium by suppressing mitochondrial permeability transition. *Korean J. Physiol. Pharmacol.* 2006; **10**:207-212.

Lee JH, Koh H, Kim M, Kim Y, Lee SY, Karess RE, Lee SH, Shong M, Kim JM, Kim J, Chung J. Energy-dependent regulation of cell structure by AMP-activated protein kinase. *Nature* 2007; **447**(7147):1017–1020.

Lemjabbar H, Li D, Gallup M, Sidhu S, Drori E, Basbaum C. Tobacco smoke-induced lung cell proliferation mediated by tumor necrosis factor alpha-converting enzyme and amphiregulin. *J. Biol. Chem*. 2003; **278**:26202– 26207.

Li Q, Zhang Q, Wang M, Zhao S, Ma J, Luo N, Li N, Li Y, Xu G, Li J. Interferon-gamma and tumor necrosis factor-alpha disrupt epithelial barrier function by altering lipid composition in membrane microdomains of tight junction. *Clin. Immunol.* 2007; **126**:67–80.

Lieb J. Remission of rheumatoid arthritis and other disorders of immunity in patients taking monoamine oxidase inhibitors. *J. immunopharmacol.* 1983; **5:**353-357.

Lin A, Song C, Kenis G, Bosmans E, De Jongh R, Scharpe S, Maes M. The in vitro immunosuppressive effects of moclobemide in healthy volunteers. *J. Affect. Disord.* 2000; **58**(1):69-74.

Lodes MJ, Cong Y, Elson CO, Mohamath R, Landers CJ, et al. Bacterial flagellin is a dominant antigen in Crohn disease. *J. Clin. Investig.* 2004; **113**:1296–306.

Lu YC, Yeh WC, Ohashi PS. LPS/TLR4 signal transduction pathway. *Cytokine* 2008; **42**:145–151.

Ma TY, Boivin MA, Ye D, Pedram A, Said HM. Mechanism of TNF-α modulation of Caco-2 intestinal epithelial tight junction barrier: role of myosin light-chain kinase protein expression. *Am. J. Physiol. Gastrointest. Liver Physiol.* 2005; **288**:G422–G430.

Madara JL. Tight junction dynamics: is paracellular transport regulated? *Cell* 1988; **53**:497-498.

Madara JL, Stafford J. Interferon-gamma directly affects barrier function of cultured intestinal epithelial monolayers. *J. Clin. Invest.* 1989; **83**:724-727.

Madara JL. Maintenance of the macromolecular barrier at cell extrusion sites in intestinal epithelium: physiological rearrangement of tight junctions. *J. Membr. Biol.* 1990; **116**:177-184.

Magyar K, Vizi ES, Ecseri Z, Knoll J. Comparative pharmacological analysis of the optical isomers of phenyl-isopropyl-methyl-propinylamine (E-250). *Acta. Physiol. Acad. Sci. Hung.* 1967; **32**:377-387.

Magyar K. Inhibitors of monoamine oxidase. *Verlag: Basel* 1993.

Magyar K, Szende B, Lengyel J, Tarczali J, Szatmary I: The pharmacology of B-type selective monoamine oxidase inhibitors; milestones in (−) deprenyl research. *J. Neural. Transm.* 1998; **48**(suppl):29-43.

Magyar K, Szende B. (−)-Deprenyl, a selective MAO-B inhibitor, with apoptotic and anti-apoptotic properties. *Neurotoxicology* 2004; **25**:233-242.

Martinez-Lacaci I, Johnson GR, Salomon DS, Dickinson RB. Characterization of a novel amphiregulin-related molecule in 12-O-tetradecanoylphorbol-13-acetate-treated breast cancer cells. *J. Cell Physiol.* 1996; **169**(3):497-508.

Mascia F, Mariani V, Girolomoni G, Pastore S. Blockade of EGF receptor induced a deranged chemokine expression in keratinocytes leading to enhanced skin inflammation. *Am. J. Pathol.* 2003; **163**:303-312.

Matsubara K, Senda T, Uezono T, Awaya T, Ogawa S, Chiba K, Shimizu K, Hayase N, Kimura K. L-Deprenyl prevents the cell hypoxia induced by dopaminergic neurotoxins, MPP(+) and beta-carbolinium: a microdialysis study in rats. *Neurosci. Lett.* 2001; **302**:65-68.

Mazzio EA, Harris N, Soliman KF. Food constituents attenuate monoamine oxidase activity and peroxide levels in C6 astrocyte cells. *Planta. Med.* 1998; **64**(7):603-606.

Mazzon E, Cuzzocrea S. Role of TNF-α in lung tight junction alteration in mouse model of acute lung inflammation. *Respir. Res.* 2007; **8**:75.

McKenzie JA, Ridley AJ. Roles of Rho/ROCK and MLCK in TNF-α-induced changes in endothelial morphology and permeability. *J. Cell. Physiol.* 2007; **213**:221–228.

McNamara BP, Koutsouris A, O'Connell CB, Nougayrede JP, Donnenberg MS, Hecht G. Translocated EspF protein from enteropathogenic Escherichia coli disrupts host intestinal barrier function. *J. Clin. Invest.* 2001; **107**(5):621-629.

Merchant NB, Voskresensky I, Rogers CM, LaFleur B, Dempsey PJ, Graves-Deal R, Revetta F, Foutch AC, Rothenberg ML, Washington MK, Coffey RJ. TACE/ADAM-17: A component of the epidermal growth factor receptor axis and a promising therapeutic target in colorectal cancer. *Clin. Cancer Res.* 2008; **14**(4):1182-1191.

Miller SI, Ernst RK, Bader MW. LPS, TLR4 and infectious disease diversity. *Nat. Rev. Microbiol.* 2005; **3**:36-46.

Miyaguchi K. Ultrastructure of the zolula adherens revealed by rapid-freeze deep-etching. *Journal of Structural Biology* 2000; **132**:169–178.

Moriez R, Salvador-Cartier C, Theodorou V, Fioramonti J, Eutamene H, Bueno L. Myosin light chain kinase is involved in lipopolysaccharide induced disruption of colonic epithelial barrier and bacterial translocation in rats. *Am. J. Pathol.* 2005; **167**(4):1071–1079.

Morita K, Furuse M, Fujimoto K, Tsukita S. Claudin multigene family encoding foru-transmembrane domain protein components of tight junction strands. *Proc. Natl. Acad. Sci. U. S. A.* 1999; **96**:511–516.

Mucida D, Park Y, Kim G, Turovskaya O, Scott I, Kronenberg M, Cheroutre H. Reciprocal TH17 and regulatory T cell differentiation mediated by retinoic acid. *Science* 2007; **317**:256–260.

Mullin JM, Laughlin KV, Marano CW, Russo LM, Soler AP. Modulation of tumor necrosis factor–induced increase in renal (LLC-PK1) transepithelial permeability. *Am. J. Physiol.* 1992; **263**:F915–924.

Myers TJ, Brennaman LH, Stevenson M, Higashiyama S, Russell WE, Lee DC, Sunnarborg SW. Mitochondrial reactive oxygen species mediate GPCR-induced TACE/ADAM17-dependent transforming growth factor-alpha shedding. *Mol. Biol. Cell.* 2009; **20**:5236-5249.

Nagatsu T, Sawada M. Molecular mechanism of the relation of monoamine oxidase B and its inhibitors to Parkinson's disease: possible implications of glial cells. *J. Neural Transm. Suppl.* 2006; **71**:53–65.

Nair NPV, Ahmed SK, Kin NMK. Biochemistry and Pharmacology of reversible inhibitors of MAO-A agents: Focus on Moclobemide. *J Psychiatr Neurosci* 1993; **18**(5):214-225.

Nakagome K, Nagata M. Pathogenesis of airway inflammation in bronchial asthma. *Auris Nasus Larynx* 2011; **38**(5):555-563.

Nakajima T, Honda T, Domon H, Okui T, Kajita K, Ito H, Takahashi N, Maekawa T, Tabeta K, Yamazaki K. Periodontitis-associated up-regulation of systemic inflammatory mediator level may increase the risk of coronary heart disease. *J. Periodont. Res.* 2010; **45**:116–122.

Naoi M, Maruyama W, Yi H, Akao Y, Yamaoka Y, Shamoto-Nagai M. Neuroprotection by propargylamines in Parkinson's disease: intracellular mechanism underlying the anti-apoptotic function and search for clinical markers. *J. Neural. Transm. Suppl.* 2007; **72**:121-31.

Nguyen DH, Catling AD, Webb DJ, Sankovic M, Wlker LA, Somlyo AV, Weber MJ, Gonias SL. Myosin light chain kinase functions downstream of Ras/ERK to promote migration of urokinase-type plasminogen activator-stimulated cells in an integrin selective manner. *J. Cell. Biol.* 1999; **146**:149–164.

Normanno N, Selvam MP, Qi CF, Saeki T, Johnson G, Kim N, et al. Amphiregulin as an autocrine growth factor for c-Ha-ras- and c-erBb-2- transformed human mammary epithelial cells. *Proc. Natl. Acad. Sci. USA* 1994; **91**(7):2790-2794.

Noti M, Corazza N, Mueller C, Berger B, Brunner T. TNF suppresses acute intestinal inflammation by inducing local glucocorticoid synthesis. *The Journal of Experimental Medicine* 2010; **207**(5):1057-1066.

Nusrat A, von Eichel-Streiber C, Turner JR, Verkade P, Madara JL, Parkos CA. Clostridium difficile toxins disrupt epithelial barrier function by altering membrane microdomain localization of tight junction proteins. *Infec. Immun.* 2001; **69**(3):1329-1336.

Obert G, Peiffer I, Servin AL. Rotavirus-induced structural and functional alterations in tight junctions of polarized intestinal Caco-2 cell monolayers. *J. Virol.* 2000; **74**(10):4645-4651.

Ohtsu H, Dempsey PJ, Eguchi S. ADAMs as mediators of EGF receptor transactivation by G protein-coupled receptors. *Am. J. Physiol. Cell Physiol.* 2006; **291**:C1–C10.

Otto T, Rembrink K, Goepel M, Meyer-Schwickerath M, Rubben H. E-cadherin: a marker for differentiation and invasiveness in prostatic carcinoma. *Urol. Res.* 1993; **21**(5):359–362.

Palfreymann MG, McDonald IA, Bey P, Schechter PJ, Sjoerdsma A. Design and early clinical evaluation of selective inhibitors of monoamine oxidase. *Prog. Neuropsychopharmacol. Biol. Psychiatry* 1988; **12**(6):967-987.

Park HS, Jung HY, Park EY, Kim J, Lee WJ, Bae YS. Cutting edge: direct interaction of TLR4 with NAD(P)H oxidase 4 isozyme is essential for lipopolysaccharide-induced production of reactive oxygen species and activation of NF-B. *J. Immunol.* 2004; **173**:3589–3593.

Pastore S, Mascia F, Mariani V, Girolomoni G. The epidermal growth factor receptor system in skin repair and inflammation. *Journal of Investigative Dermatology* 2008; **128**:1365-1374.

Perez-Moreno M, Jamora C, Fuchs E. Sticky business: orchestrating cellular signals at adherens junctions. *Cell* 2003; **112**:535–548.

Piepkorn M, Underwood R, Henneman C, Smith L. *J. Invest. Dermatol.* 1995; **105**:802–809.

Plowman GD, Green JM, McDonald VL, Neubauer MG, Disteche CM, Todaro GJ, et al. The amphiregulin gene encodes a novel epidermal growth factor-related protein with tumor-inhibitory activity. *Mol. Cell. Biol.* 1990; **10**(5):1969-1981.

Podolsky DK. Inflammatory bowel disease. *N. Engl. J. Med.* 2002; **347:**417–429.

Poltorak A, He X, Smirnova I, Liu MY, Van Huffel C, Du X, et al. Defective LPS signaling in C3H/HeJ and C57BL/10ScCr mice. Mutations in Tlr4 gene. *Science* 1998; **282**:2085–2088.

Powell DW. Barrier function of epithelia. *Am. J. Physiol.* 1981; **241**:G275-G288.

Powrie F, Leach MW, Mauze S, Menon S, Caddle LB, Coffman RL. Inhibition of Th1 responses prevents inflammatory bowel disease in *scid* mice reconstituted with CD45RBhi CD4+ T cells. *Immunity* 1994; **1**:553–562.

Prenzel N, Zwick E, Daub H, Leserer M, Abraham R, Wallasch C, and Ullrich A. EGF receptor transactivation by G-protein-coupled receptors requires metalloproteinase cleavage of proHB-EGF. *Nature (Lond)* 1999; **402**:884–888.

Putnins EE, Sanaie AR, Wu Q, Firth JD. CD-14 and Toll-like receptors 2 and 4 regulate lipopolysaccharide induction of KGF-1 protein expression. *Infect. Immun*. 2002; **70**: 6541-6548.

Quaroni A, Wands J, Trelstad RL, and Isselbacher KJ. Epithelial cell cultures from rat small intestine. *J. Cell. Biol.* 1979; **80**:248–265.

Raddatz R, Parini A, Lanier SM. Imidazoline/guanidinium binding domains on monoamine oxidases. Relationship to subtypes of imidazoline-binding proteins and tissue-specific

interaction of imidazoline ligands with monoamine oxidase B. *J. Biol. Chem*. 1995; **270**:27961–27968.

Rademacher TW, Parekh RB, Dwek RA. Glycobiology. *Annu. Rev. Biochem.* 1988; **57**:785-838.

Raetz CRH, Whitfield C. Lipopolysaccharide endotoxins. *Annu. Rev. Biochem.* 2002; **71**:635–700.

Raffel DM, Wieland DM. Influence of vesicular storage and monoamine oxidase activity on [11C]phenylephrine kinetics: studies in isolated rat heart. *J. Nucl. Med.* 1999; **40**(2):323-330.

Rakoff-Nahouman S, Paglino J, Eslami-Varzaneh F, Edberg S, Medzhitov R. Recognition of commensal microflora by Toll-like receptors is required for intestinal homeostasis. *Cell* 2004; **118**:229-241.

Rao RK, Basuroy S, Rao VU, Karnaky Jr KJ, Gupta A. Tyrosine phosphorylation and dissociation of occludin-ZO-1 and E-cadherin-beta-catenin complexes from the cytoskeleton by oxidative stress. *Biochem. J.* 2002; **368**:471-481.

Rieder CR, Williams AC, Ramsden DB. Selegiline increases heme oxygenase-1 expression and the cytotoxicity produced by dopamine treatment of neuroblastoma SK-N-SH cells. *Braz. J. Med. Biol. Res.* 2004; **37**:1055-1062.

Riese DJ, Stern DF. Specificity within the EGF family/ErbB receptor family signaling network. *Bioessays* 1998; **20**:41-48.

Robson MC, Kucukcelebi A, Carp SS, Hayward PG, Hui PS, Cowan WT Ko F, Cooper DM. Maintenance of wound bacterial balance. *Am. J. Surg.* 1999; **178**:399-402.

Rodriguez P, Heyman M, Candalh C, Blaton MA, Bouchaud C. Tumour necrosis factor-alpha induces morphological and functional alterations of intestinal HT29 cl.19A cell monolayers. *Cytokine* 1995; **7**:441–448.

Rumelhard M, Ramgolam K, Auger F, Dazy AC, Blanchet S, Marano F, Baeza-Squiban A. Effects of $PM_{2.5}$ components in the release of amphiregulin by human airway epithelial cells. *Toxicology Letters* 2007; **168**:155–164.

Runswick S, Mitchell T, Davies P, Robinson C, Garrod DR. Pollen proteolytic enzymes degrade tight junctions. *Respirology.* 2007; **12**(6):834-42.

Sadikot RT, Zeng H, Yull FE, Li B, Cheng DS, Kernodle DS, Jansen ED, Contag CH, Segal BH, Holland SM, et al. p47*phox* deficiency impairs NF-B activation and host defense in *Pseudomonas pneumonia*. *J. Immunol.*2004; **172**:1801–1808.

Saitou M, Fujimoto K, Doi Y, Itoh M, Fujimoto T, Furuse M, Takano H, Noda T, Tsukita S. Occludin-deficient embryonic stem cells can differentiate into polarized epithelial cells bearing tight junctions. *J. Cell Biol.* 1998; **141**:397-408.

Saitou M, Furuse M, Sasaki H, Schulzke JD, Fromm M, et al. Complex phenotype of mice lacking occludin, a component of tight junction strands. *Mol. Biol. Cell* 2000; **11**(12):4131–4142.

Salomon DS, Brandt R, Ciardiello F, Normanno N. Epidermal growth factor-related peptides an their receptors in human malignancies. *Crit. Rev. Oncol. Hematol.* 1995; **19**(3):183-232.

Sanders SE, Madara JL, McGuirk DK, Gelman DS, Colgan SP. Assessment of inflammatory events in epithelial permeability: a rapid screening method using fluorescent dextrans. *Epithelial Cell Biol.* 1995; **4**:25-34.

Sanders CJ, Yu Y, MooreDA3rd,Williams IR, Gewirtz AT. Humoral immune response to
flagellin requires T cells and activation of innate immunity. *J. Immunol.* 2006;
177:2810–18.

Sanderson MP, Dempsey PJ, Dunbar AJ. Control of ErbB signaling through metalloprotease
mediated ectodomain shedding of EGF-like factors. *Growth Factors* 2006; 24(**2**):121-
136.

Sanlioglu S, Williams CM, Samavati L, Butler NS, Wang G, McCray PB Jr, Ritchie TC,
Hunninghake GW, Zandi E, Engelhardt JF: Lipopolysaccharide induces Rac1-
dependent reactive oxygen species formation and coordinates tumor necrosis factor-α
secretion through IKK regulation of NF-κB. *J. Biol. Chem.* 2001; **276**:30188–30198.

Sartor RB. Mechanisms of disease: Pathogenesis of Crohn's disease and ulcerative colitis.
Nat. Clin. Pract. Gastroenterol. Hepatol. 2006; **3**:390-407.

Sauer H, Klimm B, Hescheler J, Wartenberg M. Activation ofp90RSK and growth
stimulation of multicellular tumor spheroids are dependent on reactive oxygen species
generated after purinergic receptor stimulation by ATP. *FASEB J.* 2001; **15**:2539 –
2541.

Sawada M, Imamura K, Nagatsu T. Role of cytokines in inflammatory process in
Parkinson's disease. *J. Neural. Transm. Suppl.* 2006; **70**:373–381.

Schafer B, Gschwind A, Ullrich A. Multiple G-protein-coupled receptor signals converge on
the epidermal growth factor receptor to promote migration and invasion. *Oncogene*
2004a; **23**:991-999.

Schafer B, Marg B, Gschwind A, Ullrich A. Distinct ADAM metalloproteinases regulate G
protein coupled receptor-induced cell proliferation and survival. *J. Biol. Chem*. 2004b;

279:47929-47938.

Scharl M, Paul G, Barrett KE, McCole DF. Adenosine monophosphate activated protein kinase mediates the interferon-γ-induced decrease in intestinal epithelial barrier function. *J. Biol. Chem.* 2009; **284**:27952-27563.

Schneeberger EE, Lynch RD. The tight junction: a multifunctional complex. *Am. J. Physiol. Cell. Physiol.* 2004; **284**:1213-1228.

Schroeder HE, Listgarten MA. The gingival tissues: the architecture of periodontal protection. *Periodontol. 2000* 1997; **13**:91-120.

Schwarz BT, Wang F, Shen L, Clayburgh DR, Su L, Wang Y, Fu YX, Turner JR. LIGHT signals directly to intestinal epithelia to cause barrier dysfunction via cytoskeletal and endocytic mechanisms. *Gastroenterology* 2007; **132**(7):2383–2394.

Scott KG, Meddings JB, Kirk DR, Lees-Miller SP, Buret AG. Intestinal infection with Giardia spp. reduces epithelial barrier function in a myosin light chain kinase-dependent fashion. *Gastroenterology* 2002; **123**:1179–1190.

Serkova N, Brand A, Christians U, Leibfritz D. Evaluation of the effects of immunosuppressants on neuronal and glil cells in vitro by multinuclear magnetic resonance spectroscopy. *Biochim. Biophys. Acta.* 1996; **1314**:93-104.

Shao MX, Nadel JA. Dual oxidase 1-dependent MUC5AC mucin expression in cultured human airway epithelial cells. *Proc. Natl. Acad. Sci. USA* 2005; **102**:767–772.

Shen L, Turner JR. Actin depolymerization disrupts tight junctions via caveolae-mediated endocytosis. *Mol. Biol. Cell* 2005; **16**:3919–36.

Shen L, Black ED, Witkowski ED, Lencer WI, Guerriero V, et al. Myosin light chain phosphorylation regulates barrier function by remodeling tight junction structure. *J.*

Cell Sci. 2006; **119**:2095-2106.

Shen L, Weber CR, Turner JR. The tight junction protein complex undergoes rapid and continuous molecular remodeling at steady state. *J. Cell Biol.* 2008; **181**:683-695.

Shen L. Functional morphology of the gastrointestinal tract. *Curr.Top. Microbiol. Immunol*. 2009; **337**:1-35.

Shih JC, Chen K, Ridd MJ. Monoamine oxidase: from genes to behavior. *Annu. Rev. Neurosci.* 1999; **22**:197-217.

Shoyab M, McDonald VL, Bradley JG, Todaro GJ. Amphiregulin: a bifunctional growth-modulating glycoprotein produced by the phorbol 12-myristate 13-acetate-treated human breast adenocarcinoma cell line MCF-7. *Proc. Natl. Acad. Sci. U S A* 1988; **85**(17):6528-6532.

Shoyab M, Plowman GD, McDonald VL, Bradley JG, Todaro GJ. Structure and function of human amphiregulin: a member of the epidermal growth factor family. *Science* 1989; **243**(4894 pt1):1074-1076.

Simon DB, Lu Y, Choate KA, Velazquez H, Al-Sabban E, Praga M, Casari G, Bettinelli A, Colussi G, Rodriguez-Soriano J, McCredie D, Milford D, Sanjad S, Lifton RP. Paracellin-1, a renal tight junction protein required for paracellular Mg^{2+} resorption. *Science* 1999; **285**(5424):103-106.

Simovitch M, Sason H, Cohen S, Zahavi, EE, Melamed-Book N, Weiss A, Aroeti B, Rosenshine, I. EspM inhibits pedestal formation by enterohaemorrhagic Escherichia coli and enteropathogenic E. coli and disrupts the architecture of a polarized epithelial monolayer. *Cell. Microbiol*. 2010; **12**:489–505.

Singh B, Schneider M, Knyazev P, Ullrich A. UV-induced EGFR signal transactivation is

dependent on proligand shedding by activated metalloprotease in skin cancer cell lines. *Int. J. Cancer* 2009; **124**:531-539.

Song J, Li J, Lulla A, Evers BM, and Chung DH. Protein kinase D protects against oxidative stress-induced intestinal epithelial cell injury via Rho/ROK/PKC-delta pathway activation. *Am. J. Physiol.* 2006; **290:**1469–1476.

Soond SM, Everson B, Riches DWH, Murphy G. ERK-mediated phosphorylation of Thr735 in TNF-alpha converting enzyme and its potential role in TACE protein trafficking. *J. Cell Sci.* 2005; **118**:2371–2380.

Sorensen BS, Torring N, Bor MV, Nexo E. Quantitation of the mRNA expression of the epidermal growth factor system: selective induction of heparin-binding epidermal growth factor-like growth factor and amphiregulin expression by growth factor stimulation of prostate stromal cells. *J. Lab. Clin. Med.* 2000; **136**(3):209-217.

Sousa S, Cabanes D, El-Amraoui A, Petit C, Lecuit M, Cossart P. Unconventional myosin VIIa and vezatin, two proteins crucial for Listeria entry into epithelial cells. *J. Cell Sci.* 2004; **117**:2121-2130.

Stamatovic SM, Keep RF, Wang MM, Jankovic I, Andjelkovic AV. Caveolae-mediated internalization of occludin and claudin-5 during CCL2- induced tight junction remodeling in brain endothelial cells. *J. Biol. Chem.* 2009; **284**:19053–19066.

Sternlicht MD, Sunnarborg SW. The ADAM17–amphiregulin–EGFR Axis in Mammary Development and Cancer. *J. Mammary Gland. Biol. Neoplasia* 2008; **13**:181–194.

Sternlicht MD. Review: Key stages in mammary gland development, The cues that regulate ductal branching morphogenesis. *Breast Cancer Research* 2006, **8**:201-212.

Stevenson BR, Anderson JM, Goodenough DA, Mooseker MS. Tight junction structure and

ZO-1 content are identical in two strains of Madin-Darby canine kidney cells which differ in transepithelial resistance. *J. Cell Biol.* 1988; **107**:2401-2408.

Suenaert P, Bulteel V, Lemmens L, Noman M, Geypens B, et al. Anti-tumor necrosis factor treatment restores the gut barrier in Crohn's disease. *Am. J. Gastroenterol.* 2002; **97**:2000–2004.

Sunnarborg AW, Hinkle CL, Stevenson M, Russell WE, Rasaka CS, Peschon JJ, Castner BJ, Gerhart MJ, Paxton RJ, Black RA, Lee DC. Tumor necrosis factor-α converting enzyme (TACE) regulates epidermal growth factor receptor ligand availability. *The Journal of Biological Chemistry* 2002; **277**(15):12838-12845.

Sutmuller RP, den Brok MH, Kramer M, Bennink EJ, Toonen LW, et al. Toll-like receptor 2 controls expansion and function of regulatory T cells. *J. Clin. Investig.* 2006; **116**:485–494.

Szende B, Bokonyi G, Bocsi J, Keri G, Timar F, Magyar K. Anti-apoptotic and apoptotic action of (−)-deprenyl and its metabolites. *J. Neural. Transm.* 2001; **108**:25-33.

Takarada H, Cattoni M, Sugimoto A, Rose GG. Ultrastructural studies of human gingival III. Changes of the basal lamina in chronic periodontitis. *J. Periodont. Res.* 1974a; **45**:288-296.

Takashiba S, Naruishi K, Murayama Y. Perspective of cytokine regulation for periodontal treatment: fibroblast biology. *J. Periodontol.* 2003; **74**:103-110.

Talavera D, Castillo AM, Dominguez MC, Guiterrez AE, Meza I. IL8 release, tight junction and cytoskeleton dynamic reorganization conducive to permeability increase are induced by dengue virus infection of microvascular endothelial monolayers. *J. Gen. Virol.* 2004; **85**:1801-1813.

Tamion F, Richard V, Lyoumi S, Daveau M, Bonmarchand G, Leroy J, Thuillez C, Lebreton JP . Gut ischemia and mesenteric synthesis of inflammatory cytokines after hemorrhagic or endotoxic shock. *Am. J. Physiol.* 1997; **273**:G314–G321.

Tatton WG, Ju WY, Holland DP, Tai C, Kwan M. (-)-Deprenyl reduces PC12 cell apoptosis by inducing new protein synthesis. *J. Neurochem.* 1994; **63**(4):1572-1575.

Tatton WG, Wadia JS, Ju WY, Chalmers-Redman RM, Tatton NA. (-)-Deprenyl reduces neuronal apoptosis and facilitates neuronal outgrowth by altering protein synthesis without inhibiting monoamine oxidase. *J. Neural. Transm. Suppl.* 1996; **48**:45-59.

Tatton WG, Chalmers-Redman RM, Ju WY, Wadia J, Tatton NA. Apoptosis in neurodegenerative disorders: potential for therapy by modifying gene transcription. *J. Neural Transm. Suppl.* 1997; **49**:245-268.

Tatton WG, Chalmers-Redman RM, Ju WJ, Mammen M, Carlile GW, Pong AW, Tatton NA. Propargylamines induce antiapoptotic new protein synthesis in serum- and nerve growth factor (NGF)-withdrawn, NGF-differentiated PC-12 cells. *J. Pharmacol. Exp. Ther.* 2002; **301**:753-64.

Taylor CT, Dzus AL, Colgan SP. Autocrine regulation of epithelial permeability by hypoxia: role for polarized release of tumor necrosis factor α. *Gastroenterology* 1998; **114**:657–668.

Thannickal VJ, Day RM, Klinz SG, Bastien MC, Larios JM, Fanburg BL. Ras-dependent and -independent regulation of reactive oxygen species by mitogenic growth factors and TGF-β1. *FASEB J* 2000; **14**:1741–1748.

Tharakan B, Whaley JG, Hunter FA, Smythe WR, Childs EW. (−)-Deprenyl inhibits vascular hyperpearmeability after hemorrhagic shock. *SHOCK* 2010; **33**(1):56-63.

Thiery JP. Cell adhesion in development: a complex signaling network. *Curr. Opin. Genet. Dev.* 2003; **13**(4):365–371.

Thomas T. Monoamine oxidase-B inhibitors in the treatment of Alzheimer's disease. *Neurobiol. Aging* 2000; **21**(2):343-348.

Thorne B, Plowman G. *Mol. Cell. Biol.* 1994; **14**:1635–1646.

Tipton K, Boyce S, O'Sullivan J, Davies G, Healy J. Monoamine oxidases: certainties and uncertainties. *Curr. Med. Chem.* 2004; **11**:1965-1982.

Tiruppathi, C., Naqvi, T., Sandoval, R., Mehta, D, Malik, A. B. Synergistic effects of tumour necrosis factor-α and thrombin in increasing endothelial permeability. *Am. J. Physiol. Lung Cell. Mol. Physiol.* 2001; **281**:L958–L968.

Tomofuji T, Azuma T, Kusano H, Sanbe T, Ekuni D, Tamaki N, Yamamoto T, Watanabe T. Oxidative damage of periodontal tissue in the rat periodontitis model: effects of a high-cholesterol diet. *FEBS Lett.* 2006; **580**:3601–3604.

Toronyi E, Hamar J, Magyar K, Szende B. Antiapoptotic effect of (−)-deprenyl in rat kidney after ischemia-reperfusion. *Med. Sci. Monit.* 2002; **8**:BR65-BR68.

Tsukita S, Furuse M, Itoh M. Multifunctional strands in tight junctions. *Nat. Rev. Mol. Cell Biol.* 2001; **2**:285-293.

Turksen K, Troy TC. Barriers built on claudins. *Journal of Cell Science* 2004; **117**:2435-2447.

Turksen K, Troy TC. Junctions gone bad: Claudins and loss of the barrier in cancer. *Biochimica et Biophysica Acta* 2011; **1816**:73-79.

Turner J. Intestinal mucosal barrier function in health and disease. *Nature Reviews Immunology*. 2009; **9**:799-809.

Uematsu S, Fujimoto K, Jang MH, Yang BG, Jung YJ, et al. Regulation of humoral and
cellular gut immunity by lamina propria dendritic cells expressing Toll-like receptor 5.
Nat. Immunol. 2008; **9**:769–776.

Ulich TR, Howard SC, Remick DG, Wittwer A, Yi ES, Yin S, Guo K, Welply JK, Williams
JH. Intratracheal administration of endotoxin and cytokines. VI. Antiserum to CINC
inhibits acute inflammation. *AJP - Lung Physiol* 1995; **268**(2):L245-L250.

Umeda K, Ikenouchi J, Katahira-Tayama S, Furuse K, Sasaki H, Nakayama M, Matsui T,
Tsukita S, Furuse M, Tsukita S. ZO-1 and ZO-2 independently determine where
claudins are polymerized in tight-junction strand formation. *Cell* 2006; **126**:741–754.

Ungaro R, Fukata M, Hsu D, Hernandez Y, Breglio K, Chen A, Xu R, Sotolongo J, Espana
C, Zaias J, Elson G, Mayer L, Kosco-Vilbois M, Abreu MT. A novel Toll-like receptor
4 antagonist antibody ameliorates inflammation but impairs mucosal healing in murine
colitis. *Am. J. Physiol. Gastrointest. Liver Physiol.* 2009; **296**(6):G1167-1179.

Utech M, Ivanov AI, Samarin SN, Bruewer M, Turner JR, Mrsny RJ, Parkos CA, Nusrat A.
Mechanism of IFN-γ-induced endocytosis of tight junction proteins: Myosin II-
dependent vacuolarization of the apical plasma membrane. *Mol. Biol. Cell* 2005;
16(10):5040–5052.

Van Itallie CM, Rahner C, Anderson JM. Regulated expression of claudin-4 decrease
paracellular conductance through a selective decrease in sodium permeability. *J. Clin.
Invest.* 2001; **107**:1319-1327.

Van Itallie CM, Fanning AS, Anderson JM. Reversal of charge selectivity in cation or anion-
selective epithelial cell lines by expression of different claudins. *Am. J. Physiol. Renal
Physiol.* 2003; **285**:F1078–F1084.

Van Itallie CM, Holmes J, Bridges A, Gookin JL, Coccaro MR, Proctor W, Colegio OR, Anderson JM. The density of small tight junction pores varies among cell types and is increased by expression of claudin-2. *J. Cell. Sci*. 2008; **121**:298-305.

Van Itallie CM, Fanning AS, Bridges A, Anderson JM. ZO-1 stabilizes the tight junction solute barrier through coupling to the perijunctional cytoskeleton. *Mol. Biol. Cell* 2009; **20**:3930–3940.

van Vliet SJ, den Dunnen J, Gringhuis SI, Geijtenbeek TB, van Kooyk Y. Innate signaling and regulation of Dendritic cell immunity. *Curr. Opin. Immunol.* 2007; **19**:435–440.

Vijay-Kumar M, Sanders CJ, Taylor RT, Kumar A, Aitken JD, et al. Deletion of TLR5 results in spontaneous colitis in mice. *J. Clin. Investig.* 2008; **117**:3909–3921.

Wadia JS, Chalmers-Redman ME, Ju WJ, Carlile GW, Phillips JL, Fraser AD, Tatton WG. Mitochondrial membrane potential and nuclear changes in apoptosis caused by serum and nerve growth factor withdrawal: time course and modification by (−)-deprenyl. *J. Neurosci.* 1998; **18**(3):932-947.

Wallace JL, Graham S, Whittle BJR. Gastrointestinal plasma leakage in endotoxic shock. Inhibition by prostoglandin E_2 and by a platelet-activating factor antagonist. *Can. J. Physiol. Pharmacol.* 1987; **65**:1428-1432.

Wang F, Graham WV, Wang Y, Witkowski ED, Schwarz BT, Turner JR. Interferon-γ and tumor necrosis factor α synergize to induce intestinal epithelial barrier dysfunction by up-regulating myosin light chain kinase expression. *Am. J. Pathol.* 2005; **166**: 409–419.

Wang J, Lopez-Fraga M, Rynko A, Lo DD. TNFR and LTbetaR agonists induce follicle-associated epithelium and M cell specific genes in rat and human intestinal epithelial

cells. *Cytokine* 2009;**47**(1):69–76.

Watson CJ, Rowland M, Warhurst G. Functional modeling of tight junctions in intestinal

cell monolayers using polyethylene glycol oligomers. *Am. J. Physiol. Cell Physiol.*

2001; **281**:C388-C397.

Watson CJ, Hoare CJ, Garrod DR, Carlson GL, Warhurst G. Interferon-γ selectively

increases epithelial permeability to large molecules by activating different populations

of paracellular pores. *J. Cell Sci.* 2005; **118**:5221-5230.

Weber CR, Nalle SC, Tretiakova M, Rubin DT, Turner JR. Claudin-1 and claudin-2

expression is elevated in inflammatory bowel disease and may contribute to early

neoplastic transformation. *Lab. Invest.* 2008; **88**:1110–1120.

Werb Z, Yan Y. A cellular striptease act. *Science* 1998; **282**(5392):1279-1280.

Werner P, Cohen G. Glutathione disulfide (GSSG) as a marker of oxidative injury to brain

mitochondria. *Ann. NY Acad. Sci.* 1993; **679**:364–369.

West AP, Koblansky AA, Ghosh S. Recognition and signaling by toll-like receptors. *Annu.*

Rev. Cell Dev. Biol. 2006; **22**:409–437.

Weyler W, Hsu YP, Breakefield XO. Biochemistry and genetics of monoamine oxidase.

Pharmacol. Ther. 1990; **47**:391–417.

Whaley JG, Tharakan B, Smith B, Hunter FA, Childs EW. (−)-Deprenyl inhibits thermal-

injury-induced apoptotic signaling and hyperpermeability in microvascular endothelial

cells. *Journal of Burn Care & Research* 2009; **30**(6):1018-1027.

Wheelock MJ, Johnson KR. Cadherins as modulators of cellular phenotype *Annu. Rev. Cell*

Dev. Biol. 2003; **19**:207–235.

Willmarth NE, Ethier SP. Amphiregulin as a novel target for breast cancer therapy. *J*

Mammary Gland Biol. Neoplasia 2008; **13**:171–179.

Wine E, Ossa JC, Gray-Owen SD, Sherman PM. Adherent-invasive Escherichia coli, strain LF82 disrupts apical junctional complexes in polarized epithelia. *BMC Microbiol.* 2009; **9**(180):1-11.

Wisner DM, Harris LR, Green CL, Poritz LS. Opposing Regulation of the Tight Junction Protein Claudin-2 by Interferon-γ and Interleukin-4. *Journal of Surgical Research* 2008; **144**:1–7.

Wong WK, Ou XM, Chen K, Shih JC. Activation of human monoamine oxidase B gene expression by a protein kinase C MAPK signal transduction pathway involves c-Jun and Egr-1. *J. Biol. Chem.* 2002; **277**:22222-22230.

Wray C, Mao Y, Pan J, Chandrasena A, Piasta F, Frank JA. Claudin-4 augments alveolar epithelial barrier function and is induced in acute lung injury. *Am. J. Physiol. Lung Cell. Mol. Physiol.* 2009; **297**(2):L219–L227.

Wroblewski LE, Shen L, Ogden S, Romero–Gallo J, LaPierre LA, Israel DA, Turner JR, Peek RM Jr. Helicobacter pylori dysregulation of gastric epithelial tight junctions by urease-mediated myosin II activation. *Gastroenterology* 2009; **136**:236–246.

Wu RM, Chiueh CC, Pert A, Murphy DL. Apparent antioxidant effect of *l*-deprenyl on hydroxyl radical formation and nigral injury elicited by MPP$^+$ in vivo. *Eur. J. Pharmacol.* 1993; **243**:241-247.

Xavier RJ, Podolsky DK. Unravelling the pathogenesis of inflammatory bowel disease. *Nature* 2007; **448**:427-434.

Xu L, Ma J, Seigel GM, Ma JX. L-Deprenyl blocking apoptosis and regulating gene expression in cultured retinal neurons. *Biochem. Pharmacol.* 1999; **58**:1183-1190.

Youdim MB, Finberg JP. Monoamine oxidase B inhibition and the "cheese effect" *J. Neural. Transm.* Suppl. 1987; **25**:27-33.

Youdim MBH, Weinstock M. Therapeutic applications of selective and non-selective inhibitors of monoamine oxidase A and B that do not cause significant tyramine potentiation. *Neurotoxicology* 2004; **25**:243-250.

Youdim MB, Buccafusco JJ. CNS Targets for multi-functional drugs in the treatment of Alzheimer's and Parkinson's diseases. *J. Neural Transm.* 2005; **112**(4):519-537.

Yu AS, Enck AH, Lencer WI, Schneeberger EE. Claudin-8 expression in Madin-Darby canine kidney cells augments the paracellular barrier to cation permeation. *J. Biol. Chem*. 2003; **278**(19):17350–17359.

Yu ASL, Cheng MH, Angelow S, Gunzel D, Kanzawa SA, et al. Molecular basis for cation selectivity in claudin-2-based paracellular pores: identification of an electrostatic interaction site. *J. Gen. Physiol.* 2009; **133**:111–127.

Zabner J, Winter M, Excoffon KJ, Stoltz D, Ries D, Shasby S, Shasby MJ. Histamine alters E-cadherin cell adhesion to increase human airway epithelial permeability *Appl. Physiol*. 2003; **95**(1):394–401.

Zeissig S, Bojarski C, Buergel N, Mankertz J, Zeitz M, Fromm M, and Schulzke JD. Downregulation of epithelial apoptosis and barrier repair in active Crohn's disease by tumor necrosis factor-alpha antibody treatment. *Gut* 2004; **53**:1295–1302.

Zhang Z, Oliver P, Lancaster JJ, Schwarzenberger PO, Joshi MS, Cork J, Kolls JK. Reactive oxygen species mediate tumor necrosis factor α-converting, enzyme-dependent ectodomain shedding induced by phorbol myristate acetate. *FASEB J*. 2001; **15**:303–305.

Zhu Q, Chen K, Shih J. Bidirectional promoter of human monoamine oxidase A (MAO A) controlled by transcriptional factor Sp 1. *J. Neurosci.* 1994; **14**:7393-7403.

Zolotarevsky Y, Hecht G, Koutsouris A, Gonzalez DE, Quan C, et al. A membrane-permeant peptide that inhibits MLC kinase restores barrier function in in vitro models of intestinal disease. *Gastroenterology* 2002; **123**:163–172.

Zuany-Amorim C, Hastewell J, Walker C. Toll-like receptors as potential therapeutic targets for multiple diseases. *Nat. Rev. Drug Discov.* 2002; **1**:797–807.

Appendix: One-Way ANOVA Analysis with Tukey's Test

Statistical analysis was performed using "A Calculating Companion for Brunette's Critical Thinking" (http://www.dmbru.net/Calculating_Companion/tests.php, Website and all applets copyright © 2008, DM Brunette).

A. Statistical Analysis of Figure 4 Data

Degrees of Freedom (df) = 6
Critical Value (q_c) = 4.34 (p<0.05) and 6.33 (p<0.01).

AR Treated Groups from Barrier Model TER Analysis

a) *48-hour treatment:*
 One-way ANOVA analysis: F = 1.074, P = 5.143. F must be at least 5.143 to reach p<0.05. Therefore, the null hypothesis (H_o) is not rejected.

b) *96-hour treatment:*
 One-way ANOVA analysis: F = 2.731, P = 5.143. F must be at least 5.143 to reach p<0.05. Therefore, H_o is not rejected.

c) *144-hour treatment:*
 One-way ANOVA analysis: F = 10.158, P = 5.143. F must be at least 5.143 to reach p<0.05. Therefore, H_o is rejected.
 Tukey's Test: H_o of two groups being similar is rejected if q ≥ to q_c.
 - q value of 6.239 was found between CTL and AR(10ng/ml).
 - All other comparisons do not reject H_o.

TNF-α Treated Groups from Barrier Model TER Analysis

a) *48-hour treatment:*
 One-way ANOVA analysis: F = 17.55, P = 5.143. F must be at least 5.143 to reach p<0.05. Therefore, H_o is rejected.
 Tukey's Test:
 - q value of 5.46 was found between CTL and TNF-α (5ng/ml).
 - q value of 8.234 was found between TNF-α(5ng/ml) and TNF-α (10ng/ml).
 - All other comparisons do not reject H_o.

b) *96-hour treatment:*
 One-way ANOVA analysis: H_o is not rejected at p<0.05. F = 14.775, P = 5.143. F must be at least 5.143 to reach p<0.05. Therefore, H_o is rejected.
 Tukey's Test:
 - q value of 7.675 was found between CTL and TNF-α (10ng/ml).
 - All other comparisons do not reject H_o.

c) *144-hour treatment:*

One-way ANOVA analysis: H_o is not rejected at $p<0.05$. F = 70.917, P = 5.143. F must be at least 5.143 to reach $p<0.05$. Therefore, H_o is rejected.

Tukey's Test:
- q value of 11.915 was found between CTL and TNF-α (5ng/ml).
- q value of 16.266 was found between CTL and TNF-α (10ng/ml).
- q value of 4.351 was found between TNF-α (5ng/ml) and TNF-α (10ng/ml).

B. Statistical Analysis of Figure 5 Data

MAO-A/B Inhibitor TER Experiment

$df = 8$
$q_c = 4.53$ (p<0.05) and 6.20 (p<0.01).

a) *48-hour treatment:*
   One-way ANOVA analysis: F = 40.083, P = 4.066. F must be at least 4.066 to reach p<0.05. Therefore, H_o is rejected.
   Tukey's Test:
   - q value of 8.406 was found between phenelzine (40µM) and phenelzine (5µM).
   - q value of 13.22 was found between phenelzine (40µM) and CTL.
   - q value of 13.608 was found between phenelzine (40µM) and LPS (5µg/ml).
   - q value of 4.814 was found between phenelzine (5µM) and CTL.
   - q value of 5.203 was found between phenelzine (5µM) and LPS (5µg/ml).
   - all other comparisons do not reject H_o.

b) *96-hour treatment:*
   One-way ANOVA analysis: F = 800.326, P = 4.066. F must be at least 4.066 to reach p<0.05. Therefore, H_o is rejected.
   Tukey's Test:
   - q value of 34.765 was found between phenelzine (40µM) and phenelzine (5µM).
   - q value of 58.674 was found between phenelzine (40µM) and CTL.
   - q value of 60.812 was found between phenelzine (40µM) and LPS (5µg/ml).
   - q value of 23.908 was found between phenelzine (5µM) and CTL.
   - q value of 26.047 was found between phenelzine (5µM) and LPS (5µg/ml).
   - all other comparisons do not reject H_o.

c) *144-hour treatment:*
   One-way ANOVA analysis: F = 601.684, P = 4.066. F must be at least 4.066 to reach p<0.05. Therefore, H_o is rejected.
   Tukey's Test:
   - q value of 11.981 was found between phenelzine (40µM) and phenelzine (5µM).
   - q value of 41.117 was found between phenelzine (40µM) and CTL.
   - q value of 52.546 was found between phenelzine (40µM) and LPS (5µg/ml).
   - q value of 29.136 was found between phenelzine (5µM) and CTL.
   - q value of 40.565 was found between phenelzine (5µM) and LPS (5µg/ml).
   - q value of 11.429 was found between CTL and LPS (5µg/ml).

MAO-A/B Inhibitor TNF-α ELISA Analysis

df = 8
q_c = 4.34 (p<0.05) and 6.33 (p<0.01).

96-hour treatment:
     One-way ANOVA analysis: F = 63.552, P = 4.066. F must be at least 4.066 to reach p<0.05. Therefore, H_o is rejected.
     Tukey's Test:
- q value of 7.686 was found between LPS (5μg/ml) and CTL.
- q value of 13.993 was found between LPS (5μg/ml) and phenelzine (5μM).
- q value of 18.328 was found between LPS (5μg/ml) and phenelzine (40μM).
- q value of 6.307 was found between CTL and phenelzine (5μM).
- q value of 10.642 was found between CTL and phenelzine (40μM).
- q value of 4.34 was found between phenelzine (5μM) and phenelzine (40μM).

MAO-A/B Inhibitor AR ELISA Analysis

df = 8
q_c = 4.34 (p<0.05) and 6.33 (p<0.01).

96-hour treatment:
     One-way ANOVA analysis: F = 88.194, P = 4.066. F must be at least 4.066 to reach p<0.05. Therefore, H_o is rejected.
     Tukey's Test:
- q value of 13.528 was found between LPS (5μg/ml) and CTL.
- q value of 18.323 was found between LPS (5μg/ml) and phenelzine (5μM).
- q value of 21.2 was found between LPS (5μg/ml) and phenelzine (40μM).
- q value of 4.795 was found between CTL and phenelzine (5μM).
- q value of 7.672 was found between CTL and phenelzine (40μM).
- all other comparisons do not reject H_o.

MAO-B Inhibitor TER Experiment

df = 10
q_c = 4.65 (p<0.05) and 6.14 (p<0.01).

a) *48-hour treatment:*
     One-way ANOVA analysis: F = 10.687, P = 3.478. F must be at least 3.478 to reach p<0.05. Therefore, H_o is rejected.
     Tukey's Test:
- q value of 6.627 was found between deprenyl (40μM) and pargyline (5μM).
- q value of 6.635 was found between deprenyl (40μM) and deprenyl (5μM).
- q value of 6.686 was found between deprenyl (40μM) and pargyline (40μM).
- q value of 8.449 was found between deprenyl (40μM) and CTL.
- all other comparisons do not reject H_o.

b) *96-hour treatment:*

     One-way ANOVA analysis: F = 60.213, P = 3.478. F must be at least 3.478 to reach $p < 0.05$. Therefore, H_o is rejected.

     Tukey's Test:
- q value of 16.156 was found between deprenyl (40μM) and deprenyl (5μM).
- q value of 17.022 was found between deprenyl (40μM) and pargyline (40μM).
- q value of 17.174 was found between deprenyl (40μM) and pargyline (5μM).
- q value of 18.606 was found between deprenyl (40μM) and CTL.
- all other comparisons do not reject H_o.

c) *144-hour treatment:*

     One-way ANOVA analysis: F = 44.879, P = 3.478. F must be at least 3.478 to reach $p < 0.05$. Therefore, H_o is rejected.

     Tukey's Test:
- q value of 7.492 was found between deprenyl (40μM) and deprenyl (5μM).
- q value of 12.364 was found between deprenyl (40μM) and pargyline (40μM).
- q value of 12.735 was found between deprenyl (40μM) and pargyline (5μM).
- q value of 17.758 was found between deprenyl (40μM) and CTL.
- q value of 4.871 was found between deprenyl (5μM) and pargyline (40μM).
- q value of 5.243 was found between deprenyl (5μM) and pargyline (5μM).
- q value of 10.265 was found between deprenyl (5μM) and CTL.
- all other comparisons do not reject H_o.

MAO-B Inhibitor TNF-α ELISA Analysis

df = 10
q_c = 4.65 ($p < 0.05$) and 6.14 ($p < 0.01$).

96-hour treatment:

     One-way ANOVA analysis: F = 20.106, P = 3.478. F must be at least 3.478 to reach $p < 0.05$. Therefore, H_o is rejected.

     Tukey's Test:
- q value of 12.126 was found between CTL and deprenyl (40μM).
- q value of 7.795 was found between CTL and deprenyl (5μM).
- q value of 7.507 was found between pargyline (5μM) and deprenyl (40μM).
- q value of 7.507 between pargyline (40μM) and deprenyl (40μM).
- all other comparisons do not reject H_o.

MAO-B Inhibitor AR ELISA Analysis

df = 10
q_c = 4.65 (p<0.05) and 6.14 (p<0.01)..

96-hour treatment:

    One-way ANOVA analysis: F = 34.222, P = 3.478. F must be at least 3.478 to reach p<0.05. Therefore, H_o is rejected.

    Tukey's Test:
- q value of 6.411 was found between pargyline (5μM) and pargyline (40μM).
- q value of 6.673 was found between deprenyl (5μM) and pargyline (40μM).
- q value of 14.918 was found between deprenyl (40μM) and pargyline (40μM).
- q value of 4.972 was found between CTL and pargyline (5μM).
- q value of 13.479 was found between CTL and deprenyl (40μM).
- q value of 5.234 was found between CTL and deprenyl (5μM).
- q value of 8.506 was found between deprenyl (40μM) and pargyline (5μM).
- q value of 8.244 was found between deprenyl (40μM) and deprenyl (5μM).
- all other comparisons do not reject H_o.

MAO-A Inhibitor TER Experiment

df = 10
q_c = 4.65 (p<0.05) and 6.14 (p<0.01).

a) *48-hour treatment:*

    One-way ANOVA analysis: F = 31.621, P = 3.478. F must be at least 3.478 to reach p<0.05. Therefore, H_o is rejected.

    Tukey's Test:
- q value of 6.42 was found between moclobemide (5μM) and CTL.
- q value of 9.304 was found between moclobemide (5μM) and clorgyline (5μM).
- q value of 14.536 was found between moclobemide (5μM) and clorgyline (40μM).
- q value of 6.257 was found between moclobemide (40μM) and clorgyline (5μM).
- q value of 11.489 was found between moclobemide (40μM) and clorgyline (40μM).
- q value of 8.116 was found between CTL and clorgyline (40μM).
- q value of 5.232 was found between clorgyline (5μM) and clorgyline (40μM).
- all other comparisons do not reject H_o.

b) *96-hour treatment:*

One-way ANOVA analysis: F = 49.586, P = 3.478. F must be at least 3.478 to reach $p < 0.05$. Therefore, H_o is rejected.

Tukey's Test:
- q value of 8.208 was found between moclobemide (5μM) and moclobemide (40μM).
- q value of 8.536 was found between moclobemide (5μM) and CTL.
- q value of 12.728 was found between moclobemide (5μM) and clorgyline (5μM).
- q value of 19.266 was found between moclobemide (5μM) and clorgyline (40μM).
- q value of 11.059 was found between moclobemide (40μM) and clorgyline (40μM).
- q value of 10.73 was found between CTL and clorgyline (40μM).
- q value of 6.538 was found between clorgyline (5μM) and clorgyline (40μM).
- all other comparisons do not reject H_o

c) *144-hour treatment:*

One-way ANOVA analysis: F = 73.695, P = 3.478. F must be at least 3.478 to reach $p < 0.05$. Therefore, H_o is rejected.

Tukey's Test:
- q value of 10.09 was found between moclobemide (5μM) and CTL.
- q value of 12.395 was found between moclobemide (40μM) and moclobemide (5μM).
- q value of 17.885 was found between moclobemide (5μM) and clorgyline (5μM).
- q value of 22.687 was found between moclobemide (5μM) and clorgyline (40μM).
- q value of 7.795 was found between CTL and clorgyline (5μM).
- q value of 12.597 was found between CTL and clorgyline (40μM).
- q value of 5.489 was found between moclobemide (40μM) and clorgyline (5μM).
- q value of 10.292 was found between moclobemide (40μM) and clorgyline (40μM).
- q value of 4.803 was found between clorgyline (5μM) and clorgyline (40μM).
- all other comparisons do not reject H_o.

MAO-A Inhibitor TNF-α ELISA Analysis

df = 10
q_c = 4.65 (p<0.05) and 6.14 (p<0.01).

96-hour treatment
      One-way ANOVA analysis: F = 63.57, P = 3.478. F must be at least 3.478 to reach p<0.05. Therefore, H_o is rejected.
      Tukey's Test:
- q value of 12.216 was found between clorgyline (40μM) and clorgyline (5μM).
- q value of 16.094 was found between clorgyline (40μM) and moclobemide (40μM).
- q value of 16.482 was found between clorgyline (40μM) and CTL.
- q value of 20.942 was found between clorgyline (40μM) and moclobemide (5μM) .
- q value of 8.726 was found between clorgyline (5μM) and moclobemide (5μM).
- q value of 4.848 was found between moclobemide (40μM) and moclobemide (5μM).
- all other comparisons do not reject H_o.

MAO-A Inhibitor AR ELISA Analysis

df = 10
q_c = 4.65 (p<0.05) and 6.14 (p<0.01)..

96-hour treatment:
      One-way ANOVA analysis: F = 27.47, P = 3.478. F must be at least 3.478 to reach p<0.05. Therefore, H_o is rejected.
      Tukey's Test:
- q value of 9.542 was found between clorgyline (40μM) and clorgyline (5μM).
- q value of 10.13 was found between clorgyline (40μM) and CTL.
- q value of 10.837 was found between clorgyline (40μM) and moclobemide (40μM).
- q value of 13.899 was found between clorgyline (40μM) and moclobemide (5μM) .
- all other comparisons do not reject H_o.

C. Statistical Analysis of Figure 6 Data

<u>PLE TER Experiment</u>

df = 6
q_c = 4.34 (p<0.05) and 6.33 (p<0.01).
a) *48-hour treatment:*
     One-way ANOVA analysis: F = 37.595, P = 5.143. F must be at least 5.143 to reach p<0.05. Therefore, H_o is rejected.
     Tukey's Test:
- q value of 4.35 was found between CTL and L (5μg/ml)+D (40μM).
- q value of 12.104 was found between LPS (5μg/ml) and L (5μg/ml)+D (40μM).
- q value of 7.755 was found between LPS (5μg/ml) and CTL.

b) *96-hour treatment:*
     One-way ANOVA analysis: F = 35.913, P = 5.143. F must be at least 5.143 to reach p<0.05. Therefore, H_o is rejected.
     Tukey's Test:
- q value of 4.39 was found between CTL and L (5μg/ml)+D (40μM).
- q value of 11.853 was found between LPS (5μg/ml) and L (5μg/ml)+D (40μM).
- q value of 7.463 was found between LPS (5μg/ml) and CTL.

c) *144-hour treatment:*
     One-way ANOVA analysis: F = 26.427, P = 5.143. F must be at least 5.143 to reach p<0.05. Therefore, H_o is rejected.
     Tukey's Test:
- q value of 3.5 was found between CTL and L (5μg/ml)+D (40μM).
- q value of 10.122 was found between LPS (5μg/ml) and L (5μg/ml)+D (40μM).
- q value of 6.622 was found between LPS (5μg/ml) and CTL.

<u>PLE TNF-α ELISA Analysis</u>

df = 6
q_c = 4.34 (p<0.05) and 6.33 (p<0.01).

a) *48-hour treatment:*
     One-way ANOVA analysis: F = 10.204, P = 5.143. F must be at least 5.143 to reach p<0.05. Therefore, H_o is rejected.
     Tukey's Test:
- q value of 2.428 was found between CTL and L (5μg/ml)+D (40μM).
- q value of 3.904 was found between LPS (5μg/ml) and L (5μg/ml)+D (40μM).
- q value of 6.332 was found between LPS (5μg/ml) and CTL.

b) *96-hour treatment:*

One-way ANOVA analysis: F = 8.857, P = 5.143. F must be at least 5.143 to reach p<0.05. Therefore, H$_o$ is rejected.

Tukey's Test:
- q value of 1.836 was found between CTL and L (5μg/ml)+D (40μM).
- q value of 3.985 was found between LPS (5μg/ml) and L (5μg/ml)+D (40μM).
- q value of 5.821 was found between LPS (5μg/ml) and CTL.

c) *144-hour treatment:*

One-way ANOVA analysis: F = 9.186, P = 5.143. F must be at least 5.143 to reach p<0.05. Therefore, H$_o$ is rejected.

Tukey's Test:
- q value of 2.148 was found between CTL and L (5μg/ml)+D (40μM).
- q value of 5.983 was found between LPS (5μg/ml) and L (5μg/ml)+D (40μM).
- q value of 3.835 was found between LPS (5μg/ml) and CTL.

IEC-6 TER Experiment

df = 6
q$_c$ = 4.34 (p<0.05) and 6.33 (p<0.01).

a) *48-hour treatment:*

One-way ANOVA analysis: F = 19.778, P = 5.143. F must be at least 5.143 to reach p<0.05. Therefore, H$_o$ is rejected.

Tukey's Test:
- q value of 3.098 was found between CTL and L (5μg/ml)+D (40μM).
- q value of 8.77 was found between LPS (5μg/ml) and L (5μg/ml)+D (40μM).
- q value of 5.671 was found between LPS (5μg/ml) and CTL.

b) *96-hour treatment:*

One-way ANOVA analysis: F = 86.194, P = 5.143. F must be at least 5.143 to reach p<0.05. Therefore, H$_o$ is rejected.

Tukey's Test:
- q value of 10.143 was found between CTL and L (5μg/ml)+D (40μM).
- q value of 18.541 was found between LPS (5μg/ml) and L (5μg/ml)+D (40μM).
- q value of 8.397 was found between LPS (5μg/ml) and CTL.

c) *144-hour treatment:*

One-way ANOVA analysis: F = 56.694, P = 5.143. F must be at least 5.143 to reach p<0.05. Therefore, H$_o$ is rejected.

Tukey's Test:
- q value of 2.462 was found between CTL and L (5μg/ml)+D (40μM).

- q value of 14.097 was found between LPS (5µg/ml) and L (5µg/ml)+D (40µM).
- q value of 11.635 was found between LPS (5µg/ml) and CTL.

IEC-6 TNF-α ELISA Analysis
df = 6
q_c = 4.34 (p<0.05) and 6.33 (p<0.01).

a) *48-hour treatment:*
    One-way ANOVA analysis: F = 73.346, P = 5.143. F must be at least 5.143 to reach p<0.05. Therefore, H_o is rejected.
    Tukey's Test:
- q value of 2.057 was found between CTL and L (5µg/ml)+D (40µM).
- q value of 13.698 was found between LPS (5µg/ml) and L (5µg/ml)+D (40µM).
- q value of 15.755 was found between LPS (5µg/ml) and CTL.

b) *96-hour treatment:*
    One-way ANOVA analysis: F = 19.786, P = 5.143. F must be at least 5.143 to reach p<0.05. Therefore, H_o is rejected.
    Tukey's Test:
- q value of 1.217 was found between CTL and L (5µg/ml)+D (40µM).
- q value of 8.24 was found between LPS (5µg/ml) and L (5µg/ml)+D (40µM).
- q value of 7.024 was found between LPS (5µg/ml) and CTL.

c) *144-hour treatment:*
    One-way ANOVA analysis: F = 68.987, P = 5.143. F must be at least 5.143 to reach p<0.05. Therefore, H_o is rejected.
    Tukey's Test:
- q value of 5.732 was found between CTL and L (5µg/ml)+D (40µM).
- q value of 10.636 was found between LPS (5µg/ml) and L (5µg/ml)+D (40µM).
- q value of 16.369 was found between LPS (5µg/ml) and CTL.

MDCK-I TER Experiment

df = 14
q_c = 4.83 (p<0.05) and 6.08 (p<0.01).

a) *48-hour treatment:*
     One-way ANOVA analysis: F = 22.42, P = 2.848. F must be at least 2.848 to reach p<0.05. Therefore, H_o is rejected.
    Tukey's Test:
- q value of 8.034 was found between CTL and L (0.25µg/ml)+D (40µM).
- q value of 9.789 was found between LPS (0.25µg/ml) and L (0.25µg/ml)+D (40µM).

- q value of 10.641 was found between LPS (1μg/ml) and L (0.25μg/ml)+D (40μM).
- q value of 11.638 was found between LPS (5μg/ml) and L (0.25μg/ml)+D (40μM).
- q value of 6.477 was found between L (1μg/ml)+D (40μM) and CTL.
- q value of 8.233 was found between LPS (0.25μg/ml) and L (1μg/ml)+D (40μM).
- q value of 9.085 was found between LPS (1μg/ml) and L (1μg/ml)+D (40μM).
- q value of 10.081 was found between LPS (5μg/ml) and L (1μg/ml)+D (40μM).
- q value of 4.878 was found between CTL and L (5μg/ml)+D (40μM).
- q value of 6.634 was found between LPS (0.25μg/ml) and L (5μg/ml)+D (40μM).
- q value of 7.486 was found between LPS (1μg/ml) and L (5μg/ml)+D (40μM).
- q value of 8.482 was found between LPS (5μg/ml) and L (5μg/ml)+D (40μM).
- all other comparisons do not reject H_o.

b) *96-hour treatment:*

One-way ANOVA analysis: F = 62.804, P = 2.848. F must be at least 2.848 to reach $p<0.05$. Therefore, H_o is rejected.

Tukey's Test:
- q value of 13.435 was found between CTL and L (5μg/ml)+D (40μM).
- q value of 14.659 was found between LPS (0.25μg/ml) and L (5μg/ml)+D (40μM).
- q value of 16.919 was found between LPS (1μg/ml) and L (5μg/ml)+D (40μM).
- q value of 17.74 was found between LPS (5μg/ml) and L (5μg/ml)+D (40μM).
- q value of 12.576 was found between L (0.25μg/ml)+D (40μM) and CTL.
- q value of 13.8 was found between LPS (0.25μg/ml) and L (0.25μg/ml)+D (40μM).
- q value of 16.06 was found between LPS (1μg/ml) and L (0.25μg/ml)+D (40μM).
- q value of 16.881 was found between LPS (5μg/ml) and L (0.25μg/ml)+D (40μM).
- q value of 10.783 was found between CTL and L (1μg/ml)+D (40μM).
- q value of 12.007 was found between LPS (0.25μg/ml) and L (1μg/ml)+D (40μM).
- q value of 14.267 was found between LPS (1μg/ml) and L (1μg/ml)+D (40μM).
- q value of 15.088 was found between LPS (5μg/ml) and L (1μg/ml)+D (40μM).
- all other comparisons do not reject H_o.

c) *144-hour treatment:*

 One-way ANOVA analysis: F = 99.304, P = 2.848. F must be at least 2.848 to reach $p<0.05$. Therefore, H_o is rejected.

 Tukey's Test:
- q value of 4.93 was found between L(1µg/ml)+D (40µM) and L (5µg/ml)+D (40µM).
- q value of 18.059 was found between CTL and L (5µg/ml)+D (40µM).
- q value of 19.955 was found between LPS (0.25µg/ml) and L (5µg/ml)+D (40µM).
- q value of 21.372 was found between LPS (5µg/ml) and L (5µg/ml)+D (40µM).
- q value of 21.471 was found between L (5µg/ml)+D (40µM) and LPS (1µg/ml).
- q value of 17.252 was found between CTL and L (0.25µg/ml)+D (40µM).
- q value of 19.148 was found between LPS (0.25µg/ml) and L (0.25µg/ml)+D (40µM).
- q value of 20.565 was found between LPS (5µg/ml) and L (0.25µg/ml)+D (40µM).
- q value of 20.664 was found between LPS (1µg/ml) and L (0.25µg/ml)+D (40µM).
- q value of 13.128 was found between CTL and L (1µg/ml)+D (40µM).
- q value of 15.025 was found between LPS (0.25µg/ml) and L (1µg/ml)+D (40µM).
- q value of 16.442 was found between LPS (5µg/ml) and L (1µg/ml)+D (40µM).
- q value of 16.54 was found between LPS (1µg/ml) and L (1µg/ml)+D (40µM).
- all other comparisons do not reject H_o.

MDCK-I TNF-α ELISA Analysis

df = 6
q_c = 4.34 ($p<0.05$) and 6.33 ($p<0.01$).

a) *48-hour treatment:*

 One-way ANOVA analysis: F = 55.451, P = 5.143. F must be at least 5.143 to reach $p<0.05$. Therefore, H_o is rejected.

 Tukey's Test:
- q value of 11.423 was found between LPS (5µg/ml) and L (5µg/ml)+D (40µM).
- q value of 13.987 was found between LPS (5µg/ml) and CTL.
- q value of 2.565 was found between L (5µg/ml)+D (40µM) and CTL.

b) *96-hour treatment:*

 One-way ANOVA analysis: F = 12.422, P = 5.143. F must be at least 5.143 to reach p<0.05. Therefore, H_o is rejected.

 Tukey's Test:
- q value of 5.815 was found between LPS (5μg/ml) and L (5μg/ml)+D (40μM).
- q value of 6.358 was found between LPS (5μg/ml) and CTL.
- q value of 0.543 was found between L (5μg/ml)+D (40μM) and CTL.

c) *144-hour treatment:*

 One-way ANOVA analysis: F = 24.827, P = 5.143. F must be at least 5.143 to reach p<0.05. Therefore, H_o is rejected.

 reject H_o:
- q value of 8.355 was found between LPS (5μg/ml) and L (5μg/ml)+D (40μM).
- q value of 8.881 was found between LPS (5μg/ml) and CTL.
- q value of 0.526 was found between L (5μg/ml)+D (40μM) and CTL.

D. Statistical Analysis of Figure 12 Data

TNF-α ELISA Analysis

df = 10
q_c = 4.65 (p<0.05) and 6.14 (p<0.01).

a) *48-hour treatment:*
    One-way ANOVA analysis: F = 6.468, P = 3.478. F must be at least 3.478 to reach p<0.05. Therefore, H_o is rejected.
    Tukey's Test:
- q value of 6.839 was found between LPS (1μg/ml) and CTL.
- all other comparisons do not reject H_o.

b) *96-hour treatment:*
    One-way ANOVA analysis: F = 4.401, P = 3.478. F must be at least 3.478 to reach p<0.05. Therefore, H_o is rejected.
    Tukey's Test:
- q value of 5.564 was found between LPS (1μg/ml) and CTL.
- all other comparisons do not reject H_o.

c) *144-hour treatment:*
    One-way ANOVA analysis: F = 5.605, P = 3.478. F must be at least 3.478 to reach p<0.05. Therefore, H_o is rejected.
    Tukey's Test:
- q value of 5.222 was found between LPS (1μg/ml) and CTL.
- q value of 4.964 was found between LPS (0.5μg/ml) and CTL.
- all other comparisons do not reject H_o.

E. Statistical Analysis of Figure 13 Data

AR ELISA Analysis

df = 14
q_c = 4.83 (p<0.05) and 6.08 (p<0.01).

a) *48-hour treatment:*
 One-way ANOVA analysis: F = 9.002, P = 2.848. F must be at least 2.848 to reach p<0.05. Therefore, H_o is rejected.
 Tukey's Test:
- q value of 5.544 was found between LPS (1μg/ml) and L (5μg/ml)+D (40μM).
- q value of 7.156 was found between LPS (1μg/ml) and L (0.5μg/ml)+D (40μM).
- q value of 7.191 was found between LPS (1μg/ml) and L (1μg/ml)+D (40μM).
- q value of 4.995 was found between LPS (5μg/ml) and L (5μg/ml)+D (40μM).
- q value of 6.606 was found between LPS (5μg/ml) and L (0.5μg/ml)+D (40μM).
- q value of 6.642 was found between LPS (5μg/ml) and L (1μg/ml)+D (40μM).
- q value of 4.83 was found between LPS (0.5μg/ml) and L (0.5μg/ml)+D (40μM).
- q value of 4.861 was found between LPS (0.5μg/ml) and L (1μg/ml)+D (40μM).
- all other comparisons do not reject H_o.

b) *96-hour treatment:*
 One-way ANOVA analysis: F = 109.026, P = 2.848. F must be at least 2.848 to reach p<0.05. Therefore, H_o is rejected.
 Tukey's Test:
- q value of 5.413 was found between LPS (5μg/ml) and LPS (0.5μg/ml).
- q value of 11.231 was found between LPS (5μg/ml) and CTL.
- q value of 22.26 was found between LPS (5μg/ml) and L (5μg/ml)+D (40μM).
- q value of 22.631 was found between LPS (5μg/ml) and L (0.5μg/ml)+D (40μM).
- q value of 22.665 was found between LPS (5μg/ml) and L (1μg/ml)+D (40μM).
- q value of 4.998 was found between LPS (1μg/ml) and LPS (0.5μg/ml).
- q value of 10.816 was found between LPS (1μg/ml) and CTL.
- q value of 21.845 was found between LPS (1μg/ml) and L (5μg/ml)+D (40μM).

- q value of 22.216 was found between LPS (1μg/ml) and L (0.5μg/ml)+D (40μM).
- q value of 22.249 was found between LPS (1μg/ml) and L (1μg/ml)+D (40μM).
- q value of 5.818 was found between LPS (0.5μg/ml) and CTL.
- q value of 16.847 was found between LPS (0.5μg/ml) and L (5μg/ml)+D (40μM).
- q value of 17.218 was found between LPS (0.5μg/ml) and L (0.5μg/ml)+D (40μM).
- q value of 17.252 was found between LPS (0.5μg/ml) and L (1μg/ml)+D (40μM).
- q value of 11.029 was found between CTL and L (5μg/ml)+D (40μM).
- q value of 11.4 was found between CTL and L (0.5μg/ml)+D (40μM).
- q value of 11.434 was found between CTL and L (1μg/ml)+D (40μM).
- all other comparisons do not reject H_o.

c) *144-hour treatment:*

One-way ANOVA analysis: F = 139.524, P = 2.848. F must be at least 2.848 to reach p<0.05. Therefore, H_o is rejected.

Tukey's Test:
- q value of 7.841 was found between LPS (5μg/ml) and LPS (0.5μg/ml).
- q value of 16.729 was found between LPS (5μg/ml) and CTL.
- q value of 25.396 was found between LPS (5μg/ml) and L (0.5μg/ml)+D (40μM).
- q value of 25.824 was found between LPS (5μg/ml) and L (5μg/ml)+D (40μM).
- q value of 25.866 was found between LPS (5μg/ml) and L (1μg/ml)+D (40μM).
- q value of 7.536 was found between LPS (1μg/ml) and LPS (0.5μg/ml).
- q value of 16.423 was found between LPS (1μg/ml) and CTL.
- q value of 25.091 was found between LPS (1μg/ml) and L (0.5μg/ml)+D (40μM).
- q value of 25.518 was found between LPS (1μg/ml) and L (5μg/ml)+D (40μM).
- q value of 25.56 was found between LPS (1μg/ml) and L (1μg/ml)+D (40μM).
- q value of 8.888 was found between LPS (0.5μg/ml) and CTL.
- q value of 17.555 was found between LPS (0.5μg/ml) and L (0.5μg/ml)+D (40μM).
- q value of 17.983 was found between LPS (0.5μg/ml) and L (5μg/ml)+D (40μM).
- q value of 18.025 was found between LPS (0.5μg/ml) and L (1μg/ml)+D (40μM).
- q value of 8.668 was found between CTL and L (0.5μg/ml)+D (40μM).
- q value of 9.095 was found between CTL and L (5μg/ml)+D (40μM).
- q value of 9.137 was found between CTL and L (1μg/ml)+D (40μM).

- all other comparisons do not reject H_o.

F. Statistical Analysis of Figure 14 Data.

df = 14
q_c = 4.83 (p<0.05) and 6.08 (p<0.01).

AR TER Experiment

144-hour treatment:
    One-way ANOVA analysis: F = 27.217, P = 2.848. F must be at least 2.848 to reach p<0.05. Therefore, H_o is rejected.
    Tukey's Test:
- q value of 5.204 was found between AR (1ng/ml)+D(10μM) and AR (1ng/ml).
- q value of 6.778 was found between AR (1ng/ml)+D(10μM) and CTL.
- q value of 8.802 was found between AR (1ng/ml)+D(10μM) and AR (5ng/ml).
- q value of 12.296 was found between AR (1ng/ml)+D(10μM) and AR (10ng/ml)+D(10μM).
- q value of 15.749 was found between AR (1ng/ml)+D(10μM) and AR (10ng/ml).
- q value of 7.732 was found between AR (5ng/ml)+D(10μM) and AR (10ng/ml)+D(10μM).
- q value of 11.185 was found between AR (5ng/ml)+D(10μM) and AR (10ng/ml).
- q value of 7.092 was found between AR (1ng/ml) and AR (10ng/ml)+D(10μM).
- q value of 10.545 was found between AR (1ng/ml) and AR (10ng/ml).
- q value of 5.519 was found between CTL and AR (10ng/ml)+D(10μM).
- q value of 8.972 was found between CTL and AR (10ng/ml).
- q value of 6.947 was found between AR (5ng/ml) and AR (10ng/ml).
- all other comparisons do not reject H_o.

G. Statistical Analysis of Figure 15 Data.

<u>TER Experiment</u>

$df = 10$
$q_c = 4.65$ (p<0.05) and 6.14 (p<0.01).

a) *48-hour treatment:*
    One-way ANOVA analysis: F = 22.333, P = 3.478. F must be at least 3.478 to reach p<0.05. Therefore, H_o is rejected.
    Tukey's Test:
- q value of 7.178 was found between H (0.1mM)+D (5μM) and H_2O_2 (0.1mM).
- q value of 12.571 was found between H (0.1mM)+D (5μM) and H_2O_2 (0.5mM).
- q value of 9.302 was found between H (0.1mM)+D (10μM) and H_2O_2 (0.5mM).
- q value of 8.21 was found between CTL and H_2O_2 (0.5mM).
- q value of 5.393 was found between H_2O_2 (0.1mM) and H_2O_2 (0.5mM).
- all other comparisons do not reject H_o.

b) *96-hour treatment:*
    One-way ANOVA analysis: F = 17.98, P = 3.478. F must be at least 3.478 to reach p<0.05. Therefore, H_o is rejected.
    Tukey's Test:
- q value of 6.032 was found between H (0.1mM)+D (5μM) and H_2O_2 (0.1mM).
- q value of 11.211 was found between H (0.1mM)+D (5μM) and H_2O_2 (0.5mM).
- q value of 8.842 was found between H (0.1mM)+D (10μM) and H_2O_2 (0.5mM).
- q value of 7.01 was found between CTL and H_2O_2 (0.5mM).
- q value of 5.179 was found between H_2O_2 (0.1mM) and H_2O_2 (0.5mM).
- all other comparisons do not reject H_o.

c) *144-hour treatment:*
    One-way ANOVA analysis: F = 377.883, P = 3.478. F must be at least 3.478 to reach p<0.05. Therefore, H_o is rejected.
    Tukey's Test:
- q value of 4.898 was found between H (0.1mM)+D (5μM) and H (0.1mM)+D (10μM).
- q value of 14.058 was found between H (0.1mM)+D (5μM) and CTL.
- q value of 31.263 was found between H (0.1mM)+D (5μM) and H_2O_2 (0.1mM).
- q value of 46.888 was found between H (0.1mM)+D (5μM) and H_2O_2 (0.5mM).
- q value of 9.16 was found between H (0.1mM)+D (10μM) and CTL.

- q value of 26.365 was found between H (0.1mM)+D (10μM) and H_2O_2 (0.1mM).
- q value of 41.99 was found between H (0.1mM)+D (10μM) and H_2O_2 (0.5mM).
- q value of 17.205 was found between CTL and H_2O_2 (0.1mM).
- q value of 32.83 was found between CTL and H_2O_2 (0.5mM).
- q value of 15.625 was found between H_2O_2 (0.1mM) and H_2O_2 (0.5mM).

AR ELISA Analysis

df = 8
q_c = 4.53 (p<0.05) and 6.20 (p<0.01).

a) *48-hour treatment:*
   One-way ANOVA analysis: F = 35.821, P = 4.066. F must be at least 4.066 to reach p<0.05. Therefore, H_o is rejected.
   Tukey's Test:
- q value of 11.251 was found between H_2O_2 (0.1mM) and H+D (5μM).
- q value of 11.537 was found between H_2O_2 (0.1mM) and H+D (10μM).
- q value of 12.872 was found between H_2O_2 (0.1mM) and CTL.
- all other comparisons do not reject H_o.

b) *96-hour treatment:*
   One-way ANOVA analysis: F = 33.829, P = 4.066. F must be at least 4.066 to reach p<0.05. Therefore, H_o is rejected.
   Tukey's Test:
- q value of 8.267 was found between H_2O_2 (0.1mM) and CTL.
- q value of 12.533 was found between H_2O_2 (0.1mM) and H+D (5μM).
- q value of 12.133 was found between H_2O_2 (0.1mM) and H+D (10μM).
- all other comparisons do not reject H_o.

c) *144-hour treatment:*
   One-way ANOVA analysis: F = 14.42, P = 4.066. F must be at least 4.066 to reach p<0.05. Therefore, H_o is rejected.
   Tukey's Test:
- q value of 4.797 was found between H_2O_2 (0.1mM) and CTL.
- q value of 7.39 was found between H_2O_2 (0.1mM) and H+D (5μM).
- q value of 8.556 was found between H_2O_2 (0.1mM) and H+D (10μM).
- all other comparisons do not reject H_o.

H. Statistical Analysis of Figure 16 Data

LPS ± Deprenyl Treatment of MDCK-I Barrier Model

df = 8
q_c = 4.53 (p<0.05) and 6.20 (p<0.01).

144-hour treatment:
      One-way ANOVA analysis: F = 11.451, P = 4.066. F must be at least 4.066 to reach p<0.05. Therefore, H_o is rejected.
      Tukey's Test:
- q value of 8.147 was found between Deprenyl (10μM) and CTL.
- q value of 5.376 was found between L (10μg/ml)+D (10μM) and CTL.
- all other comparisons do not reject H_o.

AR Treatment of MDCK-I Barrier Model

df = 8
q_c = 4.53 (p<0.05) and 6.20 (p<0.01).

144-hour treatment:
      One-way ANOVA analysis: F = 1.067, P = 4.066. F must be at least 4.066 to reach p<0.05. Therefore, H_o is not rejected.

TNF-α Treatment of MDCK-I Barrier Model

df = 8
q_c = 4.53 (p<0.05) and 6.20 (p<0.01).

144-hour treatment:
      One-way ANOVA analysis: F = 25.139, P = 4.066. F must be at least 4.066 to reach p<0.05. Therefore, H_o is rejected.
      Tukey's Test:
- q value of 11.31 was found between TNF-α (1ng/ml) and TNF-α (10ng/ml).
- q value of 9.332 was found between CTL and TNF-α (10ng/ml).
- q value of 8.687 was found between TNF-α (5ng/ml) and TNF-α (10ng/ml).
- all other comparisons do not reject H_o.

H₂O₂ Treatment of MDCK-I Barrier Model

df = 8
q_c = 4.53 (p<0.05) and 6.20 (p<0.01).

144-hour treatment:
　　One-way ANOVA analysis: F = 48.859, P = 4.066. F must be at least 4.066 to reach p<0.05. Therefore, H_o is rejected.
　　Tukey's Test:
- q value of 16.239 was found between H$_2$O$_2$ (0.05mM) and H$_2$O$_2$ (0.5mM).
- q value of 11.975 was found between H$_2$O$_2$ (0.1mM) and H$_2$O$_2$ (0.5mM).
- q value of 11.938 was found between CTL and H$_2$O$_2$ (0.5mM).
- all other comparisons do not reject H_o.